UNIVERSITY of CALIFORNIA

Santa Barbara

Modifying Membrane Properties with Conjugated Oligoelectrolytes and Elucidating the Charge Transfer Mechanisms

A Dissertation submitted in partial satisfaction of the

requirements for the degree

Doctor of Philosophy

in

Materials

by

Chelsea Elizabeth Catania

Committee in charge:

Professor Guillermo C. Bazan, Chair
Professor Frederick W. Dahlquist
Professor Cyrus R. Safinya
Professor Omar A. Saleh
Professor David L. Valentine

December 2016

The dissertation of Chelsea Elizabeth Catania is approved.

Professor Frederick W. Dahlquist

Professor Cyrus R. Safinya

Professor Omar A. Saleh

Professor David L. Valentine

Professor Guillermo C. Bazan, Committee Chair

November 2016

Modifying Membrane Properties with Conjugated Oligoelectrolytes and Elucidating the Charge Transfer Mechanisms

by

Chelsea Elizabeth Catania

dedicated to my mother, my father, and my sister

Acknowledgements

I would like to start by acknowledging my advisor, Professor Guillermo Bazan, for giving me the opportunity to explore this research and for his patience with me as it took us through new territories. I am lucky to have worked in such a well-equipped laboratory—which I too often took for granted. Thanks to Professor Bazan's tireless work securing funding, scientific progress was never halted for a lack of supply. I'd also like to thank Gui for the seemingly minuscule comments that have made such huge impacts on my research. For example, that first question he posed to me of "*why does the internal resistance decrease?*" that led me down this rabbit-hole. I have a tendency to think of all of the possibilities and an urge to explain everything at once. Gui helped me hone my vision into manageable pieces of work and put our accomplishments in perspective—although there is more to learn, we have come far. I can truly say that I would not have grown into the independent scientist I am today if it weren't for Prof. Bazan's mentorship and for that, I'll be eternally grateful.

I would like to thank my committee members who have supported me throughout; Profs. Omar Saleh, Cyrus Safinya, Rick Dahlquist and David Valentine. Omar has been a role model for myself, as well as many who have sat through his classes, for his quality of teaching, brilliance, and humor. I have

learned tremendously from taking his classes and attempting to emulate his standard of science. Cyrus has never had a lack of ideas. He has been particularly helpful for my research on liposomes and general life/career advice. Rick has been extremely generous with his time and resources. I have gone to him many times throughout my studies to discuss ideas, plan experiments, borrow lab supplies and confirm my sanity. I have always left these discussions feeling motivated and excited about my experiments. I am lucky to have met Dave Valentine and grateful for his support. His love of and communication of science has been inspiring for me. Spending a month at sea with his group on the R/V Atlantis was a once-in-a-lifetime experience that I would have never experienced if it were not for Dave. I will remember it fondly. I feel truly blessed to have had these professors on my committee.

My life would not be the same if it were not for Caroline Ajo-Franklin. I accomplished a significant portion of my thesis work in her lab at the Molecular Foundry. I have an infinite amount of appreciation for her work, advice and encouragement. I'd also like to thank Prof. Michaela TerAvest and the rest of the Ajo-Franklin group. The Biological Nanostructures facilities of the Molecular Foundry would not be such a productive and welcoming environment if it were not for the leadership of Ron Zuckermann and the skilled staff members. My stay in Berkeley would not have been possible if it weren't for Rachelle Andone,

Kyle Dunn, Andrew Yip and even Caroline, who have all graciously hosted me during this time.

I have had the opportunity and pleasure to work with, learn from, and enjoy the company of many wonderful group members. Special thanks to the "Bioteam", consisting of past and present members: Dr. Logan Garner, Dr. Jenny Du, Dr. Huijie Hou, Dr. Alex Thomas, Dr. Nathan Kirchhofer, Dr. Hengjing Yan, Zach Rengert, Alex Moreland, Dr. Bing Wang, and Samantha McCuskey. Our project and experience would have not been the same if we were not a great team.

I would like to separately acknowledge a few members, the first being Dr. Logan Garner. I started this project under Logan's wing as he prepared to wrap up the end of his graduate studies. I learned early on from his tricks on how to be efficient and accurate in our bench work, as well as how to not break stuff or hurt oneself in lab. He was both encouraging and critical, making for a great mentor. Dr. Huijie Hou taught me everything I know about fabricating devices. She was a pleasure to learn from, had an admirable work ethic and was generous with her support and mentorship. Huijie hosted me twice, when I visited Prof. Bruce Logan's lab and again for a conference. Dr. Hengjing Yan helped me in many ways to develop as a scientist; with experimental design, presentation help, and communication in lab. Often, she challenged me and I

felt like I had to yell at her, but mainly just to meet her natural volume and energy. I blame Dr. Jenny Du for being the reason why I joined this group in the first place. Her optimistic, can-do attitude is contagious. She advocated for others and was a keeper of peace and fairness, which strongly influenced our team atmosphere. Dr. Alex Thomas and I shared an office (and snacks) for most of my graduate career and supported each other tremendously. We grew scientifically together, shared ideas, and vented frustrations. Alex always had my back in tough times. I can't imagine this experience without him. Dr. Nate Kirchhofer felt like the equivalent of a lab sibling— sometimes working with him was challenging and we fought for attention, but we pulled through, learned a lot from each other and developed a great friendship. Zach Rengert and I worked on a project together in record time in the end of my studies and it was the most fun I ever had in lab. There were many scientific discussions, venting sessions, and philosophical conversations; I can't thank him enough for being awesome to work with and an even more awesome friend.

I have had the pleasure of being welcomed into many groups which have been a source of emotional support throughout my studies; my roommates, friends, other laboratories and student groups. I have much love for the group of women in my cohort, aka "the GSG" (for Girl Study Group), without whom I wouldn't have gotten through classes, exams, and other life events. Shoutout to

my friends; Dr. Kristin Denault, for being the best and basically sharing our life together, Alan Liu and Matt Idso, for thesis writing company, Dr. Jason Douglas and Leo Lamontagne, for always being there and countless good times, Dr. Stacy Kowsz, for the best hugs, and the many others I wish I could go on about, who have made this a home-away-from-home. I would like to especially thank Prof. Ram Seshadri for including me in his group activities, for rides home from the bus stop, and for generously sharing his love of the symphony and arts with UCSB students. I am inspired by the care he has for his own, and even not his own, students. Dave Valentine's group and his father, Prof. Ray Valentine, have also been a great source of support, encouragement, and science discussion. The many members of the Graduate Students for Diversity in Science (GSDS) have developed an inclusive student community on campus that have opened many opportunities; I am thankful to have been a part of GSDS and excited for their future.

I would like to thank the administrative and technical staff of the Center for Polymers and Organic Solids (CPOS), Institute for Collaborative Biotechnologies (ICB), CNSI Biological Nanostructures Lab (BNL), Materials Research Laboratory (MRL), and the Materials Department. This work would not have been possible without funding by the National Science Foundation Graduate Research Fellowship under Grant No. DGE 1144085 as well as from ICB. Travel

grants from the MRL enabled me to attend most of the conferences that I participated in during my studies, as well as my visit to Prof. Bruce Logan's lab, who graciously invited me to visit his lab and learn from his students. Additionally, outreach events coordinated by MRL Outreach staff, Dotti Pak, Julie Standish, Mary McGuan and Frank Kinnaman, enforced my love for science by enabling me to give back to the community. I would like to thank Profs. Tresa Pollock and Carlos Levi for truly caring for the Materials Department and all of the Materials students.

Last, I'd like to thank my family. Lisa Ferrera, my best friend, who drove with me from Florida to California, came back to see me defend, and has always been a source of support and love. My sister, Cassie, who has been a grounding force and an inspiration in terms of finding one's passion and spirit. My parents, who have raised me to be the person I am today, supported my decisions, and encouraged me to pursue my dreams and find happiness. Without them, none of this would have been possible.

Curriculum Vitæ

Chelsea Elizabeth Catania

Education

2011–2016 Ph.D. in Materials, University of California, Santa Barbara, CA, USA.

2006–2011 B.S. in Materials Science and Engineering, University of Florida, Gainesville, FL, USA.

Publications

8. **Catania, Chelsea**; Ajo-Franklin, Caroline M.; Bazan, Guillermo C.; "Membrane Permeabilization by Conjugated Oligoelectrolytes Accelerates Whole-Cell Catalysis." *RSC Advances*, **2016**, 6 (102), 100300-100306. [**doi**]

7. **Catania, Chelsea**; Thomas, Alexander W.; Bazan, Guillermo C.; "Tuning cell surface charge in *E. coli* with conjugated oligoelectrolytes." *Chemical Science* **2016**, 7 (3), 2023-2029. [**doi**]

6. Yan, Henging; **Catania, Chelsea**; Bazan, Guillermo C.; "Membrane-Intercalating Conjugated Oligoelectrolytes: Impact on Bioelectrochemical Systems." *Adv. Mater.* **2015**, 27 (19), 2958-2973. [**doi**]

5. Thomas, Alexander W.; **Catania, Chelsea**; Garner, Logan E.; Bazan, Guillermo C.; "Pendant ionic groups of conjugated oligoelectrolytes govern their ability to intercalate into microbial membranes." *Chem. Commun.* **2015**, 51 (45), 9294-9297. [**doi**]

4. Du, Jenny; **Catania, Chelsea**; Bazan, Guillermo C.; "Modification of abiotic-biotic interfaces with small molecules and nanomaterials for improved bioelectronics." *Chem. Mater.* **2013**, 26 (1), 686-697. [**doi**]

3. Hou, Huijie; Chen, Xiaofen; Thomas, Alexander W.; **Catania, Chelsea**; Kirchhofer, Nathan D.; Garner, Logan E.; Han, Arum; Bazan, Guillermo C.; "Conjugated oligoelectrolytes increase power generation in *E. coli* microbial fuel cells." *Adv. Mater.* **2013**, 25 (11), 1593-1597. [**doi**]

2. Wang, Yan; Azaïs, Thierry; Robin, Marc; Vallée, Anne; **Catania, Chelsea**; Legriel, Patrick; Pehau-Arnaudet, Gérard;, Babonneau, Florence; Giraud-Guille, Marie-Madeleine; Nassif, Nadine; "The predominant role of collagen in the nucleation, growth, structure and orientation of bone apatite." *Nature Mater.* **2012**, 11 (8), 724-733. [**doi**]

1. Vigier, Sylvain; **Catania, Chelsea**; Baroukh, Brigitte; Saffar, Jean-Louis; Giraud-Guille, Marie-Madeleine; "Dense Fibrillar Collagen Matrices Sustain Osetoblast Phenotype *In Vitro* and Promote Bone Formation in Rat Calvaria Defect." *Tissue Engineering Part A* **2011**, 17 (7-8), 889-896. [**doi**]

Abstract

Modifying Membrane Properties with Conjugated Oligoelectrolytes and Elucidating the Charge Transfer Mechanisms

by

Chelsea Elizabeth Catania

Cellular membranes exist across all domains of life, essentially acting as a barrier that separates the conditions of life from the non-living environment. In gram-negative bacteria, such as *Escherichia coli*, the cell envelope is comprised of an outer membrane (OM), a peptidoglycan layer (ca. 35–55 nm) and an inner membrane (IM). The core structural component to each membrane is the lipid bilayer, which is electrically insulating and impermeable to most ions and polar molecules. Membrane proteins are the other major component in microbial membranes, conferring function to the membrane and enabling the passive and active transport of ions, molecules and water. Critical biological processes, such as energy generation and molecular sensing, are inherently electronic—driven by the flow of electrons and ions across the membranes of cells. Thus, modification of the transmembrane flux of ions or electrons may enable manipulation of

a wide-range of intracellular biological processes pertinent to biotechnological applications.

Conjugated oligoelectrolytes (COEs) are a class of small molecules designed for membrane modification. The structure of COEs are described by a π-conjugated, phenylenevinylene backbone of a few repeat units tethered at the two terminal ends by ionic functionalities. COEs have been demonstrated to spontaneously intercalate and align in lipid bilayers, thereby allowing modification of membrane properties and function of cells in bioelectrochemical systems. One COE, namely DSSN+, has been applied in a variety of microbial electronic devices utilizing Yeast, *E. coli*, *Shewanella oneidensis*, and even naturally occurring microorganisms in wastewater to improve current generation. It is generally acknowledged that ability of COEs to intercalate into microbial membranes is paramount for increasing charge transfer in bioelectrochemical systems, however the specific mechanism of action is not well understood. Previous investigations on the mechanism for improved current in *S. oneidensis* suggest that DSSN+ amplifies the native biological electron transfer pathway. However, this suggested mechanism does not universally apply across microbial species. For example, COEs have been demonstrated to increase in current and power generation in *E. coli* microbial fuel cells and this organism lacks a native extracellular electron transfer pathway.

A unifying mechanism by which COEs improve charge transfer processes and modify microbial membranes is the underlying motivation for this work. First, COEs varying in length and structural features are compared with respect to their association with *E. coli*. Quantification of COEs associated with the cell reveals a morphologically impossible amount, approaching or surpassing a 1:1 lipid:COE ratio, indicating association is not exclusive to membrane intercalation. Using zeta potential measurements on COE modified cells, it is determined that COEs are able to tune cell surface charge. Second, considering permeabilization as one possible mode for improved bioelectrochemical performance, the effect of DSSN+ on the permeability of the inner and outer membrane of *E. coli* is examined, revealing a plausible explanation. Lastly, performance of *E. coli* in bioelectrochemical systems is examined while taking these effects on membrane properties into consideration. An ultimate hypothesis is proposed, that the combined effects of COEs on membrane properties are the underlying cause for the increased current in *E. coli*. A better understanding of the effects of COEs on microbial membrane properties can thus inform the molecular design of future COEs and uncover potential new areas of application.

Contents

List of Figures

List of Tables

Chapter 1

Introduction

1.1 Motivation

The field of bioelectronics takes advantage of innate cellular behavior for the "transduction" of chemical information into electronic information and vice versa. [2] Many biological processes such as energy generation and signal transduction are inherently electronic—driven by the flow of electrons and ions across the membranes of cells. [3] Barriers to charge transport across the biotic-abiotic interface constitute a significant obstacle to utilize such processes in high performance electronics. [4–7] Advances in the ability to manipulate charge

[1]The contents of this chapter have appeared in reference 1: H. Yan, C. Catania, and G. C. Bazan, Membrane-Intercalating Conjugated Oligoelectrolytes: Impact on Bioelectrochemical Systems, *Adv. Mater.* **27**, 2958–2973 (2015).

transfer in organisms has far reaching applications for bioenergy [4, 8], bioelectrosynthesis [9, 10], diagnostics [11–13], environmental monitoring [14–16] and bioremediation. [17, 18]

Certain microorganisms, called exoelectrogens, have evolved the innate ability for extracellular electron transfer (EET) necessary for survival in specific environments. [19–22] These microbes are inherently capable of accomplishing EET to (or from) an electrode, which they accomplish mechanistically by either direct electron transfer (DET) or mediated electron transfer (MET). [23, 24] Microorganisms capable of DET typically do so by directly transferring electrons via appendages such as outer membrane-bound redox active proteins and/or conductive pili/nanowires. [25–28] Other microorganisms interact indirectly with electrodes via the secretion of redox-active electron shuttles. [29–32] These mechanisms are depicted in Figure 1.1. While microorganisms capable of EET exist, they are not prevalent. [4] Thus, there is interest in finding general methods by which EET can be induced or improved in microorganisms to increase the breadth of potential bioelectronic applications.

For the specific application of microorganisms in microbial fuel cells (MFCs), exoelectrogenic microorganisms catalyze the conversion of chemical energy to electrical energy. A general illustration of the electron flow in MFC is provided in Figure 1.2. In brief, microorganisms in the anode chamber oxidize a sub-

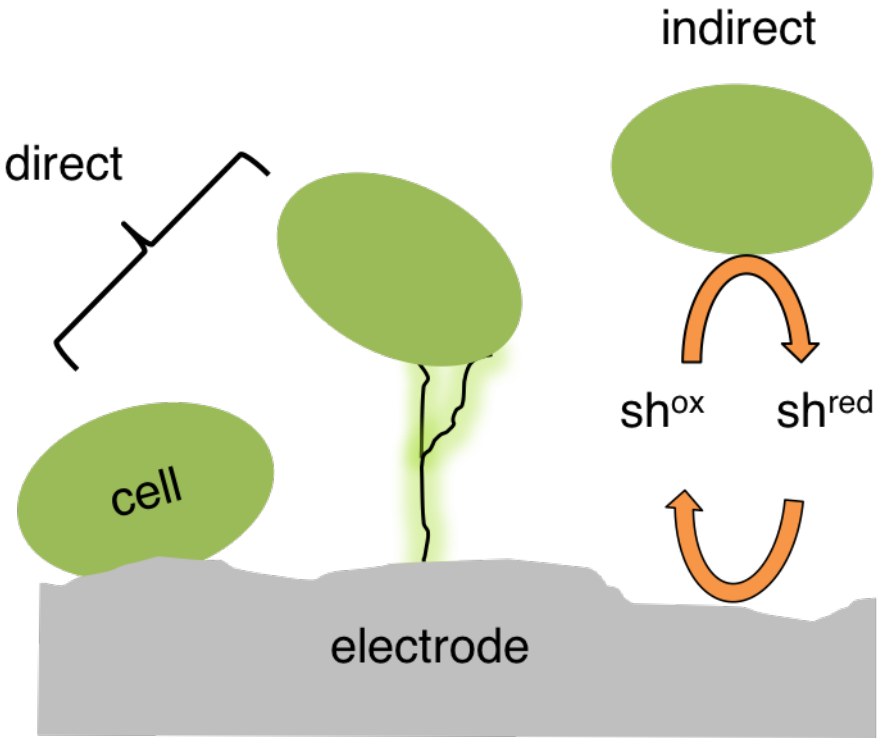

Figure 1.1: Cartoon illustration of the different mechanisms of microbial extracellular electron transfer (EET). *Left to right*: direct electron transfer through outer membrane-bound proteins; transfer through conductive appendages/pili; and mediated transport via redox active shuttles (sh).

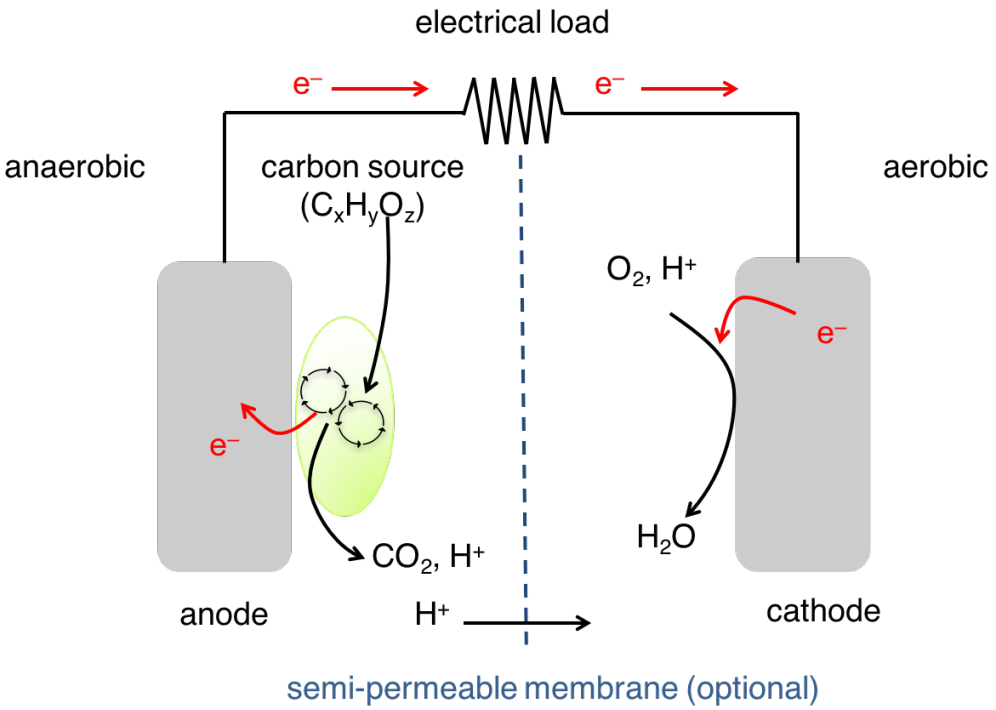

Figure 1.2: Cartoon illustration of the processes occurring in a microbial fuel cell. Microbial oxidation of a carbon source and collection of electrons at the anode, which flow through an external circuit, completed at the cathode where oxygen is reduced to water, thus generating electricity.

strate, releasing protons, electrons, and carbon-based by-products. Through the mechanisms illustrated in Figure 1.1, these electrons are donated to the anode. Electrons then flow through an external circuit across an electrical load to the cathode where oxygen is reduced to water, thus completing the circuit and generating electricity.

A variety of approaches have been examined to improve the transfer of electron equivalents in non-natively exoelectrogenic microorganisms with the purpose of improving current generation in MFCs. For example, exogenous redox mediators, such as methylene blue and neutral red, have shown to promote the ability of mediated charge transfer in weakly exoelectrogenic microorganisms, i.e. *Escherichia coli*. [33–37] However, these mediators often have undesirable features such as cellular uptake not favoring electron transfer, incompatible redox properties and possible diffusion limited kinetics. Other approaches have included bioengineering the charge-transport conduit of a model exoelectrogenic microbe, i.e. *Shewanella oneidensis* into the cell membrane of *E. coli*. [38, 39] Synthetic materials aimed at modifying electrode surfaces for better microbial attachment [40], greater surface area [41] or synthetic scaffolds [42] have been utilized to increase performance. [43] Additionally, microbes have been modified with redox active polymers [44, 45], nanoparticles [46] and carbon nanotubes [47] in order to increase their transmembrane electrical and ionic conductance. Lastly, membrane-intercalating, π-delocalized conjugated oligoelectrolytes (COEs) have been demonstrated to improve bioelectronic communication between microorganisms and electrode surfaces without acting as conventional redox shuttles. [1] The effects of COEs on bacterial membranes in relation to their mechanism for improved performance in *E. coli* MFCs is the

subject of discussion for this dissertation. These molecules have been applied to a wide range of bioelectrochemical systems as well as various microorganisms, which provide additional perspective on the potential mechanism(s) of action and are described in detail below.

1.2 Summary of conjugated oligoelectrolytes

The structures of COEs used in this contribution are distinguished by ionic functionalities tethered at the two terminal ends of a phenylenevinylene sequence, shown in Figure 1.3. Previously, COEs have been utilized to reduce charge-injection/extraction barriers as metal/organic thin-film organic-electronic devices. [48] These bolaamphiphilic structures have been shown to spontaneously intercalate into lipid bilayers with a concomitant increase in fluorescence quantum yield. [49] Polarized confocal microscopy has been used to demonstrate a preferential alignment of the COEs molecular long axis relative to the membrane plane. They have been implicated in boosting the performance of a variety of microbial electronic devices [1, 43] employing organisms ranging from non-exoelectrogenic yeast [49], to *E. coli* [50, 51] and exoelectrogenic *Shewanella oneidensis*, [52, 53] and even naturally occurring microorganisms in wastewater. [54] The most widely applied

COE used in such bioelectrochemical systems has been 1,4-bis(4'-(N,N-bis(6-(N,N,N-trimethylammonium)hexyl)amino)-styryl)stilbene tetraiodide, referred to as DSSN+. A major reason DSSN+ has been so widely used is because of its relative biocompatibility, with a minimum inhibitory concentration to growth of 256 μM in *E. coli*. [51, 55–57]

Previous studies have indicated that COEs not only increase current generation in *E. coli* MFCs but they also decrease the internal resistance, contributing to an overall increase in power production. [51] Additionally, model membrane studies have shown that COEs increase ion conductance across the membrane. [58] To add to mechanistic complexity, recent results suggest that COEs may interact with other components in the cell envelope, such as lipopolysaccharides and cholic acid. [59–61] Some of these results will be discussed in Chapter 2. The degree to which such processes dominate bioelectrochemical changes, relative to electron transfer mechanisms, is not entirely known. Regardless, it is generally acknowledged that the COEs ability to intercalate into microbial membranes is paramount for increasing charge transfer in bioelectrochemical systems. This was demonstrated due to the inability of anionic COEs to stain *E. coli* and improve MFC performance. [61]

The mechanism by which COEs improve MFC performance is the underlying motivation for this body of work and has led to tangental discoveries. For exam-

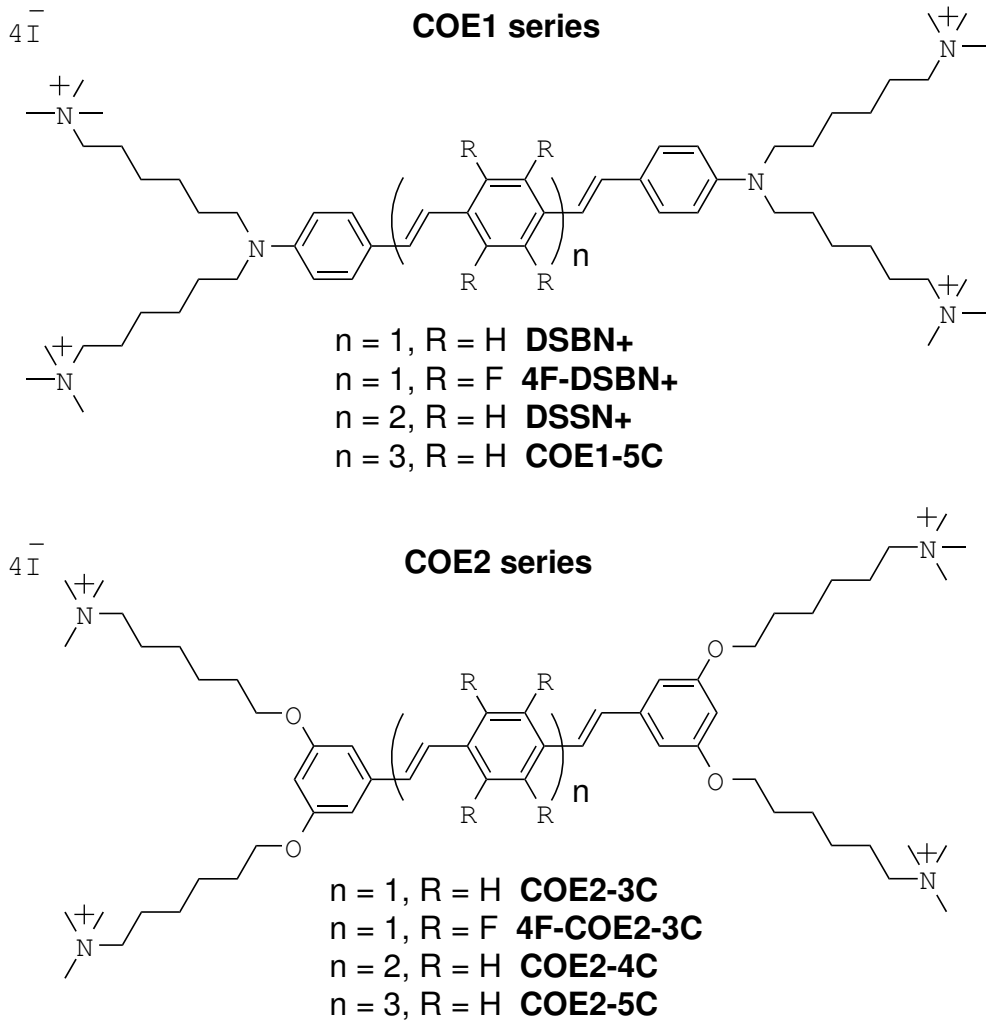

Figure 1.3: Chemical structures of COEs used in these studies.

ple, the inability of anionic COEs to intercalate into *E. coli* suggests electrostatic interactions govern intercalation and that additional cell surface components play a role in COE-cell interactions. Thus motivating the investigation of COE's ability to tune cell surface properties in Chapter 2. Discussion of the potential mechanisms of action COEs may take for increased charge transfer follows below.

1.3 Potential mechanisms of COEs in microbial extracellular electron transport

One finds in the literature various possible mechanisms by which COEs modify charge transport between microorganisms and the electrode. Inspired by previous studies on charge tunneling from a metallic electrode to a tethered redox species through similar oligophenylenevinylene (OPV) structures, the molecular structures of COEs were originally designed for molecular wire functionality. [49, 62] This idea proved consistent with cyclic voltammetry (CV) blocking experiments, where transmembrane electron transport across an insulating supported lipid bilayer between a glass carbon electrode and aqueous ferricyanide was facilitated by DSSN+ and DSBN+. [49] Moreover, the oxidation and re-

duction peaks in the ferricyanide system, at ∼0.3 V and ∼0.1 V *vs.* Ag/AgCl, respectively, are below the oxidation potential corresponding to DSSN+ and DSBN+ (∼0.55 V *vs.* Ag/AgCl), suggesting that those COEs are not acting simply like an electron shuttle, but rather they promote direct electron transport across the insulating membrane. The demonstration of this ability, along with the compatible nature of COEs with living organisms, played an important role in motivating the application in bioelectrochemical systems. However, the inherent processes pertaining to electron equivalent motion in living systems are far more complex. Since these mechanisms bear a strong influence on how to determine possible applications, they are discussed in some detail.

1.3.1 Mechanism 1: Facilitation of direct electron transfer

Much of the previous mechanistic work with COEs has utilized *S. oneidensis*. The inherent ability of *S. oneidensis* MR-1 to participate in two key EET processes makes this microorganism an interesting platform for study. The two main proposed EET mechanisms of *S. oneidensis* to an extracellular electron acceptor include: (1) direct electron transfer (DET) via terminal membrane-bound cytochromes MtrC and OmcA [21, 63–69] and/or biosynthesized nanowires [26–28, 70–74] and (2) mediated electron transfer (MET) via secreted flavin-based

molecules that act as electron shuttles. [27, 31, 32, 75–78] These EET processes are distinguishable by their characteristic redox potential ranges of -0.4 V to 0 V *vs.* Ag/AgCl for MET and 0 V to 0.2 V *vs.* Ag/AgCl for DET. Recent mechanistic studies on DSSN+ modification in *S. oneidensis* used this electrochemical identification to suggest that native cytochrome-based DET is enhanced independently of MET. [53] CV and differential pulse voltammetry (DPV) were utilized to demonstrate that the EET increase from DSSN+ addition originated from the cytochrome DET machinery, due to the enhanced catalytic CV traces and a large-amplitude peak increase at E = 0.05 V seen in DPV. Consistent with the improved efficiency of DET over MET due to diffusive losses, coulombic efficiency increased by $\sim$1.7 fold. While elevated MET signals were also observed, they were delayed, and thus argued to be a result of elevated DET.

In a related study, chronoamperometry (CA) of *S. oneidensis* biofilms poised at 0 mV and at 200 mV showed enhanced current generation when measured at 200 mV, while at 0 mV the enhancement was negligible. [79] CV analysis of these devices indicated that DSSN+ introduces a feature at E $>$ 0 mV, that is not related to mediation by flavins and correlating with the rapid increase in current output. However, while Kirchhofer et al [53] postulate that DSSN+ might physically access relative amphiphilic OmcA and MtrC in the *S. oneidensis* MR-1 membrane, effectively increasing the electronic surface areas between

cytochromes and electrode, Wang et al [79] suggest that the DSSN+ EET mechanism does not rely on the outer membrane cytochromes (OMCs). Supporting this idea, CVs of MtrC-OmcA knockout mutants grown at both potentials did not show any current boost in the CV.

In terms of the mechanistic insights attained regarding *S. oneidensis*, it is reasonable that these postulates may not be generally applicable for all microbial species. For example, while DSSN+ is able to improve current and power generation in *E. coli* MFCs, [50, 51] *E. coli* lacks an obvious homologue to cytochrome c or any other outer membrane redox able to undergo DET. [80–83] Additional consideration should be made regarding the specific effects they may have to different bacteria species in terms of the EET mechanism and thus the relevant applications, which will be further discussed subsequently.

1.3.2 Mechanism 2: Enhanced mediated electron transfer via increased membrane permeabilization

In addition to the possible transfer of electrons via DET, possible facilitation of transmembrane movement of ions, substrates and electrochemical shuttles has been considered. COE intercalation was found to facilitate the transmembrane movement of ions across mammalian membrane patches. [58] This ini-

tial study has lead to further investigation on membrane permeabilization via DSSN+ intercalation and its possible role in increased charge transport.

Sivakumar et al. found an increase in flavin concentration in *S. oneidensis* with DSSN+ addition, corresponding to an increase in ferrihydrate reduction. [84] In addition to increased flavin concentration, DSSN+ increased extracellular ATP and G6PDH activity, which was also claimed as a result of membrane permeabilization. These observations led to the proposal that membrane permeabilization could be responsible for the enhanced bioactivity. Wang et al. noted the influence of accumulated flavins on current production, but maintained that the EET mechanism of DSSN+ is independent of flavins. [79] A decrease in charge transfer resistance was also noted in the regime of $E > 0\,mV$, which was attributed to membrane structural rearrangement or a release of intracellular redox active compounds. [79] In Kirchhofer et al's study, an increase in the electrochemical current pertaining to flavins was noted as well, however it did not correlate to the increased coulombic efficiency. [53] No evidence has yet been found to support that the DSSN+ effected upstream flavin biosynthesis, suggesting instead COEs enhance the membrane permeability of redox shuttles such as flavins in *S. oneidensis*. [84]

When DSSN+ was integrated into *E. coli* membranes to induce the reduction of $HAuCl_4$ to form gold nanoparticles, electrochemical experiments by CV

were consistent with the release of electroactive cytosolic components (possibly quinones) to the medium. [85] CV traces indicated a redox process occurring at -270 mV (vs. Ag/AgCl), however it is unclear whether this current correlates to any of the quinones known to *E. coli*. [86–88] It is also worth noting that ultrapure water without any added carbon source was used in performing these experiments, potentially exposing the cells to osmotic shock, as well as inhibiting the metabolic processes that may contribute to EET. It is possible that COEs may enhance the leakage of redox shuttles to facilitate the mediated electron transport in external electron transport process, however certainty is lacking on whether these conditions correlate to the increased performance observed in MFCs.

It should be noted that some of the above mentioned mechanistic studies may have been overly focused on a DSSN+ EET mechanism that may have been exclusively explained by either MET or DET function. However, supporting experimental data may not be comprehensive at this time. For instance, bioreduction of centrifuged cells in metabolically-limited conditions with DSSN+ does not negate the possibility of alternative EET pathways in conditions relevant to device operation. [85] Similarly, the failure of DSSN+ to recover the EET pathway of *S. oneidensis* mutants lacking membrane-bound cytochromes suggests that DSSN+ cannot substitute the evolution-driven Mtr-pathway com-

pletely. [79] It may not necessarily indicate complete absence of enabling DET mechanism. There is, of course, the possibility that COEs modify microbial behavior in ways not presently considered, or that they perturb more than one electron transfer process.

1.3.3 Alternate mechanisms

It is possible that the mechanisms by which COEs influence the charge transfer process in cells are not independent from one another—there can be a combination of effects. Other possibilities where COEs influence charge transfer exist beyond the two mechanisms discussed above. For example, increased cell attachment to electrodes would result in an increased current generation due to increased cells capable of DET on the electrode and/or decreased diffusion time for soluble mediators participating in MET. Previous reports have observed differences in *E. coli* biofilm morphologies after treatment with COEs. [51] Additionally, it was shown that DSSN+ promotes electrode colonization in developing biofilms of *S. oneidensis*, but did not attribute this to the increase in EET. [53] These differences in biofilm morphologies must be kept in mind when using COEs in microorganisms capable of different EET processes.

Another potential mechanism COEs can effect current generation is by alter-

ing metabolic pathways and/or physiology. There has been limited investigation specifically probing COEs effects on metabolism, however studies have made relevant observations. Studies have shown that DSBN+ addition completely inhibits hydrogen gas oxidation by *Geobacter sulfurreducens* and repressed hydrogen uptake and methane production in mixed culture microbial electrolysis cells (MECs), however the specific reason for inhibition is not known. [89, 90] DSBN+ also improved COD removal, indicating that the repression of hydrogen uptake relieved the inhibition on acetate utilization by the presence of H_2, although this effect was not observed in mixed culture MECs. In this case however, adding DSBN+ to MECs did not noticeably improve current generation. In *S. oneidensis* electrochemical cells, DSSN+ increased charge collection 2.2-fold and increased lactate consumption 1.3-fold. During anaerobic respiration, *S. oneidensis* utilizes the Mtr pathway to pass electrons liberated from oxidation of organic electron donors to terminal electron acceptors. Introduction of the Mtr pathway into non-electrogenic organisms, i.e. *E. coli*, has been shown to significantly alter metabolic flux. [91] Additionally, metabolic manipulations have been employed to produce greater currents from a wider range of feedstocks in exoelectrogens. [92] As such, current production is inherent to metabolic activity.

1.4 Objectives and Summary

In summary, previous work has established that COEs can spontaneously intercalate and align within lipid bilayers and boost the electrical performance of a wide range of bioelectrochemical systems. In particular, COEs have been shown to increase current and power production and decrease internal resistance in non-exoelectrogenic *E. coli* MFCs. Yet, the mechanism of improved charge transfer remains incompletely understood. The overall objective of the research presented in this dissertation is to uncover the mode of action by which COEs influence bacterial membranes. A better understanding of their interactions with cells can thus inform the molecular design of future COEs, inform us of the mode of action COEs may take to improve performance of MFCs and uncover potential new areas of application.

We utilize *E. coli* as a model organism for the investigation of COE's mode of action. Though the outward electron transfer from *E. coli* is relatively insignificant in comparison to electrogenic counterparts such as *Geobacter sulfurreducens* or *Shewanella oneidensis* for integration in METs. [93–95]. *E. coli* is an ideal model organism for deciphering the modes of action small molecules take on the cell as all genes, proteins, pathways and molecular interactions have all been extensively studied. [96, 97]

In Chapter 2, we examine the effect COEs have on cell surface properties and quantify their association with *E. coli*. In Chapter 3 we investigate the effect DSSN+ has on the permeabilities of the inner and outer membrane of *E. coli* and discuss this as a possible mode of action. In Chapter 4, we investigate the origin of electrochemical performance improvements in situ with DSSN+ modification in various device configurations. Chapter 5 summarizes our current understanding and provides a future outlook for applications of COEs. Appendix A contains additional electrochemical experimental data.

Chapter 2

Tuning surface properties of *Escherichia coli* with conjugated oligoelectrolytes

Cationic conjugated oligoelectrolytes (COEs) varying in length and structural features are compared with respect to their association with *Escherichia coli* and their effect on cell surface charge as determined by zeta potential measurements. Regardless of structural features, at high staining concentrations COEs with longer molecular dimensions associate less, but neutralize the neg-

[1]The contents of this chapter have substantially appeared in Reference 60: C. Catania, A. W. Thomas, G. C. Bazan, Tuning cell surface charge in *E. coli* with conjugated oligoelectrolytes, *Chemical Science* **2015**, 51 (45), 9294-9297.

ative surface charge of *E. coli* to a greater degree than shorter COEs. In the supplementary information section, we examine the effects of COEs on cell surface hydrophobicity and autoaggregation, finding a similar length dependence where COEs with longer molecular dimensions increase hydrophobicity and aggregation to a greater degree than shorter COEs.

2.1 Introduction

Although the manipulation of microbial cell properties offers the potential for harnessing and tuning the abilities of microorganisms, it remains a significant challenge due to the aqueous environment and overall structural complexity and diversity. [98] Genetic engineering, while effective, is limited to materials the cell itself is capable of producing. Synthetic materials and molecular systems offer possible functionalities that are not encountered in nature. With this in mind, conjugated oligoelectrolytes (COEs) are synthetic molecules generally characterized by 3 – 5 π-conjugated repeat units (RUs) equipped with pendant ionic groups to impart solubility in polar media. COEs are related to conjugated polyelectrolytes used in optoelectronics, [99–102] biosensing [98, 103–105] and bioimaging. [99–102, 106, 107] COEs thus share attractive photophysical properties similar to those of their polymeric analogs, but have much smaller

length scales, on par with biological architectures like proteins [108, 109] and lipid membranes. [49, 56, 110–112] As such, a variety of COEs have found utility in bioimaging [113–119] and biological detection schemes [108, 120–124] of their own.

While the lipid membrane intercalation of COEs is well-documented, other biological interactions of COEs and their consequences have not yet been studied. Previously we showed that an anionic COE analogous to DSSN+ was prevented from incorporating into *E. coli* membranes most likely due to electrostatic repulsion from the innate negative surface charge of the cells. [61] These negative charges occur mostly as ionized carboxyl and phosphate groups that are part of lipopolysaccharide (LPS) macromolecules composing the outer leaflet of most gram-negative bacteria. [125, 126] Thus, electrostatic attraction between cationic COEs and these anionic sugars in the outermost extensions of *E. coli* are reasonable and should allow modulation of the overall surface charge of the cells. [127–129] Furthermore, in studies concerning the effects of COEs on biological systems, COE concentrations are chosen in the low micromolar regime with no consideration given to the total number of cells; the amount of COE that associates with each cell and that which is left in solution remains to be quantified. With this purpose, we compare 8 COEs varying in molecular length and core substitutions for their association with *E. coli* and effect on cell zeta

potential, finding a remarkable length dependence on these properties.

The chemical structures of the COEs used in this study are shown in Figure 1.3; their syntheses have been described in the literature. [49, 51, 130] Their basic structure can be described by 3 – 5 phenylenevinylene repeat units (RUs) flanked on both ends by either an amine (COE1 series) or two meta-positioned alkoxy (COE2 series) linkages carrying trimethylammonium iodide terminated hexyl chains. Tetrafluorine substitution of the center phenylene ring of the 3-RU molecules offers variance of the central hydrophobic core to determine its role, if any, in cell association and cell surface charge.

2.2 Experimental methods

Cell culture

Escherichia coli K-12 (ATCC #10798) was grown aerobically in Luria Broth (10 g L^{-1} bacto tryptone, 5 g L^{-1} yeast extract, 10 g L^{-1} NaCl) overnight at 37°C with shaking.

Cell staining for microscopy

Before staining, *E. coli* was rinsed twice from the growth medium with phosphate buffered saline (PBS) containing the following: 45.7 mM NaCl, 0.9 mM KCl, 3.3 mM Na_2HPO_4 and 0.6 mM KH_2PO_4 at pH 7.4. 0.5 mL of $OD_{600nm} = 0.9$ cells were stained with 10 μM COE for 1 hour in the dark at room temperature before rinsing twice. Samples were then resuspended in 100 μL of PBS and 5 μL were dropped onto a clean glass slide and a cover slip placed on top. Cover slips were sealed with clear nail polish and all samples were imaged within 2 hours.

Confocal microscopy

All images were obtained via laser scanning confocal microscopy using an Olympus FluoView 1000S spectral scanning microscope equipped with a 60×1.30 silicon oil immersion lens. A 405 nm laser was used as the excitation source. For the COE1 series, emission was collected from 480 nm – 580 nm. For the COE2 series, emission was collected from 410 nm – 510 nm. All images were processed using ImageJ.

Cell association experiments

E. coli cells at $OD_{600nm} = 1.0$ were stained in clear 96-well plates (BD Biosciences, San Jose, CA) at 20°C for 1 hour in the dark with shaking. Total volume of each sample was 200 μL and samples were measured in triplicate. After centrifugation of the plate (3500 rpm, 4 minutes), 100 μL of supernatant was transferred to a clean well for UV-Vis absorption with a Tecan M220 Infinite Pro plate reader (Tecan, MŁnnedorf, Switzerland). Absorbance was measured at 420 nm for COE1 series and 380 nm for COE2 series molecules. Control samples with no cells were treated the same and their absorbance values represented the total COE from which the supernatant values were subtracted to give the amount associated with cells.

Zeta potential measurements

Stained, twice-rinsed cells were resuspended in PBS to their original $OD_{600nm} = 1.0$. 100 μL of each sample was diluted into 900 μL PBS for zeta potential measurements on a Malvern Zetasizer Nano ZS (Malvern Instruments, Malvern, U.K.) at 20°C . Data points given are an average of 4 biological replicates with 3 measurements each.

2.3 Results and Discussion

2.3.1 Visualization and quantification of COE association

In order to first visualize how each COE interacts with *E. coli*, we exploited the photoluminescent π-conjugated core of the molecules for fluorescence microscopy. Cells were stained with 10 μM solutions of COE for 1 hour and imaged with a laser scanning confocal microscope, the results of which are shown in Figure 2.1. As anticipated based on the bolaamphiphilic structure shared by the molecules, all COEs display an emission pattern around the edges of cells consistent with membrane intercalation. In this regard, the substitution of alkoxy pendant linkages for amine or the addition of 4 fluorine atoms to the center phenyl ring of the 3-RU COEs provides no discernible difference in terms of observable cell localization in *E. coli*.

Taking advantage of the strong visible light absorbing properties provided by the conjugated core of the molecules, [49] the amount of each COE that associates with *E. coli* in solution was quantified. Briefly, cells (OD_{600nm} = 1.0) were stained in different concentrations of COE ranging from 1 – 40 μM for 1 hour in 50 mM phosphate buffered saline (PBS) solutions. All concentrations of COE used in this study were less than the critical aggregation concentration (CAC)

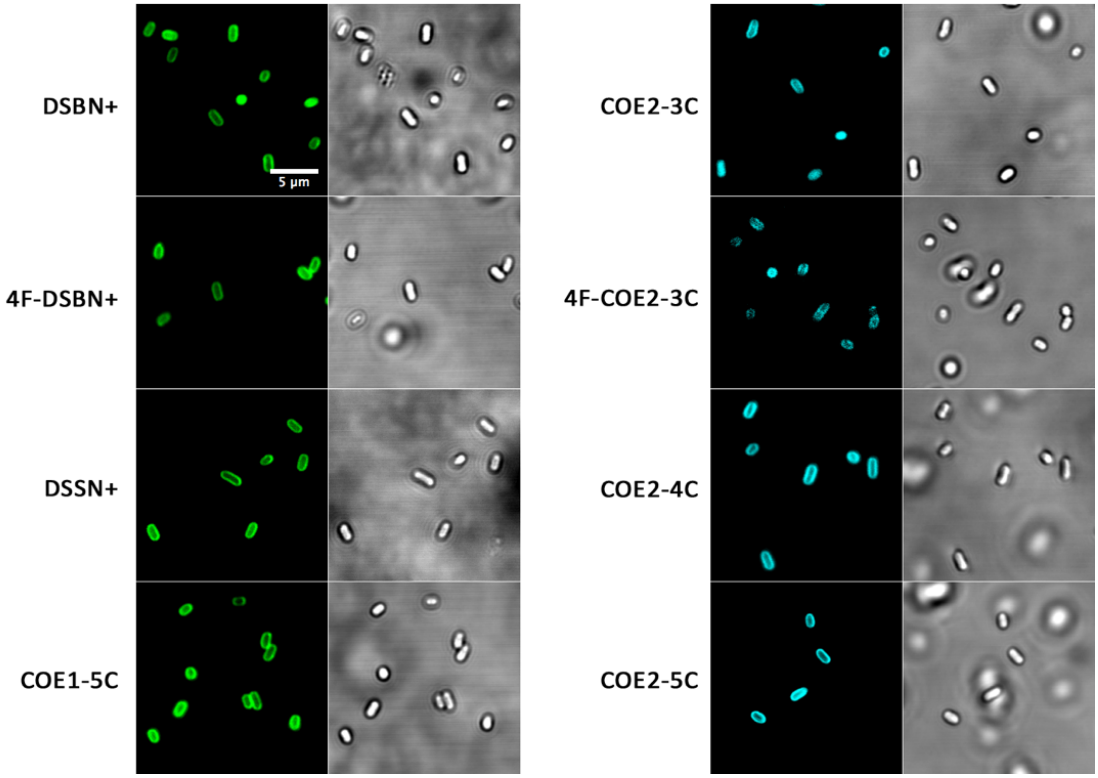

Figure 2.1: Laser scanning confocal micrographs and accompanying brightfield images of *E. coli* stained with 10 μM COE in PBS for 1 hour. Right column is COE1 series (green) and left is COE2 series (blue). Excitation wavelength was 405 nm for all images. 5 μm scale bar is the same for all images.

reported for DSBN+, which is at 0.51 mM. [131] A staining time of 1 hour was found sufficient to establish equilibrium within these experimental conditions (Figure 2.2). The cells were then centrifuged and the supernatant analysed by UV-vis absorption to determine the amount of COE left in solution (i.e. not associated with the pelleted cells). This method is illustrated in Figure 2.3 for 10 μM and 20 μM DSSN+. Comparing the control spectra of the solutions containing just DSSN+ in PBS (solid lines) to the spectra of the supernatants resulting from cell staining, one observes that at 10 μM, no discernable DSSN+ is left in solution, meaning that all COE has associated with the cells. In contrast, at 20 μM a significant absorption is observed indicating that some DSSN+ remains in the solution and did not associate with the *E. coli*.

In subsequent experiments, the amount of COE associated with cells using the UV-vis absorption method was quantified by subtracting the absorbance of the supernatant of stained and centrifuged *E. coli* at a wavelength of 420 nm (COE1 series) or 380 nm (COE2 series) from control samples that did not contain cells. Figure 2.4 shows the trends in COE/cell association for the unfluorinated COEs at different staining concentrations normalized to 1 OD_{600nm} of cells. Interestingly, at concentrations between 1 – 15 μM for all 6 COEs, 100% association is observed resulting in a linear increase in COE association with increasing staining concentration, reaching $\sim$15 nmol/OD_{600nm} associated at 15

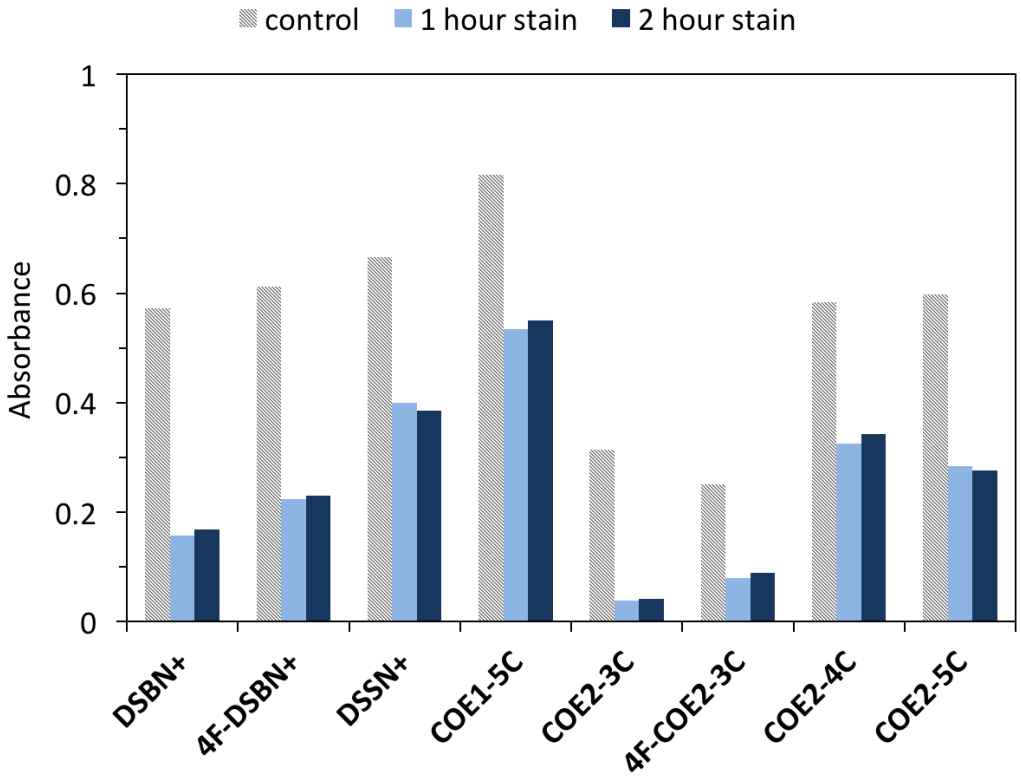

Figure 2.2: In order to demonstrate that the system had reached equilibrium after 1 hour, the supernatant of *E. coli* stained with 40 μM COE for 1 hour (light blue) and 2 hours (dark blue) were analysed by UV-vs absorption at 420 nm (COE1 series) and 380 nm (COE2 series). Note that a lower absorbance in the supernatant indicates less COE left in solution and more associated with cells. Shown in grey are 40 μM COE solutions in PBS (i.e. the amount of COE in solution with no cells present).

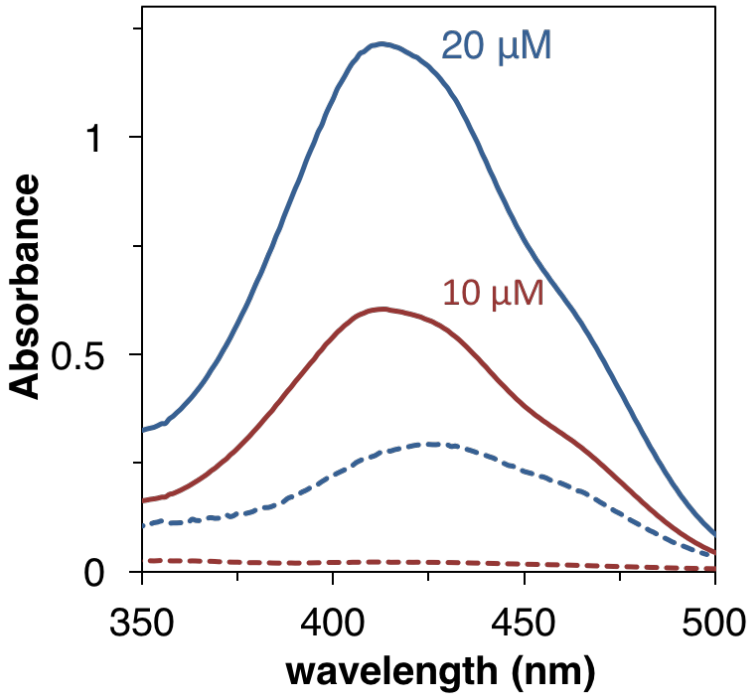

Figure 2.3: UV-vis absorption of 20 μM (blue, solid) and 10 μM (red, solid) DSSN+ in PBS. After staining *E. coli* ($OD_{600nm} = 0.9$) for 1 hour with these concentrations of DSSN+, the cells are centrifuged and the DSSN+ remaining in the supernatant (dashed lines) is measured in order to determine how much COE associates with cells.

μM staining concentration. Looking at the COE1 series in Figure 2.3, at concentrations greater than 15 μM the 4- and 5-RU COEs, DSSN+ and COE1-5C, reach a maximum association of 20 $\pm$ 0.4 nmol/OD_{600nm} and 25 $\pm$ 1.0 nmol/OD_{600nm} respectively. In contrast, the 3-RU COE, DSBN+, does not reach a plateau and attains a maximum association of 34 $\pm$ 0.2 nmol/OD_{600nm} at 40 μM staining concentration. It should be noted that for COEs with minimum inhibitory concentration (MIC) data published (DSBN+ and DSSN+), the MICs (normalized to cell count) required to reduce growth of *E. coli* are 2 orders of magnitude higher than the concentrations used in this study. [55, 56] Moreover, it is pointed out in another study, where cytotoxicity tests on *E. coli* with 20 μM of all COE1 series, that no toxicity phenomena is observed in colony forming units (CFUs). [51]

A similar trend is observed for the COE2 series in Figure 2.4b with maximum associations of 37 $\pm$ 2.4 , 18 $\pm$ 0.5, 20 $\pm$ 1.1 nmol/OD_{600nm} for the 3-, 4- and 5- RU COEs, respectively. When comparing the two series of COEs, the 3-RU COE2 series shows slightly greater maximum association than the 3-RU COE1 series DSBN+, suggesting that the structural modification afforded by the alkoxy pendant linkages provide a modest advantage in this respect. However, the comparison between the 4- and 5-RU COEs shows a slightly higher maximum association in the COE1 series than the COE2 series. Interestingly, previous cytotoxicity tests on *E. coli* with 20 μM of all COE2 series showed no toxicity

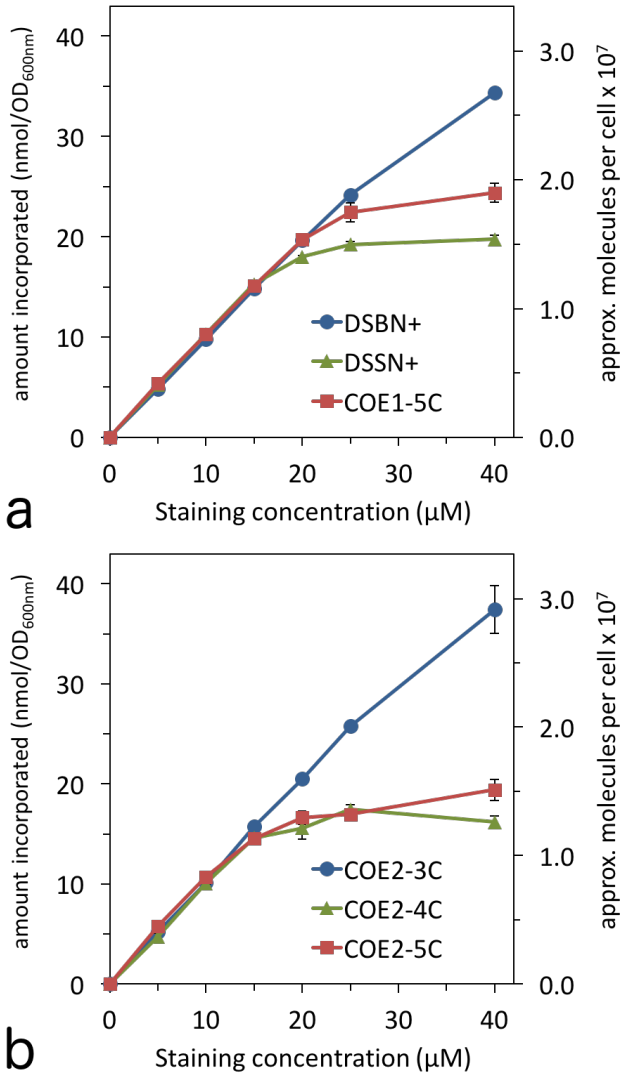

Figure 2.4: COE associated with *E. coli* cells as a function of staining concentration for (a) COE1 series and (b) COE2 series molecules. The amount of COE associated was calculated by subtracting the absorbance at 420 nm (COE1) or 380 nm (COE2) of the supernatant after centrifugation from that of a control staining solution with no cells. Approximate number of cells assuming 1 $OD_{600nm} = 10^9$ cells mL^{-1}.

for COE2-3C, while COE2-4C and COE2-5C have demonstrated a $\sim$30$\%$ loss in CFUs than controls. [51] Regardless of series type, there is a clear dependence of COE association with *E. coli* on molecular length: the amount able to associate with cells for the 4-RU and 5-RU COEs plateaus within the concentration range tested, while the 3-RU COEs do not.

On the secondary y-axes in Figure 2.4 are the estimated number of COE molecules associated per cell at each staining concentration, with 1 OD_{600nm} corresponding to a concentration of 10^9 cells per mL. [132] With this estimate, it can be seen that maximum COE associations observed in these experiments are greater than 10^7 molecules per cell for 4- and 5-RU COEs and greater than 2 $\times$ 10^7 for both 3-RU COEs. When comparing these numbers to an estimate of the number of lipids per *E. coli* cell of $\sim$2.2 $\times$ 10^7 [97] one can see that the 4- and 5-RU COEs would approach a 1:1 lipid:COE ratio in cells and the 3-RU COEs surpass this threshold at the 40 μM staining concentration. As discussed in the introduction, much evidence has been presented that COEs intercalate into microbial membranes, and up until this point, this has been the only interaction considered. With ratios at or above 1:1 lipid:COE per cell, which would be morphologically impossible, it is obvious that not all of the associated COE is intercalating into lipid bilayers. A plausible hypothesis is that some COE is associating with the outside of the *E. coli*, which, with its net negative charge

[133], is a likely candidate for electrostatic interaction with positively charged molecules. [129, 134, 135]

2.3.2 Zeta potential measurements

In order to determine the effect of COE association on cell surface charge, stained *E. coli* cells from the previous experiment were washed and resuspended in PBS buffer for zeta potential measurements [133], the results of which are shown in Figure 2.5. Unstained cells were found to have an average zeta potential of about -16 mV under these conditions, indicating a net negative charge, as expected. [134] The cells stained with COE1 series follow a trend of increasing zeta potential to more positive values as the staining concentration increases. Maximum zeta potential values of -13.1 $\pm$ 0.4, -7.8 $\pm$ 1.1, and -2.4 $\pm$ 0.4 mV are reached for the 3-, 4-, and 5-RU COEs, respectively, trending more positive with increasing molecular length. In addition, zeta potential values reflect the association trends observed in Figure 2.4a, in that the 4- and 5-RU COEs reach a plateau at a staining concentration around the same concentration that the cell association for these COEs plateaus. Despite having the highest maximum cell association of the COE1 series, the 3-RU COE causes the least change in zeta potential but reflects the association trend in Figure 2.4a in that the zeta potential

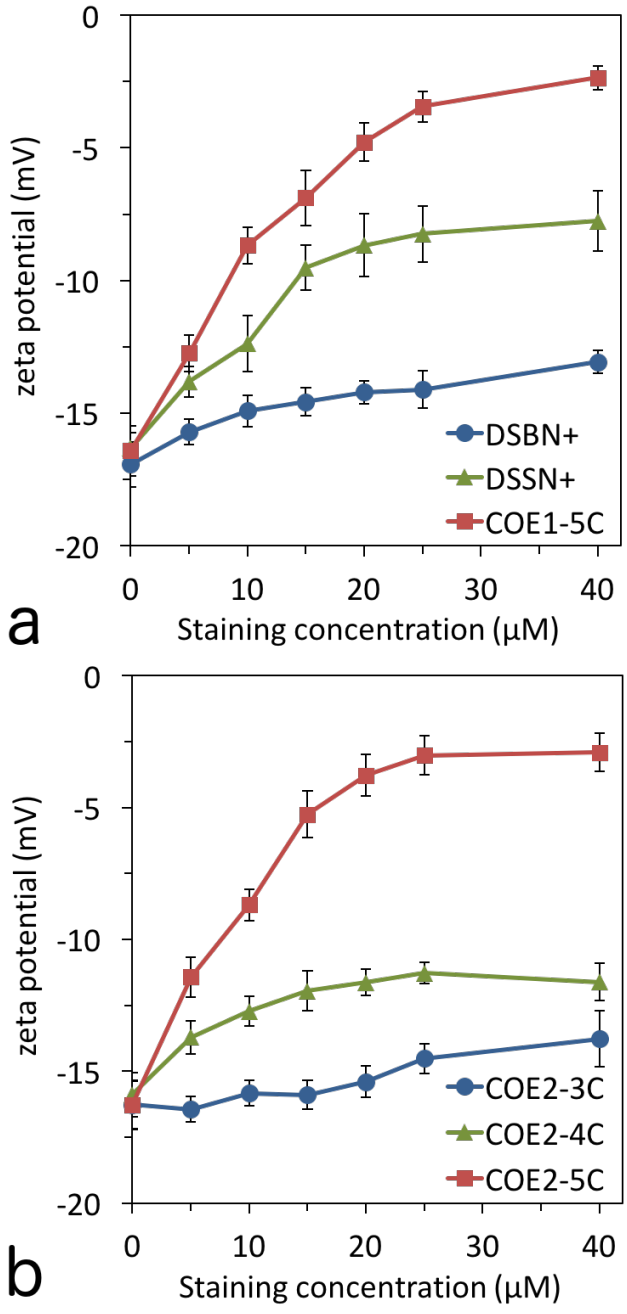

Figure 2.5: Zeta potential measurements of *E. coli* cells as a function of COE staining concentration for (a) COE1 series and (b) COE2 series. Dashed line represents the zeta potential of unstained *E. coli*.

does not appear to plateau in the concentration range tested.

The effect on *E. coli* zeta potential of the COE2 series is shown in Figure 2.5b. The COE2 series displays a similar length dependence with maximum zeta potential values for E. coli of -13.8 $\pm$ 1.1, -11.3 $\pm$ 0.6, and -2.9 $\pm$ 0.7, observed for COE2-3C, COE2-4C and COE2-5C, respectively. Cells stained by the 3- and 4-RU COE2 molecules display noticeably less positive zeta potential values than their COE1 counterparts but ultimately a similar trend follows in that cells stained by longer COEs result in more positive zeta potential values. Ultimately the change from amine to alkoxy linked pendant groups has only a minor influence on the COE zeta potential effects as a whole.

Rather than observing charge reversal towards high positive values as is seen with cells being coated with positively charged polyelectrolytes [127, 128, 134], the trend towards charge neutralization in this experiment suggests that not many of the COE positive charges are extending beyond the LPS. COEs are much smaller in size than polyelectrolytes and easily intercalate into lipid membranes and perhaps also interdigitate with the oligomeric sugars that form the core of LPS rather than coating the outside cells. In fact, this non-lipid portion of LPS in *E. coli* K12 is estimated to be $\sim$2.1 nm in length. [136, 137] This length is slightly longer than the 3-RU phenylenevinylene core and slightly shorter than the 4-RU conjugated core, which are estimated to be 1.8 nm and 2.4 nm re-

spectively. With the 5-RU core estimated to be around 3 nm, one can begin to rationalize the length scales with the zeta potential results. More specifically, the 4- and 5-RU COEs have a greater chance of spanning the full length or even extending past the outermost LPS units than do the 3-RU COEs, possibly explaining the molecular length dependence of the zeta potential results.

2.3.3 Fluorinated derivatives

Lastly, cell association and zeta potential experiments were carried out with the fluorine-substituted 3-RU COEs (4FCOEs), the results of which are plotted with the unsubstituted counterparts for comparison and are shown in Figure 2.6. Cell association for the 4FCOEs (Figure a) is largely indistinguishable from their unsubstituted counterparts until staining concentrations of ∼25–40 μM, at which point the 4FCOEs associate slightly less. At the highest staining concentration tested (40 μM), there were approximately 2.0 ($\pm$0.06) $\times$ 10^7 and 2.4 ($\pm$ 0.02) $\times$ 10^7 molecules associated per cell for 4F-DSBN+ and 4F-COE2-3C, respectively. These values are 23% and 15% less than for DSBN+ and COE2-3C, respectively. A possible explanation for this deviation at higher staining concentrations is the polar-hydrophobic nature of fluorinated compounds [138], making these molecules less likely to aggregate in the lipid membrane

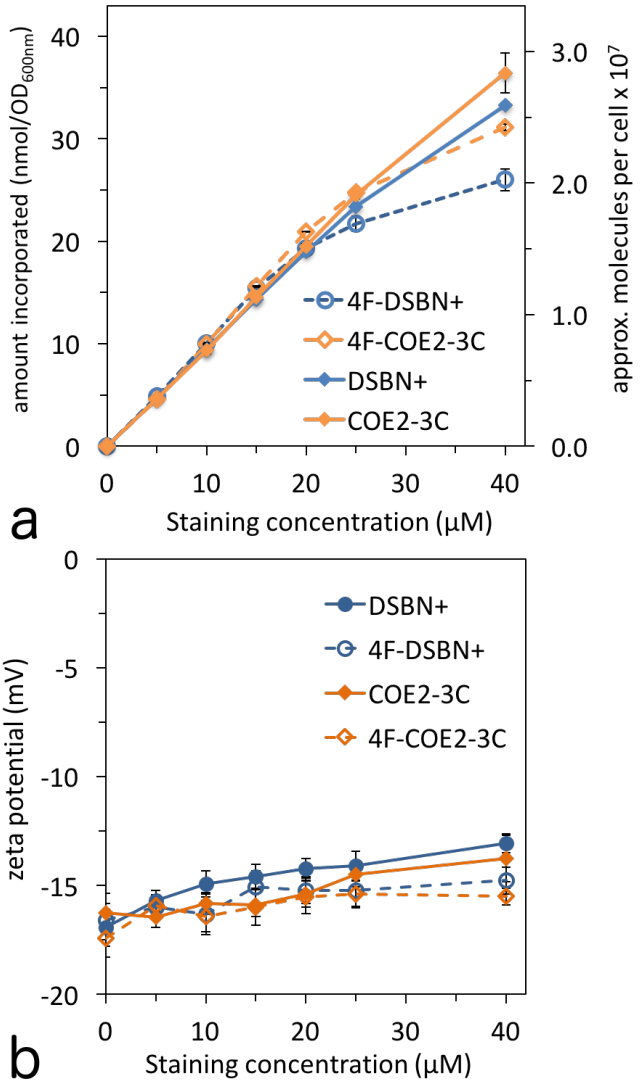

Figure 2.6: Comparison of 3-ring COEs with and without fluorine substitution. (a) COE associated with *E. coli* as a function of staining concentration. Approximate number of cells assuming $1\,\mathrm{OD}_{600nm} = 10^6$ cells per mL. (b) Zetal potential measurements of stained *E. coli* as a function of COE staining concentration. Black dashed line represents the zeta potential of unstained *E. coli*

due to interactions between the cationic pendant groups and the fluorinated core.[56] Being less likely to aggregate or pack closely would result in less overall cell association. It is worth noting, however, that aggregation of COEs in a lipid membrane has yet to be experimentally proven.

The zeta potential of *E. coli* stained with the 4FCOEs (Figure 2.6b) follows the same trend as the unfluorinated COEs, in that a gradual increase in zeta potential is observed as staining concentration increases. Cells stained with 4F-DSBN+ reach a more positive maximum (-14.8 $\pm$ 0.6 mV) than those stained with 4F- COE2-3C (-15.4 $\pm$ 0.6 mV), with both maxima being slightly less positive than the corresponding unfluorinated COEs at -13.1 $\pm$ 0.4 mV and -13.8 $\pm$ 1.1 mV, respectively. Ultimately, fluorine substitution of the center ring of 3-RU COEs has minimal influence on cell association and zeta potential of stained *E. coli*.

2.4 Conclusions

In conclusion, 8 COEs varying in length and substitutions to the aromatic core have been compared in terms of their association with *E. coli* and their effect on cell zeta potential. Confocal microscopy showed patterns consistent with lipid membrane association for all COEs. At low staining concentrations

($<$20 μM) nearly 100% of COE in solution associates with cells, leaving none remaining in the supernatant of centrifuged samples. At higher concentrations, 3-RU COEs continue to associate while 4- and 5-RU COEs plateau, reaching a maximum association that cannot be overcome by adding more COE to the staining solution. The 3-RU COEs associate past a 1:1 lipid:COE ratio while the 4- and 5-RU COEs approach it, which is morphologically impossible and indicative of cellular association not exclusive to membrane intercalation. Cells stained with COEs generally showed more positive zeta potential values with increasing staining concentration, indicating a neutralization of anionic charges of the LPS by the cationic charges of the COEs. Additionally, more positive zeta potential values were observed for longer COEs suggesting that they are able to extend beyond the negatively charged molecular constructs of the *E. coli* LPS. The other structural variations presented here, namely amine vs. alkoxy pendant linkages and fluorination of the aromatic core, proved less important than molecular length, as they had minimal effects on cell association and zeta potential, when compared to analogues with the same number of repeat units. These changes alter the photophysical properties of the molecules and thus increase the number of COEs available for applications in bioimaging[114, 115, 139–141] and optoelectronics. [142, 143] Most importantly, that the zeta potential of bacteria can be tuned by COE length and concentration has implications for technolo-

gies such as microbial electronics, wastewater treatment, and others that rely on bacterial aggregation, adhesion and biofilm formation.[144–150]

2.5 Supplementary Information

The ability to synthetically manipulate cell surface charge has profound implications for technologies such as microbial electronics, wastewater remediation and others that rely on bacterial aggregation and adhesion to surfaces. [144–150] Electrostatic and hydrophobic forces are generally recognized as being important for bacterial adhesion. Bacterial adhesion is often described as a two step event, i.e. reversible adhesion due to long-range forces and irreversible adhesion due to short-range interactions that promote direct contact, such as hydrophobic interactions and chemical bonds. [146, 151, 152] While experimental studies have shown the importance of the electric double layer in bacterial adhesion, they have also revealed discrepancies between theoretical expectations and observation. [145] Other physico-chemical properties correlate with adhesion include cell surface hydrophobicity and aggregation ability. Therefore to further characterize the effect COEs have on cell surface properties relevant to bacterial adhesion, we compare COE structures for their effects on overall hydrophobicity and autoaggregation and find a similar length depen-

dence on these properties.

2.5.1 Experimental methods

Measurements of cell surface hydrophobicity

The surface hydrophobicity of unstained and stained cells was determined using microbial adherence to hydrocarbons (MATH) using hexadecane as the adsorption solvent. [153] Cells grown overnight were washed and resuspended in 50 mM PBS to an OD_{600nm}~1.6. 1.5 mL of cells were stained with 1.5 mL of 2× the target concentration of COEs (2× 5, 10, 15, 20, 25 and 40 μM) in PBS and allowed to equilibrate at room temperature for 15 min. 1 mL of hexadecane was added to test tubes containing the cell solution, vigorously shaken by vortex for 2 min, and then left at room temperature for 30 min to allow for phase separation. After phase separation, optical density of the PBS phase was measured using a HACH DR2800 spectrophotometer at 600 nm. The results were expressed as the percentage from 3 replicates according to the formula $MATH\%$=1 – (OD /OD_{t0}) × 100, where OD_{t0} and OD are the optical densities at 600 nm before and after mixing with hexadecane, respectively.

Autoaggregation assay

Bacteria were grown overnight as described previously. Cells were then harvested by centrifugation, washed twice with 50 mM PBS and resuspended to a final OD_{600nm} of 0.98 when diluted in half. 500 μL bacterial suspension was placed in cuvettes with 500 μL of 2$\times$ the target COE concentration (2$\times$ 5, 10, 15, 20, 25 and 40 μM). Cells were incubated at room temperature for 5 hours and OD_{600nm} was measured every hour. Aggregation was expressed as a percentage of the total cell population using the formula 1 – (OD_t /OD_{t0}) $\times$ 100.

2.5.2 Cell surface hydrophobicity

In addition to surface charge, bacterial cell surface hydrophobicity is an important factor in bacterial adhesion. [154] It had been found that increased cell surface hydrophobicity would favor cell adhesion on both hydrophilic and hydrophobic surfaces. [147]*E. coli* is reported to be hydrophilic in nature [154, 155], but specific surface structures crucial for biofilm formation impart local hydrophobicity. [152] Some studies correlate adhesion to cell surface charge [156], but in most instances overall hydrophobicity has the strongest correlation. [147, 148] Here, we determined the overall hydrophobicity of *E. coli* modified with varying concentrations of COEs using microbial adherence to

hydrocarbons (MATH). [153, 157] Bacteria were grown overnight and stained with 0, 5, 10, 15, 20, 25 or 40 μM of the 3-, 4-, or 5-RU COE1 series. After staining equilibration, cells were mixed with hexadecane. Binding affinity to hexadecane was quantified as the change in OD_{600nm} after phase separation of hexadecane from the cell buffer solution.

Figure 2.7 plots the percent increase in affinity to hexadecane versus staining concentration of DSBN, DSSN and COE1-5C. Results show a similar trend as with zeta potential measurements, where longer molecular length COEs increase the hydrophobicity to a greater extent than shorter COEs. Additionally, the cells affinity to hexadecane plateaus around 25 μM staining concentration. The concentration where hydrophobicity plateaus is slightly greater than the association staining concentration plateau. This may indicate that at relatively higher concentrations, COEs may be disrupting some of the cell surface features that impart hydrophilicity, such as LPS. Future work is needed for the determination of specific interactions COEs may have with membrane components.

2.5.3 Autoaggregation

Cell aggregation, or autoaggregation, is a process of cell-to-cell immobilization that is inherently related to cell surface hydrophobicity. [147] In many

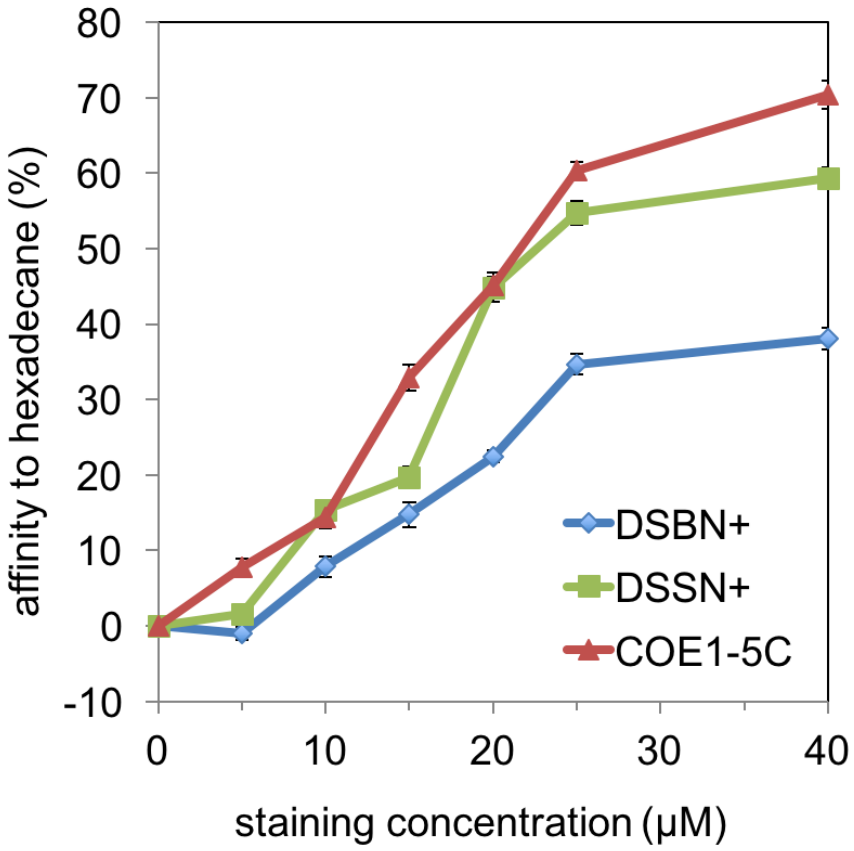

Figure 2.7: Affinity of COE-modified *E. coli* to hexadecane at various staining concentrations. Error bars show standard deviations of triplicate measurements.

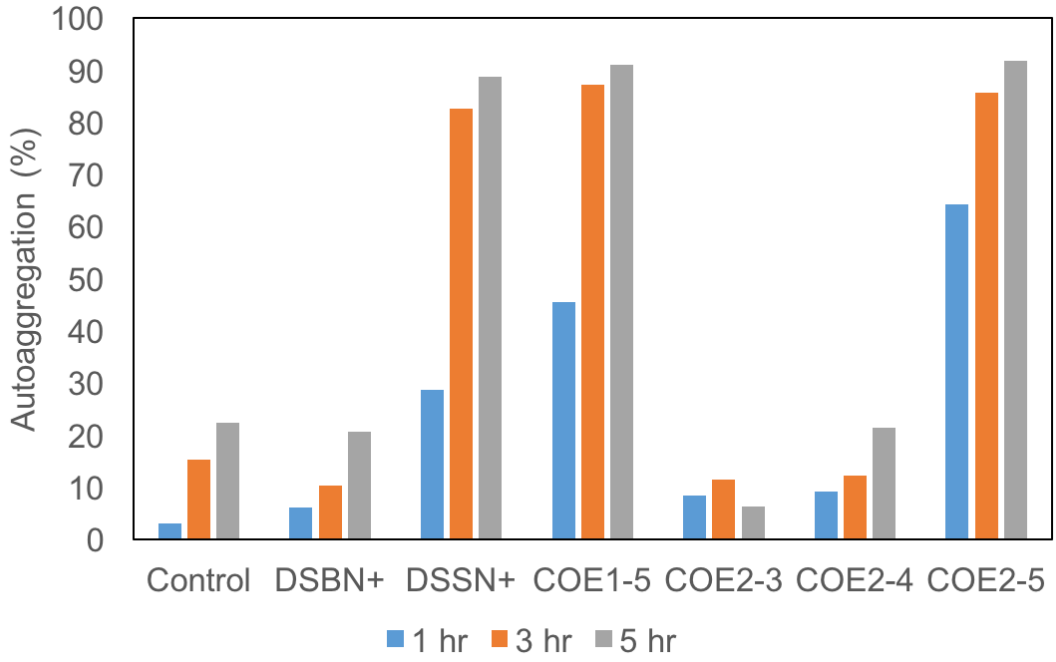

Figure 2.8: Autoaggregation of untreated *E. coli* (Control) and *E. coli* stained with 10 μM COE after 1 (blue), 3 (orange), and 5 (gray) hours.

cases, aggregation ability is related to cell adherence properties. To further characterize the effects of COEs on surface properties, autoaggregation of *E. coli* modified with varying structures of COEs was examined. Figure 2.8 shows autoaggregation of cells stained with 10 μM COE over time, where percent autoaggregation is calculated as the change in OD_{600nm} with COE treatment compared to initial. The trend in autoaggregation follows zeta potential measurements, where cells treated with COEs with longer molecular length aggregate more than shorter COEs.

Chapter 3

Permeability effects of conjugated oligoelectrolytes on *Escherichia coli*

One possible mode of action COEs may use to improve bioelectrochemical performance is by permeabilization of the cell envelope. In this chapter, we examined the effect of the tetracationic conjugated oligoelectrolyte, DSSN+, on the permeability of the inner and outer membrane of *Escherichia coli* by detecting extracellular activity of normally periplasmic and cytoplasmic enzymes. DSSN+ increases the release of the periplasmic enzyme alkaline phosphatase (ALP) up to 20-fold, but does not significantly change the release of the cyto-

[1]The contents of this chapter have substantially appeared in Reference 158 C. Catania, C. M. Ajo-Franklin, and G. C. Bazan, Membrane Permeabilization by Conjugate Oligoelectrolytes Accelerates Whole-Cell Catalysis, *RSC Advances*, **2016**, 6 (102), 100300-100306.

plasmic enzyme β-galactosidase. Additionally, DSSN+ caused a 2-fold increase in the turnover of a cytoplasmic substrate. These studies present a more complete understanding of the mechanism of action in bioelectrochemical systems and pivot future applications of COEs towards a method for improving whole-cell catalysis.

3.1 Introduction

The cell envelope acts as a protective barrier that limits the transport of ions, non-natural sugars and redox-active molecules in the cell. [97, 159, 160] In gram-negative bacteria, the envelope is comprised of an outer membrane (OM), a peptidoglycan layer and an inner membrane (IM). [126, 161–163] The common structural component to each is the lipid bilayer, which is electrically insulating and impermeable to most ions and polar molecules. In the OM, lipopolysaccharides provide a barrier to hydrophobic and most hydrophilic molecules. Small hydrophilic compounds ($<$600 Da) rely on passive diffusion through OM porins, while large hydrophilic molecules typically require specific protein-based transport mechanisms. [126, 159–164] In contrast, transport of hydrophobic molecules through the IM is relatively facile, while the transport of hydrophilic molecules typically requires specific membrane transport proteins.

[97] For reactants that do not have a natural uptake system, e.g. non-natural sugars, passive diffusion through the lipopolysaccharide layer is the only mechanism of transport. [159, 160]

The inherent barrier function of the OM can be a limitation in whole-cell bioprocesses such as bioelectrochemistry, biocatalysis, fermentation and bioremediation.[3, 165, 166] In an ideal process, uptake of substrates into the cell would not slow the rate of product formation. In practice, however, whole-cell catalyzed reactions are generally one to two orders of magnitude slower than catalysis by isolated enzymes. [167–171] Chemical and physical methods have been developed to increase membrane permeability and accelerate reaction rates despite possible complications in downstream processing, added processing steps, and excessive membrane damage or lysis. [165, 172–174] While genetic modifications can also improve permeability, they are often more effective at enhancing transport across the IM than the OM and are complicated to implement alongside other genetic modifications, such as enzyme overexpression. [175–179] Thus, there is a paucity of well-characterized, one-step methods for altering membrane permeability that do not introduce additional limitations.

Given the importance of membrane permeabilization on bioprocesses, a better understanding of how COEs alter membranes would open opportunities beyond bioelectrochemical applications. Here, we address possible impacts on

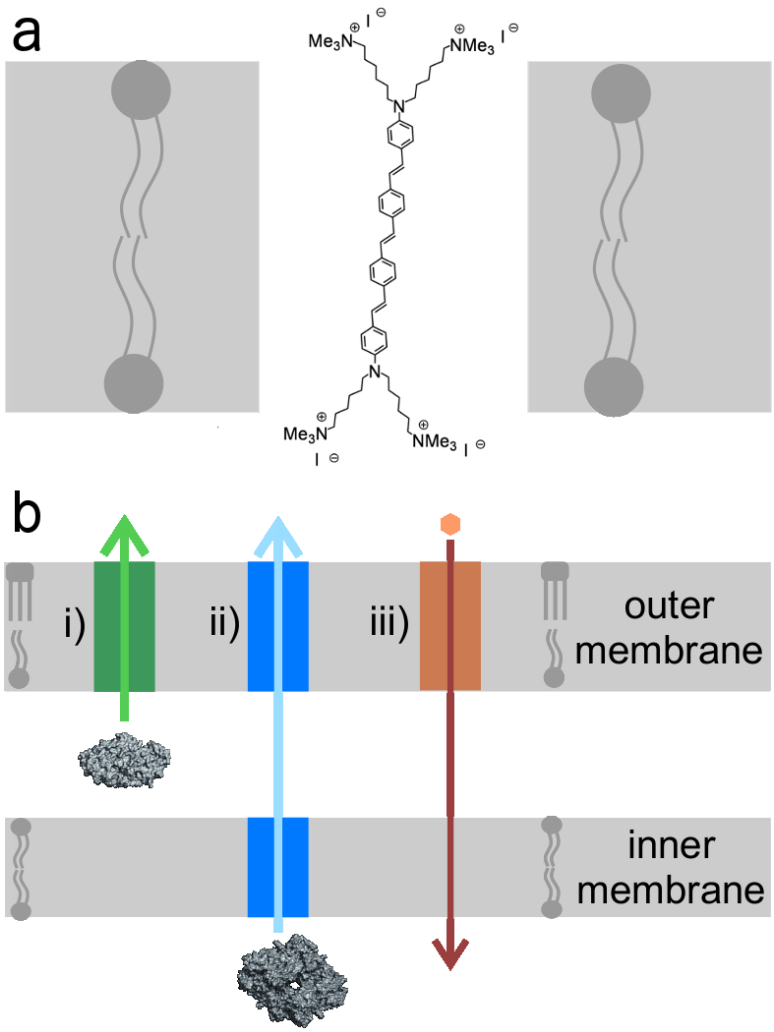

Figure 3.1: Schematic illustration depicting DSSN+ situated in the lipid bilayer (a) and the scenarios tested in this study (b). DSSN+ intercalation in the membrane may either: (i) permeabilize the OM to allow the release of periplasmic enzymes, (ii) permeabilize the IM to release cytosolic enzymes, and/or (iii) increase the rate of catalysis by intracellular enzymes by increasing the rate of transport of substrate across the cell envelope.

membrane permeabilization and whole cell catalysis by using the approach illustrated in Figure 3.1. Specifically, we examine changes in the OM and IM permeability of *E. coli* upon exposure by detecting extracellular enzymatic activity of normally periplasmic (i) and cytosolic (ii) enzymes. We find that the permeability of the OM is significantly affected by DSSN+ (scenario (i)) as indicated by extracellular enzyme activity, while we do not yet find evidence for perturbation of the IM (scenario (ii)). Furthermore, by monitoring turnover of the substrate utilized by a cytosolic enzyme (scenario (iii)), we demonstrate DSSN+ increases whole-cell biocatalysis.

3.2 Experimental Methods

Cell culture

Escherichia coli (ATTC #10798, ATCC, VA) was cultured aerobically overnight from a frozen stock by growth in Luria Broth (10 g L^{-1} bacto tryptone, 5 g L^{-1} yeast extract, 10 g L^{-1} NaCl) at 37°C with shaking. For cells cultured for β-galactosidase activity assays, Luria Broth was supplemented with 2% lactose for induction of *lacZ*. Cells were washed three times by centrifugation in M9 minimal media (6.8 g L^{-1} Na_2HPO_4, 3 g L^{-1} KH_2PO_4, 1 g L^{-1} NH_4Cl,

0.5 g L^{-1} NaCl) before use in assays.

Assay of outer membrane permeability

Cell suspensions were resuspended to a final OD_{600nm} = 1.0 in M9, stained with varying amounts of 1 mM DSSN+ in ultrapure water to achieve final concentrations of 0, 5, 10, 15 and 25 μM, and then incubated at room temperature for 1, 4 and 10 hours. Samples were removed at each time point and filtered using a 0.2 μm filter. Non-fluorescent 4-methylumbelliferyl phosphate disodium salt (MUP) from an alkaline phosphatase activity assay kit (Biovision, K422-500) was used to measure the activity of extracellular ALP. Filtered samples were incubated with 80 μM MUP at 25°C in a 96-well plate while monitoring fluorescence (Ex/Em = 360nm/440nm) over 90 min using a Spectra Max Plus 384 microplate spectrophotometer. Filtrates samples without MUP added were measured for background correction. All samples were measured in triplicate.

Assay of inner membrane permeability

Cell suspensions were resuspended to a final OD_{600nm} = 0.6 in M9, stained with varying concentrations of DSSN+ (0, 5, 10, 15 and 25 μM) and then incubated at room temperature for 5 hours. The permeability of the inner mem-

brane of *E. coli* K-12 was determined by measuring the release of β-galactosidase activity into the medium. Cell suspensions were filtered, and the resulting filtrates were incubated with 1.3 mM 2-nitrophenyl β-D-galactopyranoside (ONPG, Sigma Aldrich) at 37°C for 2 hours in a 96-well plate while monitoring the absorbance at 420 nm using a Spectra Max Absorbance plate reader. All samples were measured in triplicate.

Calibration against cell lysate

For both permeability assays, activities were compared against the activity of lysed cell suspensions. Cell suspensions of the same OD_{600nm} and same culture conditions used in the comparative assays were lysed via probe sonication in an ice bath. Complete lysis was confirmed by measuring OD_{600nm} to be equal to 0. Lysates were then serially diluted in M9 in ratios of 1:2, 1:4, 1:8, 1:16, 1:32 and 1:64 to produce solutions of 50, 25, 12.5, 6.1, 3 and 1.5$\%$ cell lysate. These solutions were then tested following the respective assay procedures. The cell lysate activities for ALP and β-galactosidase are shown in Figure 3.2 and 3.3, respectively. Specifically, to generate an ALP activity calibration curve, we calculated the average rate of fluorescence change using the slopes of plots containing fluorescence intensity *vs.* time. The resulting rates were linearly related to the amount of cell lysate in order to generate a calibration curve to deter-

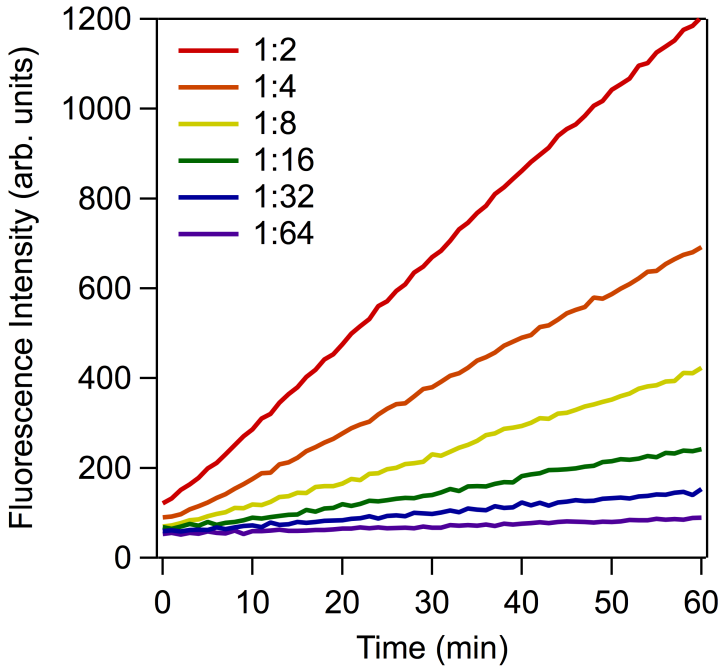

Figure 3.2: ALP activity of cell lysates dilutions (1:2, 1:4, 1:8, 1:16, 1:32, 1:64) determined by fluorescence intensity of 4-MU measured at 440 nm over time. All measurements are an average of triplicates.

mine the relative degree of cell lysis of samples. The linear trend is plotted in Figure 3.4. The same calculations were performed for β-galactosidase activity in cell lysates using the rate of absorbance change *vs.* time from the linear region.

Whole-cell ONPG turnover assay

Cell suspensions were resuspended to an $OD_{600nm} = 0.6$ in M9, stained with varying concentrations of DSSN+ (0, 5, 10, 15 and 25 μM) for 30 minutes to

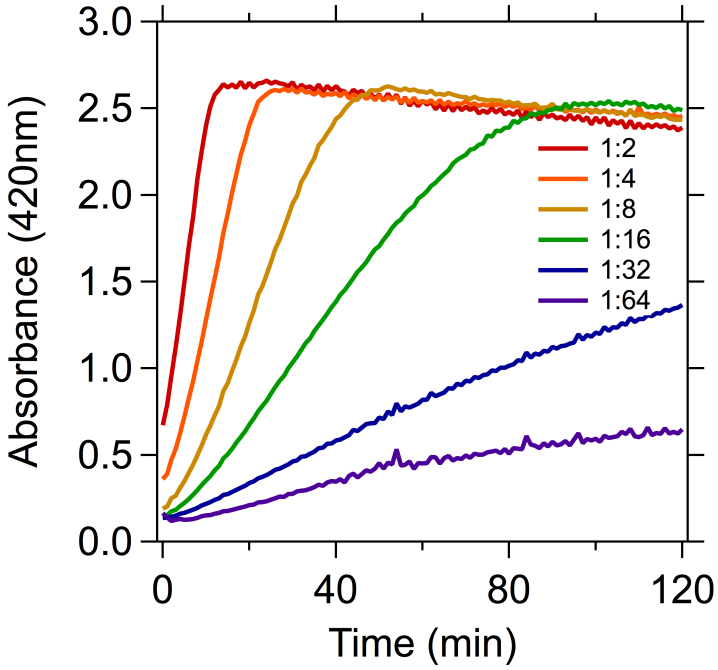

Figure 3.3: β-galactosidase activity of cell lysates dilutions (1:2, 1:4, 1:8, 1:16, 1:32, 1:64) determined by absorbance measured at 420 nm over time. All measurements are an average of triplicates.

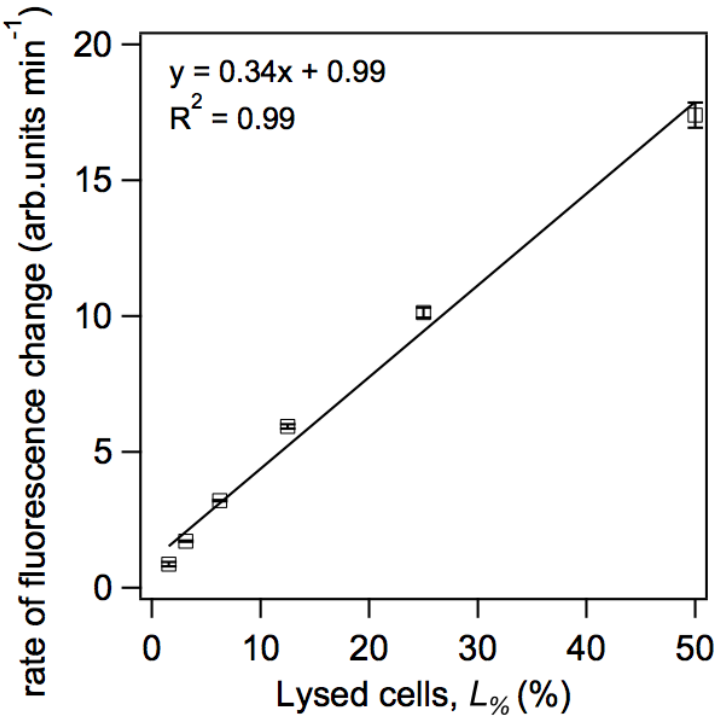

Figure 3.4: ALP calibration curve determined by measuring the rate of fluorescence change in different concentrations of cell lysate solutions, where $L_{\%}$ is equivalent to the ratio of cell lysate to buffer as a percentage.

allow for membrane intercalation, then centrifuged and resuspended in M9 to a final $OD_{600nm} = 0.6$. Cell turnover of ONPG, indicated by the linear rate of absorbance increase, was examined in triplicate for each staining concentration using a Spectra Max Absorbance plate reader to measure absorbance at 420 nm over 2 hours while cells were incubated with 1.3 mM ONPG. Background corrections were made by subtracting the absorbance at 420 nm of DSSN+ stained cell suspensions that were not incubated with ONPG.

Control test for DSSN+ interference with ALP activity

To determine whether DSSN+ has an effect on the hydrolysis of MUP or interferes with the activity of ALP, a standard curve was generated in accordance to the BioVision (#K422-500) Assay kit protocol. Using a 96-well plate, varying amounts of MUP (0, 0.1, 0.2, 0.3, 0.4, 0.5 nmol/well) were dispensed in the assay buffer. The same amount of ALP enzyme solution was added to each well. To test the effect of DSSN+, DSSN+ solution was added to each well to achieve a final concentration of 2 μM in order to mimic the maximum amount of DSSN+ left in solution after cell staining. Fluorescence was monitored in duplicates of the standard without DSSN+ and with DSSN+ at 440 nm and is plotted in Figure 3.5.

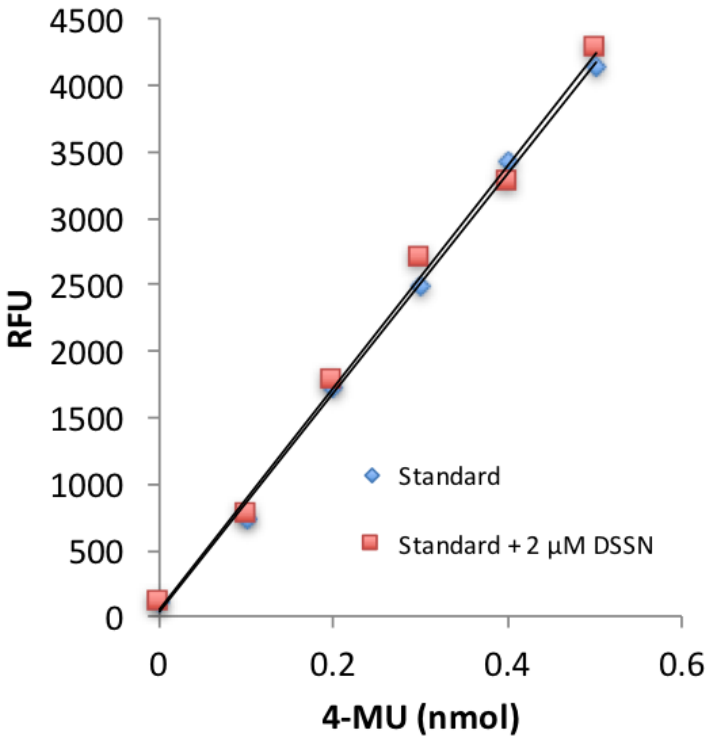

Figure 3.5: ALP hydrolysis of MUP measured by fluorescence intensity at 440 nm in standards prepared without and with DSSN+. All measurements performed in duplicate.

Control test for DSSN+ interference with β-galactosidase activity

To determine whether DSSN+ interferes with the hydrolysis of ONPG or interferes with the activity of β-galactosidase, a control experiment was performed on the standard measurements. A standard curve was generated using lysed cells that were previously stained with 10 μM DSSN+. Lysates were then serially diluted in M9 in ratios of 1:2, 1:4, 1:8, 1:16, 1:32 and 1:64 to produce solutions of 50, 25, 12.5, 6.1, 3 and 1.5% cell lysate. These solutions were then tested following the outer membrane permeability assay procedure. The β-galactosidase activities from dilutions of UT and DSSN+ modified *E. coli* lysates are shown in Figure 3.6.

3.3 Results and Discussion

3.3.1 Outer membrane permeability

A standard protocol was used to test changes in OM permeability (scenario (i) in Figure 3.1b). We measured the extracellular activity of the periplasmic enzyme alkaline phosphatase (ALP) after *E. coli* was exposed to different concentrations of DSSN+ for varying lengths of time. Specifically, *E. coli* cells were washed, resuspended in buffer, and then stained with 5, 10, 15 and 25 μM

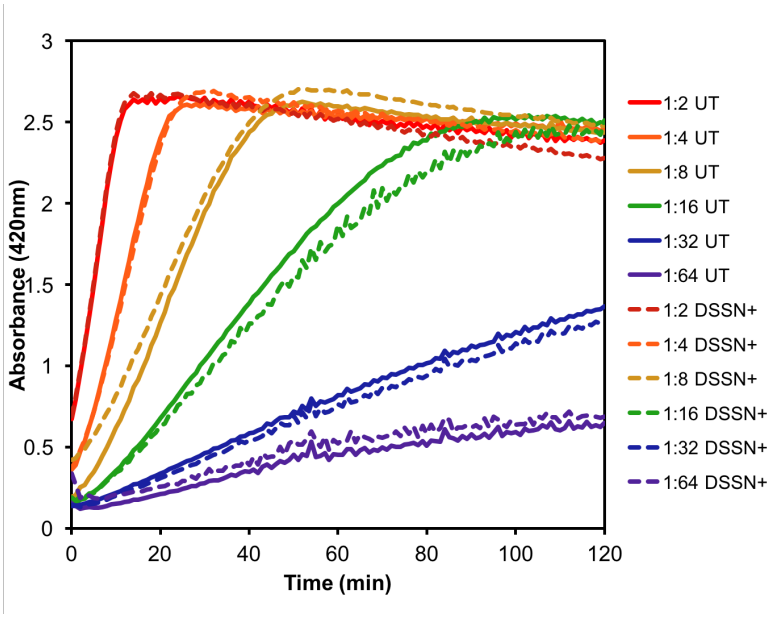

Figure 3.6: β-galactosidase activities measured by absorbance at 420 nm of different concentrations of cell lysate solutions from UT (solid lines) and 10 μM DSSN+ treated (dashed lines) cells to determine if DSSN+ interferes with hydrolysis of ONPG. Traces display an average of triplicate measurements.

DSSN+ for 1, 4 or 10 hours then filtered. The resulting filtrates were probed for extracellular ALP activity by monitoring conversion of non-fluorescent 4-methylumbelliferyl phosphate (MUP) to fluorescent 4-methylumbelliferone (4-MU). [84, 180, 181] The fluorescence intensity linearly increased over 60 min for filtrates from both unstained, untreated (UT) and DSSN+ treated cells (selected examples are shown in Figure 3.7). However, the rate of fluorescence increase was greater in filtrates from DSSN+ treated cells relative to UT cells (Fig. 3.7). Thus, DSSN+ alters the OM permeability sufficiently to facilitate periplasmic release of ALP, which is a moderately-sized macromolecule of 89 kDa. [182–184]

To quantitatively assess the degree of OM permeabilization under different conditions, we calibrated the ALP activity of different percentages of *E. coli* cell lysate. As with the filtrates of DSSN+ stained and UT samples, the 4-MU fluorescence of the cell lysates linearly increased with time (e.g. 50% cell lysate solution, Fig. 3.7). A linear trend was generated between the rate of fluorescence change and amount of cell lysate, thus providing a calibration curve between extracellular ALP activity and the relative degree of OM lysis, described as a percentage of total intracellular ALP. We use this calibration curve to determine the relative degree of cell lysis, notated by $L_{OM}\%$, in which $L_{OM}\%$ values of 100 and 0 correspond to a fully lysed and fully intact cell population, respectively.

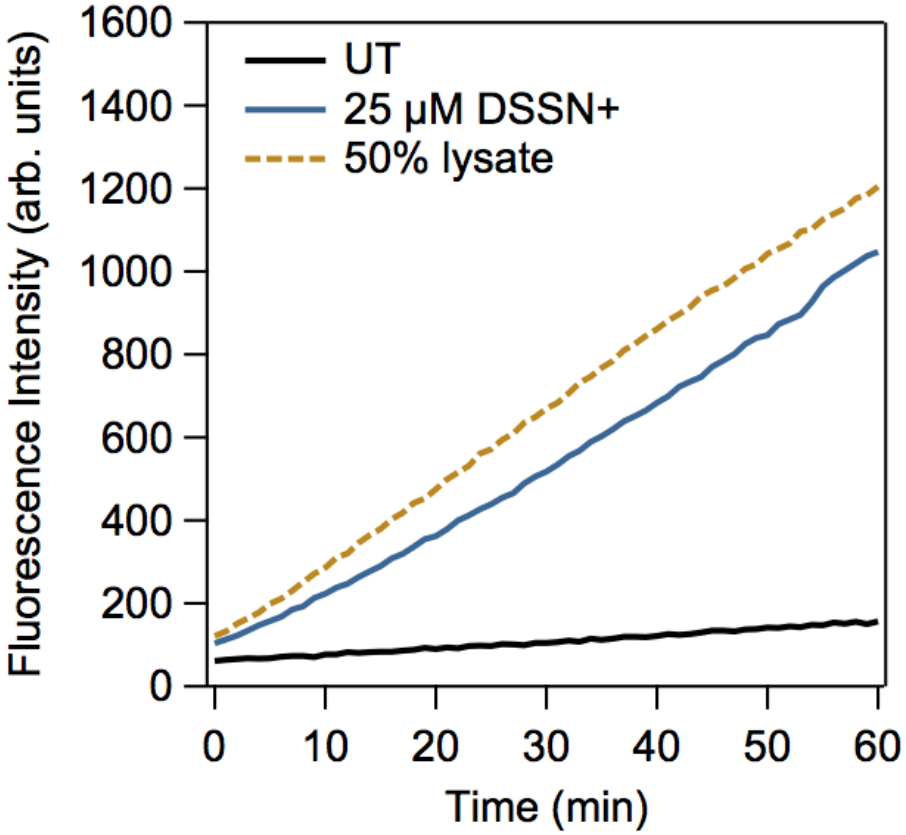

Figure 3.7: Extracellular ALP activity of filtrates from UT, *E. coli* stained with 25 μM DSSN+ for 10 hours and a 50% cell lysate solution, determined by fluorescence intensity of 4-MU measured at 440 nm over time. All measurements are an average of triplicates.

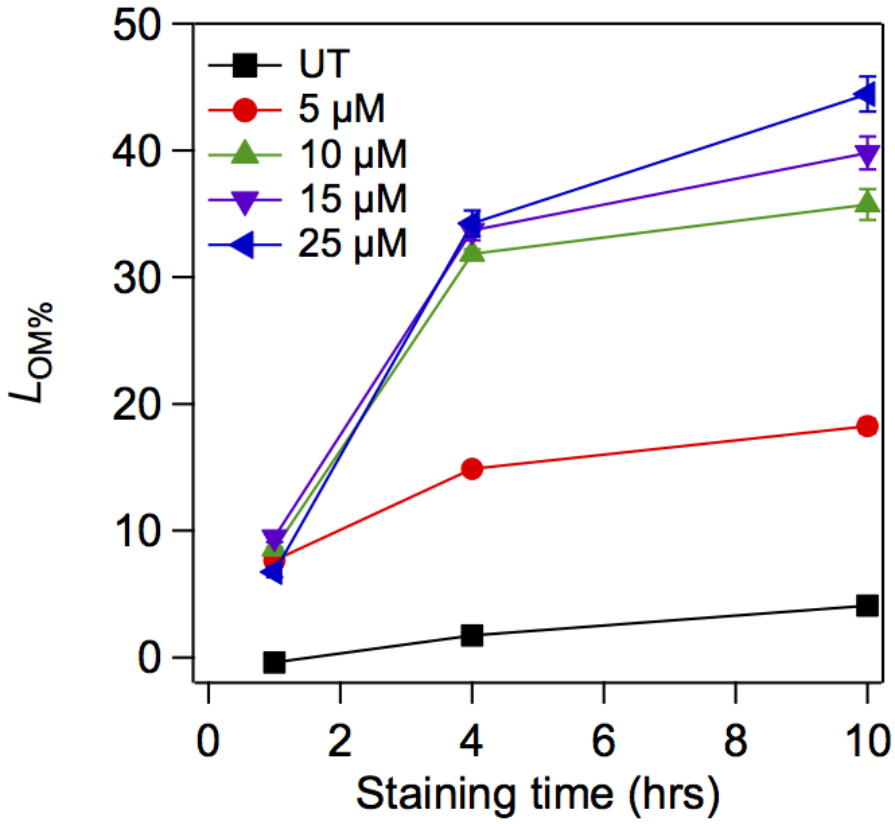

Figure 3.8: Permeabilization of the OM of *E. coli* from varying concentrations of DSSN+ measured as a percentage of total ALP activity ($L_{OM}\%$) released extracellularly over staining time. Error bars show standard deviation of an average of triplicates.

We compared the effective OM lysis of *E. coli* cells as a function of DSSN+ staining concentration and time (Figure 3.8). As summarized in Table 3.1 and plotted in Fig. 3.8, the $L_{OM}\%$ values increased with both DSSN+ staining concentration and time. Specifically, *E. coli* cells stained with the greatest DSSN+ concentration (25 μM) showed the most pronounced increase in OM permeability. The OM permeability of these cells was 20-fold higher than UT cells at 4 h, and at 10 h had the greatest $L_{OM}\%$, i.e. 45%. Given that the DSSN+ exposure in these experiments do not cause measurable cytotoxicity [51, 55, 56], these data indicate DSSN+ is able to increase OM permeability without significantly altering *E. coli* cell viability. These observations demonstrate that scenario (i), namely enzyme transport across the OM, is accelerated for cells that are labeled with DSSN+. It is worth noting that freeze/thaw methods used to release similar concentrations of recombinant proteins are poorly effective for proteins of ALPs dimensions. [185]

From Fig. 3.8, one observes that changes in OM permeability increase as the cells are exposed to more DSSN+; however, the magnitude of this increase tapers with both DSSN+ staining concentration and time. At concentrations over 10 μM, the effect of additional DSSN+ on OM lysis is diminished. It is worth pointing out that the maximum association of DSSN+ with *E. coli*, previously shown to be 20 nmol/OD_{600nm}, is equivalent to a staining concentration

Table 3.1: Effect of DSSN+ staining on OM permeability at 4 h, IM permeability at 5 h, and the rate of ONPG hydrolysis, defined as the linear rate of absorbance increase.

[DSSN+] (μM)	$L_{OM}\%$	$L_{IM}\%$	Turnover rate (a.u. min^{-}1)
0 (WT)	1.7 $\pm$ 0.12	0.8 $\pm$ 0.002	0.009 $\pm$ 0.001
5	14.9 $\pm$ 0.27	1.0 $\pm$ 0.003	0.013 $\pm$ 0.003
10	31.8 $\pm$ 0.36	1.2 $\pm$ 0.006	0.018 $\pm$ 0.007
15	33.7 $\pm$ 0.79	1.3 $\pm$ 0.005	0.018 $\pm$ 0.007
25	34.2 $\pm$ 1.01	1.3 $\pm$ 0.005	0.018 $\pm$ 0.004

of 12 μM in our experimental conditions.[60] These data thus suggest that little additional DSSN+ associates with cells above 10 μM, causing only a minor additional impact on OM permeability. Additionally, the OM permeability increases rapidly over the first 4 h of staining, then tapers for all DSSN+ concentrations. These data indicate that DSSN+ association with cells reaches a steady-state after 4 h of staining. Taken together, these data are consistent with the suggestion that the degree of OM permeability is related to the amount of DSSN+ associated with the cell and that DSSN+ association with *E. coli* cells saturates at a staining concentration of $\sim$10 μM and a staining time of $\sim$4 h.

3.3.2 Inner membrane permeability

To determine whether DSSN+ had a similar impact on IM permeability (scenario (ii) in Figure 3.1b), we measured the release of the cytoplasmic hydrolase enzyme, β-galactosidase (β-gal), into the medium, which is commonly used as an indicator of inner membrane damage. [186–189] As before, *E. coli* cells were washed in buffer, stained with varying concentrations of DSSN+ for 5 hours and then filtered. Extracellular β-gal activity in the resulting filtrates was measured by monitoring cleavage of colorless 2-nitrophenyl β-D-galactopyranoside (ONPG) into yellow o-nitrophenol (ONP) by using absorption spectroscopy. For filtrates from both UT cells and cells stained with DSSN+, the ONP absorbance at 420 nm linearly increased with time (Figure 3.9). In contrast to the ALP experiments, there was no marked difference in the rate of change of A_{420nm} between UT and DSSN+-stained cell filtrates, even when DSSN+ concentration was increased up to 25 μM. This observation indicates that IM permeability for β-gal did not change significantly upon DSSN+ staining and therefore scenario (ii) is not operational under our experimental conditions.

To more precisely quantify the effects of DSSN+ staining on IM permeability, we assessed the ONP production rate for different amounts of IM lysis and calculated $L_{IM}\%$ for each staining concentration (Table 3.1). The ONP forma-

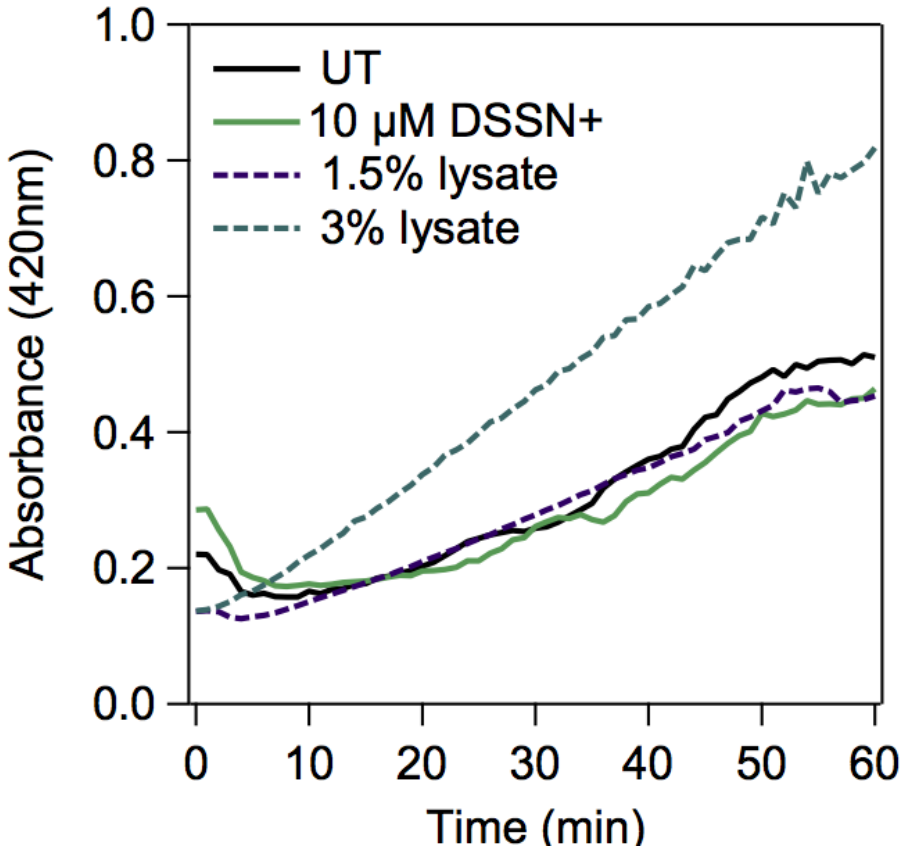

Figure 3.9: Permeation of *E.coli* IM by DSSN+ determined optically by measuring absorbance of ONP at 420 nm. Extracellular β-galactosidase activity in the filtrates from UT and 10 μM DSSN+ stained *E. coli* shown over incubation time with ONPG and compared with absorbance of 1.5% and 3% cell lysate solutions. All measurements are an average of triplicates.

tion rate for 3% cell lysate was significantly higher than both the UT and 10 μM DSSN+ stained cell filtrates (Fig. 3.9), while the rate for 1.5% lysate was comparable to these samples. These data show that the amount of β-gal released by DSSN+ staining is both comparable to unstained cells and very small. Taken together, these data indicate that the IM is not sufficiently disrupted to accelerate β-gal diffusion out of the cell. This is an important improvement to our current understanding of how DSSN+ improves charge transport in *E. coli*, which was previously suggested to be caused by cell lysis. [85]

When considering the difference DSSN+ has on OM and IM permeability, it is important to consider that the OM and IM permeabilities were probed with different size proteins. With a molecular weight of 465 kDa, β-gal is $\sim$5$\times$ larger, than ALP (MW = 89 kDa). [182–184, 190, 191] While the mode by which DSSN+ increases membrane permeability is unclear, it is possible that these changes in permeability are size dependent. Regardless, as release of β-gal is often used as evidence of cell lysis, it is clear that DSSN+ does not cause *E. coli* lysis under the experimental conditions studied here. [85, 186, 188, 189, 192]

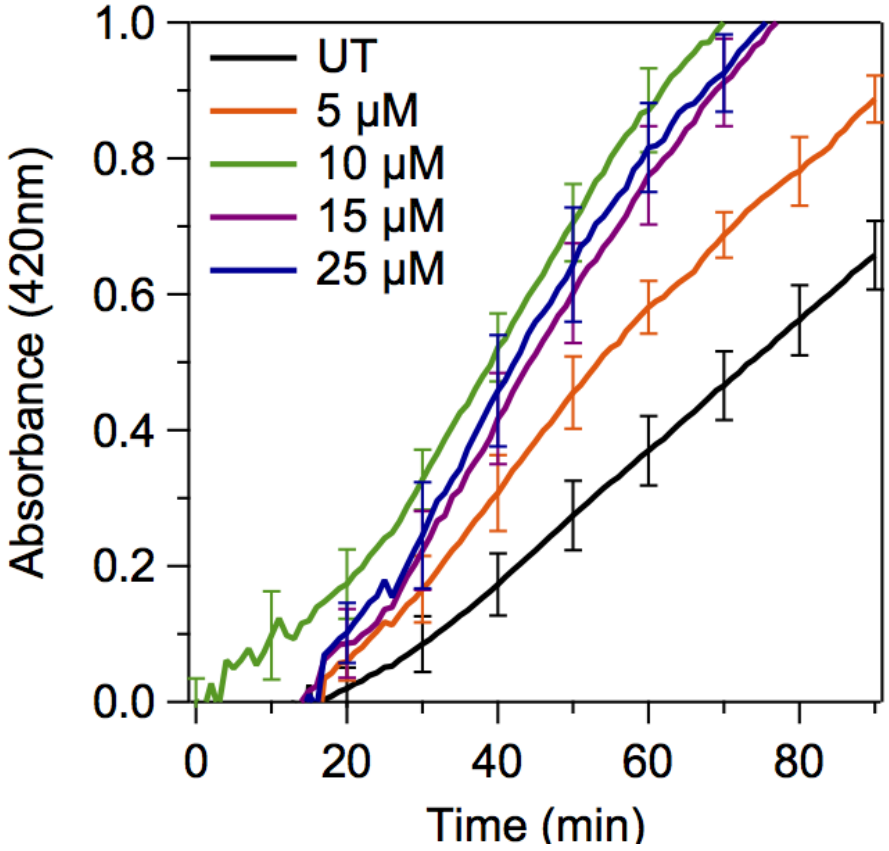

Figure 3.10: Turnover of ONPG by whole cells monitored by absorbance of ONP at 420 nm over time. Error bars are standard deviations of triplicates and plotted for every 10 minutes.

3.3.3 Influence on whole-cell catalysis

Considering the ability of DSSN+ to increase the OM permeability, we hypothesized DSSN+ could improve the transport of much smaller substrate molecules through the cell envelope (scenario (iii) in Figure 3.1b). Because ONPG hydrolysis is rate limited by its passive diffusion through the OM, we chose to test this hypothesis using a modified β-gal assay on whole *E. coli* cells stained with DSSN+.[188, 193–195] Cells were therefore incubated with varying concentrations of DSSN+ for 5 hours, washed, and then monitored for ONP production as a function of time. The time dependence of the background-corrected A_{420nm} versus time provides a measure of product formation (Figure 3.10). The faster increase in A_{420nm} for DSSN+ stained cells shows that DSSN+ stained cells produce ONP more rapidly than unstained counterparts.

To quantify the relative ONP production rate, we determined the slope of the linear region in A_{420nm} versus time plots shown in Fig. 3.10. As observed with the ALP experiments, this increase in turnover rate increased with DSSN+ staining concentration up to $\sim$10 μM. This limiting value reinforces the idea that permeability changes are proportional the amount of DSSN+ associated with the cell. [60] A comparison of these turnover rates (Table 3.1) shows that DSSN+ stained cells hydrolyzed ONPG up to 2-fold more rapidly than unstained cells.

This 2-fold increase in turnover does not match with the 20-fold increase in OM permeabilization, indicating a different rate limiting process may be occurring. Regardless, while DSSN+ staining does not release β-gal from the cytoplasm, it does increase transport of ONPG across the cell envelope, resulting in increased microbial catalysis.

While it is possible that DSSN+ may affect transport of molecules or proteins with a low molecular weight across the IM, at this point we do not have definitive proof that DSSN+ is permeabilizing or, to what extent, even reaching the IM. Regardless, this interest in structural elucidation has led to the discovery of a new way to accelerate whole-cell catalysis by improved transport across the OM. Beyond whole-cell catalysis, these observations have broader implications where membrane permeabilization is relevant, for example antimicrobial susceptibility. [159, 160]

The data presented here also offers mechanistic insight into how DSSN+ increases current production in *E. coli* microbial fuel cells (MFCs). [50, 51] In contrast to previous reports, the IM remains primarily intact under our experimental conditions. [85] Since the conditions described herein closely mimic that used in MFCs, it is unlikely that the increased extracellular electron transfer (EET) in MFCs is due to cell lysis. Rather, given the substantial increase in OM permeability with DSSN+ staining, we suggest DSSN+ increases trans-

port of redox active molecules or electron donors in the media across the OM. [50, 51] Increased transport of either set of molecules would increase the observed current in an *E. coli* MFC. Supporting this idea, increasing the permeability of the OM in *E. coli* via directed evolution [196–198], overexpression of porins [179, 195], and introduction of permeabilizers [199] have all been previously used to increase mediated EET. Additionally, a recent study demonstrated that released enzymes in certain microorganisms can mimic direct EET. [200] It is also important to note that COEs alter the physiochemical properties of the cell in a manner that may affect cell-electrode interactions. [60] Thus we cannot rule out that DSSN+ improves *E. coli* MFC performance through a combination of effects, such as increased permeability and cell attachment.

While the specific mechanism of membrane perturbation is yet to be defined experimentally, molecular dynamic simulations demonstrated distortions and disorder in the phospholipid bilayer upon COE modification and aggregation of COEs. [56] To what extent the LPS layer is modified is less well understood. It is not unreasonable to suggest COE interactions with LPS cause disorder, which is a common cause of OM permeability. [159]

3.4 Conclusions

In summary, we have shown that DSSN+ increases the permeability of the OM and improves transport of a small molecule through the cell envelope. By measuring the release of the periplasmic ALP enzyme into the extracellular medium, it is possible to unify changes in the OM permeability with accumulation of DSSN+. This process led to a 20-fold increase in OM permeability. This effect was observed in staining concentrations far below those needed for toxicity. We did not observe significant release of β-gal, indicating DSSN+ does not adequately disturb the IM to allow outward diffusion of this enzyme. This does not rule out accumulation of DSSN+ in the IM since the dimensions of the protein may be too large for diffusion. It may be possible that smaller macromolecules could diffuse, but this requires additional tests. Nonetheless, it is important to note these results have led to the discovery of a new way to accelerate whole-cell catalysis. Last, we show that DSSN+ staining increases the rate of ONP formation up to 2-fold.

The deeper understanding of DSSN+s impact on OM permeability suggests COEs may be suited for wide range of whole-cell applications.[165, 201] Here, we have shown DSSN+ improves passive transport across the OM. Thus, COEs provide a synthetic, one-step method to either release a periplasmic product

or increase transport of substrate across the OM by using specifically designed synthetic molecules with limited influence on cell viability. Thereby, use of COEs for increased transport across the OM has the potential to improve microbial catalysis, recombinant protein recovery, or even decrease antibiotic resistance, where the OM is limiting.

3.5 Supplementary Information

3.5.1 Effect of COE structure on whole-cell catalysis

We have demonstrated the ability of DSSN+ to increase the permeability of the OM and improve transport of a small molecule through the cell envelope. This investigation of solely DSSN+ was motivated based on the wide application of DSSN+ in bioelectrochemical systems.[1] These results provided important insight regarding permeabilization as a possible mode of action this COE takes on bacterial membranes, which would result in increased current generation in *E. coli* MFCs when in the presence of redox mediators. To further our understanding on the relationship between COE molecular structure and membrane properties, we continued these experiments using COEs with different molecular structures. The COE structures investigated have phenylenevinylene cores of 3–

5 repeat units (RUs) and either an amine (COE1 series) or two meta-positioned alkoxy (COE2 series) linkage groups. The chemical structures of the COEs used are shown in Figure 1.3.

To determine how COE molecular structure effects the rate of whole-cell catalysis, we followed the procedure previously described for the whole-cell ONPG turnover assay using cells stained with varying concentrations (0, 5, 10, 15, 25 and 40 μM) of COE1 series (DSBN+, DSSN+, COE1-5C) and COE2 series (COE2-3C, COE2-4C, COE2-5C) molecules. *E. coli* cells were prepared as described in Section 3.2, then resuspended to an OD_{600nm} such that $OD_{600nm} = 0.6 \pm \dot{0}.04$ in assay conditions. In contrast to the previous experiment, which incubated cells for 5 hrs with DSSN+, cells were incubated at 37°C with COE solutions for 2 hrs prior to the assay. *E. coli* from separate cultures were used for COE1 and COE2 series experiments. Whole-cell turnover of ONPG by UT and COE-treated *E. coli* was monitored via absorbance at 420 nm over time.

Figure 3.11 displays absorbance over time of control cells (untreated *E. coli*) and 25 μM COE stained *E. coli* from (a) COE1 series and (b) COE2 series. One notes that the rate of absorbance change in COE1 series molecules is fastest in DSBN+ stained cells, followed by DSSN+, then COE1-5C and the control—where the COE1-5C trace is indistinguishable from the control trace. A similar trend is observed in COE2 series stained cells, shown in Figure 3.11b, however

there is a slight rate increase in COE2-5C modified cells compared to the control. Turnover rates were calculated by fitting the linear region of the plots and taking the slope; rates are expressed in a.u. min^{-1} and listed in Table 3.2. These data demonstrate that there is a rate dependence of ONPG turnover on the molecular length, where the rate of catalysis increases with decreasing molecular length.

Negligible differences are seen between the turnover rates of COE1 and COE2 series when comparing molecules of the same backbone length (Table 3.2). However, control sample turnover rates were comparable between the COE1 and COE2 control experiments. The difference between control rates are likely because COE1 and COE2 series experiments were performed using separate *E. coli* cultures. Slight differences in handling could account for altered physiologies. Comparing COE-modified cell turnover rate with their control rate, we observe a greater net improvement with COE2 series modified cells. This likely indicates that COE2 series are permeabilizing the cell envelope to a greater extent.

ONPG turnover in whole cells modified with varying concentrations of COEs are plotted separately by COE structure as a function of A_{420nm} versus time in Figure 3.12. One notes in Figure 3.12a and b that rates of absorbance change over time generally increase with increasing concentration. Thus, cells modified with 3-RU COEs, i.e. DSBN+ and COE2-3C, show a greater sensitivity to

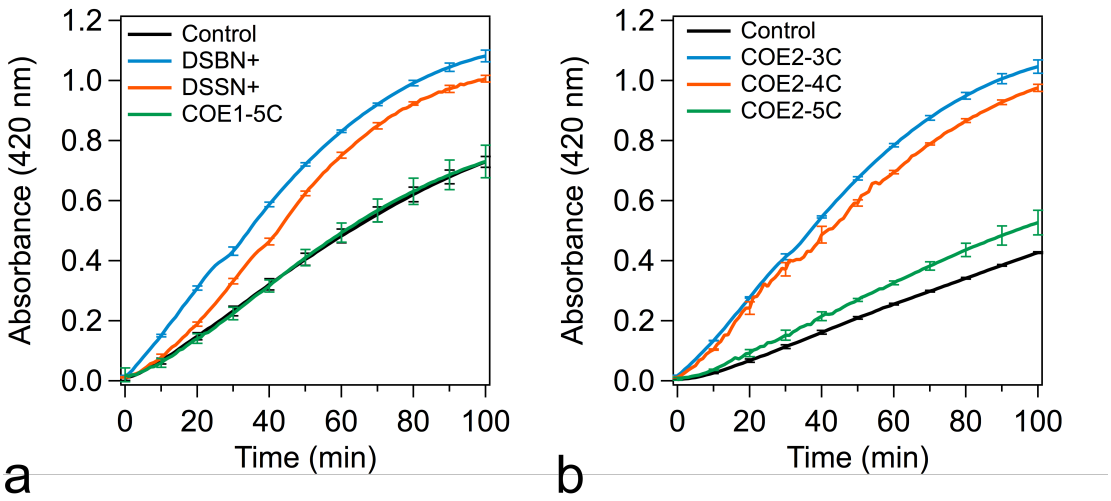

Figure 3.11: Absorbance over time measuring ONPG turnover in control (unstained) *E. coli* and *E. coli* stained with 25 μM COEs from (a) COE1 series and (b) COE2 series. All measurements are an average of triplicates, error bars are displayed every 10th measurement show standard deviation.

Table 3.2: Comparison ONPG turnover rates between untreated (UT) *E. coli* and *E. coli* cells modified with 25 μM COEs from COE1 series and COE2 series. Turnover rates expressed in terms of a.u. $\text{min}^{-}1$.

COE1 series	Turnover rate	COE2 series	Turnover rate
UT	0.008	UT	0.004
DSBN+	0.014	COE2-3C	0.013
DSSN+	0.013	COE2-4C	0.012
COE1-5C	0.008	COE2-5C	0.006

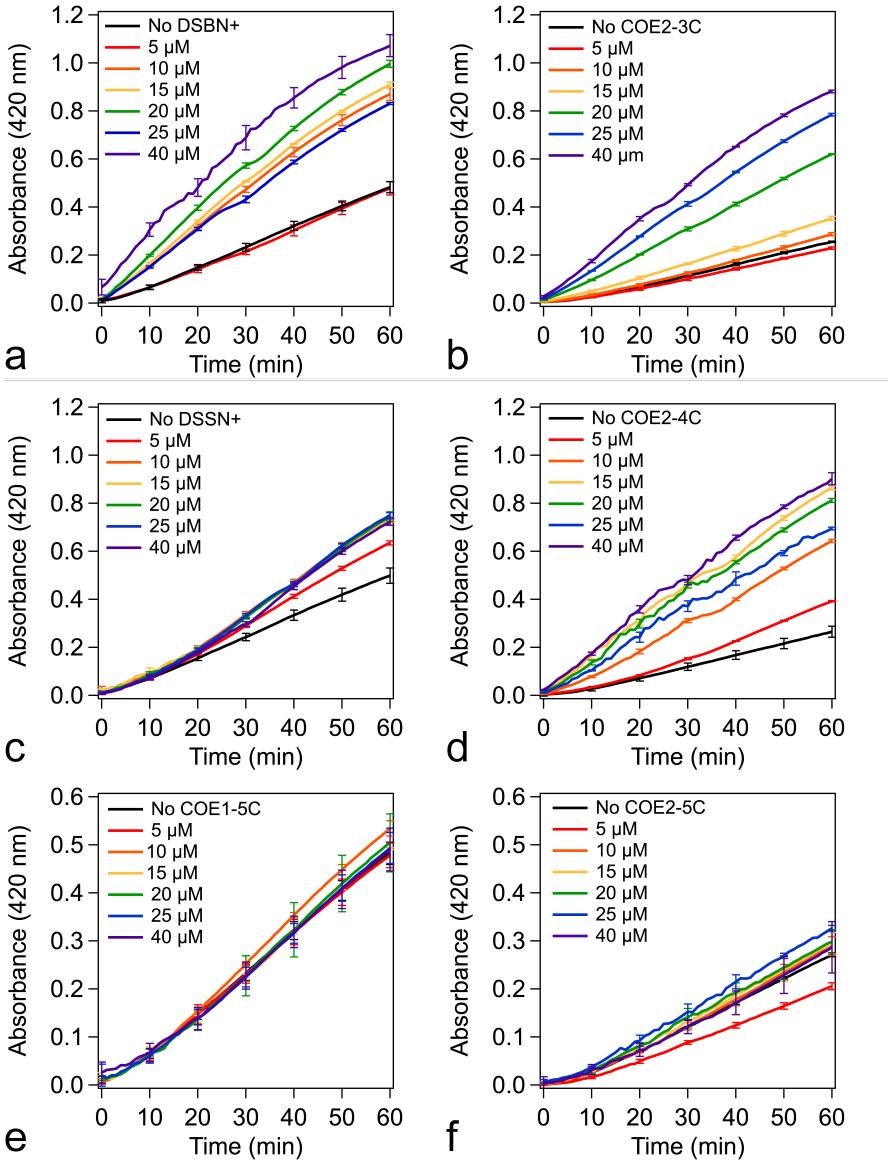

Figure 3.12: Absorbance over time measuring ONPG turnover in whole cells of *E. coli* stained with varying concentrations of (a) DSBN+, (b) COE2-3C, (c) DSSN+, (d) COE2-4C, (e) COE1-5C and (f) COE2-5C. All measurements are an average of triplicates, error bars show standard deviation.

concentration compared to the longer COEs. In longer COE structures we see a slight increase in rates of A_{420nm} with increasing concentration, however differences are less apparent between cells modified with concentrations $>10\,\mu$M. This reinforces the idea postulated in Section 3.3.3 that permeability changes are proportional to the amount of COE associated with the cell. Where, in Chapter 2, we noted plateaus in COE association with *E. coli* beginning at $\sim$15 μM for the 4- and 5-RUs, where 3-RU COEs did not exhibit plateaus in association.

Little change in ONPG turnover rates are observed between the 5-RU modified cells and controls, displayed in Figure 3.12e and f. Interestingly, at 5 μM COE2-5C, the rate of A_{420nm} over time is slower than the control. These results suggest that longer COE structures have less of an effect on whole-cell catalysis compared to the 3- and 4-RU structures. Considering this, it is likely that 5-RU COEs have less of an effect on membrane permeability.

An interesting analogy is made by comparing the relationship of molecular structure to the catalysis rate and antimicrobial effects. Yan et al has demonstrated that COE structures with longer backbone lengths are significantly less toxic than the 3-RU COE structures. [57] Another study demonstrated that the relative toxicity of DSBN+ and DSSN+ are positively correlated with the extent of mismatch between the length of backbone and the bilayer thickness. [56] Hinks et al suggested that the mode of toxicity was due to membrane thinning;

molecular dynamics simulations demonstrated that DSBN+ thinned the membrane more than DSSN+, thus perturbing it to a greater extent. It is reasonable to suggest that the trend of COE molecular structure on membrane perturbation is related to trends observed in whole-cell catalysis rate, whereby increased rates are due to increased membrane perturbation.

5-RU COEs, whose the molecular length (≈5 nm) exceeds the thickness of the bilayer (≈4 nm), are suggested to perturb lipid bilayers less than 3- and 4-RU COEs, due to their positive hydrophobic mismatch compared to the negative mismatch of 3- and 4-RU COEs. [56, 202] COE1-5C has shown to impart rigidity to the lipid bilayer and has thus been used to mitigate membrane destabilization by organic solvents. [203] Thus, the ability of this 5-RU COE to stabilize the membrane may work against increasing permeability and whole-cell catalysis. However, when applied in *E. coli* MFCs, 5-RU COEs show an increase in power production regardless of their ability to increase membrane permeability. [51] Considering 5-RU COEs influence cell surface charge to the greatest extent [60], our previous argument that the mode of action COEs take on increasing performance in MFCs is a combination of effects, such as increased permeability and cell attachment, is likely.

Chapter 4

Origin of electrochemical performance improvements in DSSN+ modified *E. coli* fuel cells

In this chapter we examine the mechanism for improved electrochemical performance of *Escherichia coli* in a variety of device configurations. First, we aim to determine whether the improved performance originates from the microbes on the electrode or by released soluble components or planktonic cells. In U-tube microbial fuel cells, we find that the mechanism of performance improvements induced by conjugated oligoelectrolytes (COEs) is dependent on physical con-

tact of microorganisms with the electrode. Modifying device configuration and conditions, we investigate the electrochemical performance in the absence of exogenous mediators and the possible effects DSSN+ has on redox activity in situ. Last, we examine the effect of DSSN+ on cell adhesion to the electrode. From these studies, we confirm that COEs increase cell accumulation on the electrode and this is the mechanism by which COEs increase current production in these conditions.

4.1 Introduction

Technologically relevant microbial electrochemical technologies (METs) such as microbial fuel cells (MFCs) and microbial electrosynthesis cells (MECs) rely on the inherent ability of microorganisms for extracellular electron transfer (EET) to or from an electrode. [4, 8, 9, 204] While electrogenic microorganisms capable of EET exist, they are not prevalent nor are they widely used in biotechnology. Thus broadening the variety of cell types capable of transferring charge across membranes is of general interest. The limited number of electrogenic microbes has led to varied approaches to the application of synthetic molecules and materials, as well as genetic modifications to influence non-electrogenic systems, as discussed in detail in Chapter 1. [43]

As such, it is desirable to modify microorganisms with synthetic structural features that enable transmembrane electron transport and that do not impede their metabolic function. As discussed in Chapter 1, COEs have been designed for this purpose and improve electrochemical performance in a variety of METs. In particular, DSSN+ is able to increase current and power generation in *E. coli* MFCs. While mechanistic studies on DSSN+ modification in *S. oneidensis* show evidence for enhanced direct electron transfer (DET) [53] and an increase in released flavins [79, 84], this mechanism would not explain such phenomena in *E. coli*. *E. coli* lacks the ability to utilize flavins as redox mediators in anaerobic conditions as well as any obvious redox or conductive membrane protein in the outer membrane capable of DET. [80, 82] Recent examination of *E. coli* modified with DSSN+ for the production of gold nanoparticles suggested that DSSN+ perturbs the membrane, leading to the release of cytosol components. [85] It is worth noting, however, that these experiments were performed in ultrapure water, potentially exposing the cells to osmotic shock, which could lead to cell damage. [56, 205, 206] Addressing these concerns in Chapter 3, we demonstrated that release of cytosolic enzymes is negligible in conditions mimicking those in an MFC. Regardless, it is unclear to what extent these observations are related to the increased power observed in MFCs.

In the first part of this chapter, we provide evidence that DSSN+ improves

current generation in *E. coli* MFCs in cells directly in contact with the electrode as opposed to planktonic cells or by extraneous species generated by cells in solution. We utilize U-tube MFCs as the test devices for the examination of extracellular electron transfer (EET) in *E. coli*. Operational MFCs were interrupted after a specific period of time and their components transferred into new MFC devices, as illustrated in Figure 4.1. This approach was used to deconvolve the overall performance into the contributions made from (i) the cells attached to the electrode and (ii) the solution components, which consist of planktonic cells and any extraneous species generated. The question we wish to answer is to what extent increased current production and power generation is a function of the modified cells in physical contact with the electrode surface or as a result of released soluble materials in the planktonic cell solution.

We find that the cells on the electrode are the underlying factor for the increased current and power generation utilizing this U-tube device configuration. However, it is possible that DSSN+ increases the cell population of loosely adhered bacteria to the electrode and that device-specific constraints prohibit an accurate account of cell populations. We hypothesize that improvements in current with COEs may be due to a combination of effects, such as increased permeability and increased population of loosely adhered bacteria to the electrode. The next question we wish to answer is three-fold; (1) to what extent is current

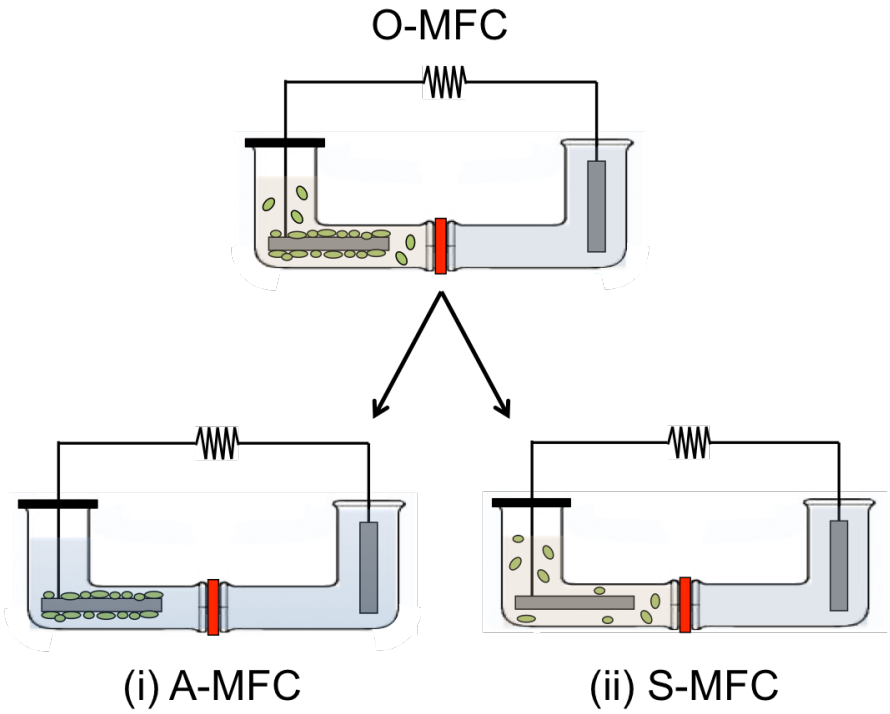

Figure 4.1: Cartoon illustration of the U-tube *E. coli* MFC devices and the separation process occurring at day 3. Anode components from the original MFCs (O-MFCs) were separated and transferred into new devices; (i) A-MFCs, which contain the anodes from O-MFCs with added LB media and (ii) S-MFCs, which contain the solution from the O-MFC anode chambers and an added carbon felt electrode.

increased in the absence of mediators, (2) if COE intercalation enables and alternate redox pathway or releases redox active species, and (3) to what extent is current increased due to increased cell adhesion.

The second part of this chapter aims to answer this question. Here, we use 3-electrode, two chamber bioreactors employing defined media as the electrolyte devoid of exogenous mediators. Use of 3-electrode bioreactors enables the ability of electrochemical characterization in situ, compared to the U-tube device configuration which lacks a reference electrode. Chronoamperometry is used to examine current improvements and cyclic voltammetry is used to examine possiblealtered redox processes in the cell or released redox active components by DSSN+ intercalation. Last, we examine cell adhesion by monitoring the decreasing planktonic cell density and examining total protein content.

4.2 Experimental Methods

Cell culture

E. coli K-12 (10798, ATCC, VA) was cultured aerobically overnight from frozen stock in sterile Luria Broth (10 g L^{-1} bacto tryptone, 5 g L^{-1} yeast extract, 10 g L^{-1} NaCl) at 37°C while shaking. In experiments utilizing defined

media bioreactors, cells were additionally centrifuged and rinsed twice in 1×M9 salts, then resuspended in 1×M9 (6.8 g/L Na_2HPO_4, 3 g/L KH_2PO_4, 1 g/L NH_4Cl, 0.5 g/L NaCl).

4.2.1 U-tube MFCs

MFC construction and operation

Twelve U-tube MFCs were constructed as reported previously. [49, 50, 54] Devices were assembled from two L-shaped glass tubes separated by a Nafion® N117 membrane and sealed using an O-ring and a 28/15 stainless steel pinch clamp. Nafion® membranes were treated by soaking at 80°C in a sequence of solutions for 1 hour each in the following order: 3% hydrogen peroxide solution, ultrapure water, 0.5 M sulfuric acid solution, and ultrapure water again. Electrodes were constructed out of carbon felt (2 cm × 5 cm) and threaded with titanium wire. The anode chamber was sealed with a silicone stopped while the cathode chamber was loosely capped with a glass scintillation vial. Assembled devices were filled with ultrapure water and sterilized by autoclaving. After autoclaving, the water was removed and concentrated, sterile DSSN+ solution (1 mM) was added to the anode chambers. The anode and cathode chambers were filled with sterile LB then inoculated with the appropriate amount of cell

culture for an optical density of 0.1 and a final DSSN+ concentration of 10 μM. Cathodes were partially submerged for the purpose of "air-wicking. The devices were connected to an external resistor (10 kΩ), a multiplexer and a digital multimeter (PXI-2575, PXI-4065, National Instruments, Austin, TX) controlled by a LabView program for automated data acquisition. Polarization measurements were taken by switching through a series of external resistors (1, 10, 51, 100, 200, 500 and 1000 kΩ) for 20 minutes at each resistance. Power density was calculated and normalized by the 2D area of the felt electrodes (10 cm^2) for comparison to previous results.[50] All devices were operated in a temperature regulated incubator at 30°C .

New U-tube MFCs were constructed to test the performance of the cells attached to the electrode and planktonic cells separately. For A-MFCs, anode electrodes with attached *E. coli* cells were carefully removed from O-MFCs and transferred into new U-tubes devices. Both anode and cathode chambers were filled with sterile LB medium and the cathode chamber was inoculated with suspended *E. coli* cells that were grown overnight. No additional DSSN+ was added. For S-MFCs, the solution was removed from the anode chambers of the O-MFCs and transferred into newly constructed U-tube devices containing carbon felt anodes. Only the cathode chambers were filled with LB medium and inoculated with *E. coli*. Remaining O-MFCs were kept operational. Each MFC

condition was run in triplicate devices.

Scanning electron microscopy (SEM)

Anodes were collected at the end of operation for SEM analysis. The carbon felt anodes were fixed in 2% formaldehyde solution prepared in 10 mM PBS for 24 hours. The electrodes were then rinsed twice in 10 mM phosphate buffer then ultrapure milli-Q water before dehydration in ethanol. Electrodes were dehydrated by soaking in a 70% and 100% ethanol solution for 30 minutes each then subsequently dried under ambient conditions for 72 hours before analysis. SEM images were taken using a FEI XL40 Sirion FEG Digital Scanning Microscope at an acceleration voltage of 5 keV.

Confocal microscopy

An approximately 1 cm^2 square was cut from the carbon felt anode electrodes for laser scanning confocal microscopy. Samples were dipped twice in PBS to dislodge loosely attached cells. Anodes without DSSN+ modification were stained with DAPI. For DAPI staining, the electrode samples were submerged in a solution of 5 μM DAPI in PBS for 30 minutes. All samples were also stained with propidium iodide (PI) in a similar fashion; submerged in a

solution of 5 μM PI in PBS for 30 min. Excessive moisture was removed via wicking with a paper towel in contact with one edge of the square sample. A large drop of silicone immersion oil was placed directly onto the sample, then the sample was placed face down onto a cover slide. Tape was used to secure the sample before imaging. Laser scanning confocal microscopy was performed using an Olympus FluoView 1000 spectral scanning microscope equipped with a 60 $\times$ 1.30 silicon oil immersion lens. Confocal laser excitation for DSSN+ and DAPI was at 405 nm with emission collected at 600 nm and 420–520 nm for DSSN+ and DAPI, respectively. Excitation for PI was at 559 nm and emission was collected at 600–700 nm. All images were processed using ImageJ.

Colony forming unit (CFU) assay

Anodes from control and test O-MFCs were removed after 3 days of operation, placed in 20 mL of 50 mM PBS and vortexed. Samples of 1 mL of PBS solution containing cells dislodged from the anodes were serially diluted in PBS. 100 μL of dilutions of 1:10^6 and 1:10^7 sample:PBS were plated on LB agar plates and incubated overnight at 30°C . Colony forming units (CFUs) were quantified by the average total number of colonies that grew overnight. All plates were made in triplicate.

4.2.2 Defined media bioreactors

Bioreactor construction and operation

Experiments were conducted in batch bioelectrochemical reactors. Reactors were comprised of two chambers containing 140 mL of solution and separated by a cation exchange membrane (CMI-7000, Membranes International, Ringwood, NJ). Each chamber was filled with the appropriate amount of solution and autoclaved at 121°C for 20 min. The working electrode chamber contained M9 growth media with 40 mM D,L-lactate, and the counter electrode chamber contained only M9 media. Vitamins, minerals and lactate solutions were filter sterilized and added after autoclaving. The working electrode was a piece of graphite felt cut to the dimensions of 2.5×2.5 cm (GF-S6-06, Electrolytica) threaded with a piece of Pt wire. The counter electrode was a piece of Pt wire and the reference electrode was Ag/AgCl in saturated KCl.

The bioreactors were kept at 30°C in an incubator, continuously sparged with N_2 gas, and stirred at ∼200 rpm by magnetic stir bars. The potential of the working electrode was set to $+0.2\,V_{Ag/AgCl}$ using a potentiostat (Model 1000B, CH Instruments). After overnight N_2 sparging and background electrochemical measurements, the working electrode chambers were inoculated with *E. coli* to a final $OD_{600mn} = 0.55 \pm 0.04$. Cells were cultured overnight and prepared

as described above. After 3.6 h, DSSN+ solution was added to the working electrode chamber of the test devices to a final concentration of 10 μM. After day 1, current was manually recorded.

Cyclic voltammetry was performed after one day of operation and day 6 of all bioreactors. Scans were run without stirring from -0.7 V to 0.5 V at 100 and 50 mV/s for two cycles and at 2 mV/s for one cycle.

Sampling from bioreactors and measurements

Samples (1.5 mL) were removed from each reactor periodically. OD_{600nm} was measured for each sample. After one week of operation, bioreactors were removed and agitated to dislodge loosely attached cells. OD_{600nm} measurements were taken before and after agitation. Total protein content of all samples and electrodes were determined using the Pierce® BCA Protein Assay Kit (No. 23225, Thermo Fisher Scientific). Briefly, cell samples were centrifuged (5 min at 12,000 rpm), resuspended in 200 μL of 0.2 M NaOH then incubated at 50°C for 40 min. Electrodes were placed in 25 mL of 0.2 M NaOH and incubated at 50°C for 1 hr. The standard procedure for the BCA Assay was followed.

4.3 Results and Discussion

4.3.1 Performance in U-tube MFCs

Performance contributions from cells on the anode *vs.* cells in solution

Briefly, MFCs were constructed in a U-tube configuration using Luria Broth (LB) as the medium and inoculated with *E.coli*. Test devices contained 10 μM DSSN+ while control devices were unmodified. Devices from the test and control groups left in operation over the course of 10 days are referred to as O-MFCs. These devices represent the original performance of test and control groups, which is considered to be the sum of contributions from cells residing on the anode surface and the planktonic cell solution. Meanwhile, groups of test and control devices were interrupted after three days of operation; anode components were separated and installed into newly constructed U-tubes, as demonstrated in Figure 4.1. Specifically, anode electrodes were installed in the anode chamber of newly constructed U-tubes and filled with LB. Representative of the performance contribution from cells on the anode, these devices are referred to as A-MFCs. Anode solutions removed were used to fill the anode chamber of devices containing new anodes. These devices were used to represent the performance contribution from soluble species; referred to as S-MFCs.

No additional DSSN+ was added to either group. All MFCs were operated in connection to an external resistance of 10 kΩ.

Averaged current traces from triplicate devices are shown in Figure 4.2. One notes that the addition of DSSN+ to the O-MFCs results in a 6.0-fold increase in current production compared to control O-MFCs over the course of operation. When separated on day 3, one observes significantly higher current production in the A-MFCs containing DSSN+. Specifically, the peak current from DSSN+ containing A-MFCs was 4.2-fold larger than from the current generated by the control devices. These data indicate DSSN+ has a significant impact on the performance of cells attached on the electrode. Inspection of Figure 4.2 also shows a slight enhancement of the S-MFCs with DSSN+ addition. However, note that both control and test S-MFCs produce less than 0.5 μA. These results clearly relate the overall improvement in current production to the cells in physical contact with the electrode.

To visualize O-MFCs as the overall sum of A- and S-MFC, representative current contributions from the cells on the electrode and soluble species, respectively, are displayed as a stacked bar graph and compared to the total current in Figure 4.3. With DSSN+ modification, the sum of current generation from A- and S-MFCs is comparable to the O-MFCs, with the most appreciable current contribution originating from the A-MFCs. All of the control devices per-

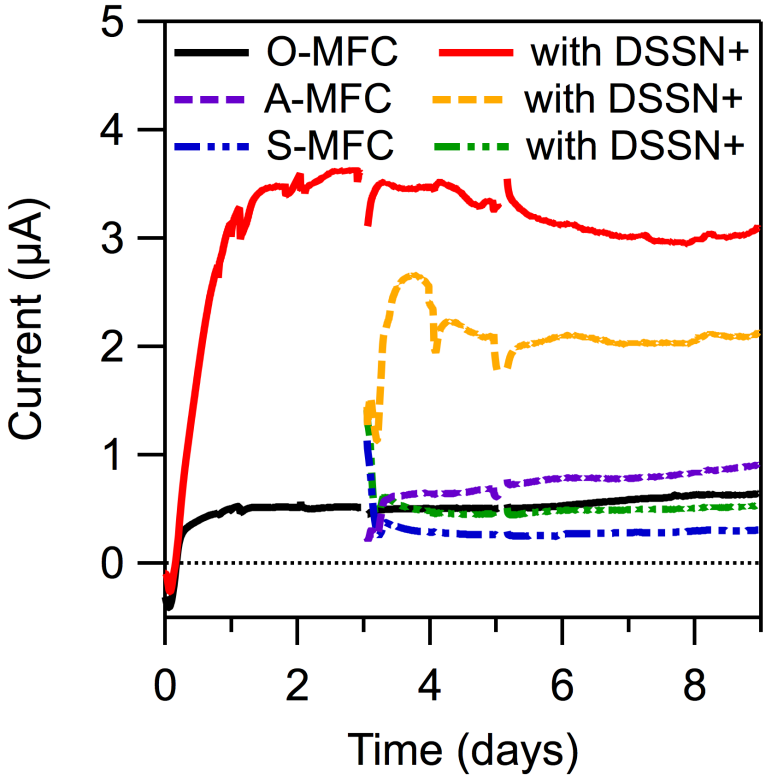

Figure 4.2: Average current generated as a function of time. Only O-MFCs with and without DSSN+ are present for the first three days. A group of O-MFCs are separated into A- and S-MFCs with and without DSSN+ at t = 3 days, while some O-MFCs are left in operation. Breaks in the traces at t = 5 days are due to polarization measurements. All measurements are an average of triplicates.

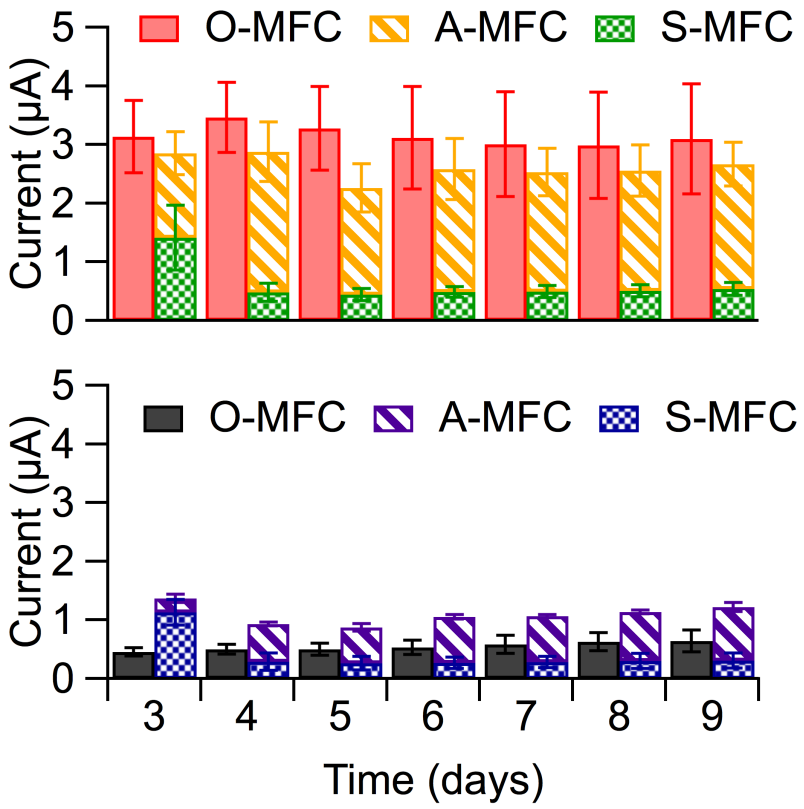

Figure 4.3: Bar graphs showing the averaged current generation at each day of the O-MFCs compared to the sum of A- and S-MFCs. Top: DSSN+ modified test devices. Bottom: control devices.

formed similarly, resulting in the sum of A- and S-MFCs to surpass the O-MFCs. These data suggest that DSSN+ enhances MFC performance by increased electron transfer occurring at the anode surface rather than through soluble cell components from the planktonic cell solution and highlights the importance of physical contact between cells and the electrode.

Polarization measurements were taken of each MFC on day 5; average power densities and the *i-V* curve are shown in Figure 4.4. DSSN+ increased the power density by ~10-fold in O-MFCs, 3.3-fold in A-MFCs and 2.3-fold in S-MFCs, following the same trend of improved power performance between devices as with improved current generation in DSSN+ modified devices. Internal resistances were calculated from the slopes of the polarization curves (Fig. 4.4b). Relative to the control group, the internal resistance decreased substantially with DSSN+ modification in the O- and A-MFCs, from 172 ± 0.5 and $169 \pm 11.2\,\mathrm{k}\Omega$ to 24.7 ± 5.1 and $57.3 \pm 20.4\,\mathrm{k}\Omega$, respectively. There was little different in the internal resistance between the control and DSSN+ S-MFCs. These data further support the conclusion that the increased MFC performance with DSSN+ is derived from the cells on the electrode surface.

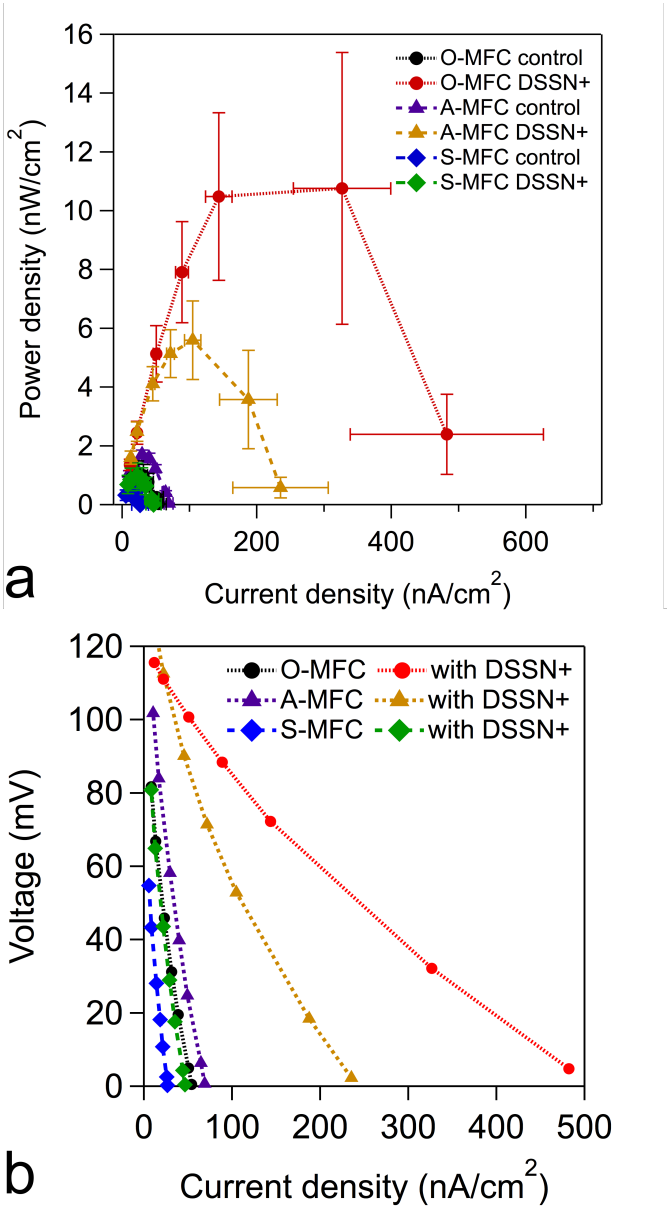

Figure 4.4: Polarization measurements from day 5 of the O-, A- and S-MFCs with and without DSSN+. (a) Calculated power densities and (b) *i-V* curves from control and test devices. All measurements are an average of triplicates.

Assessing the effect of DSSN+ on cell populations in U-tube MFCs

One possible mechanism to consider for the increased performance with DSSN+ is the increased presence of viable cells on the electrode surface. To assess this hypothesis, carbon felt anodes were examined using confocal microscopy. Electrodes were rinsed in PBS before imagining. For unmodified devices, cells were imaged by staining with 5 μM DAPI, a nucleic acid stain. In the case of DSSN+ containing electrodes, we utilized the intrinsic emission of DSSN+ for cell imaging. Cells stained with DSSN+ displayed emission patterns characteristic of membrane incorporation. To assess the viability of cells on the anode, all anodes were additionally stained with 5 μM propidium iodide (PI), which is used as an indicator for dead cells or cells with compromised membrane integrity. [207] The results of these staining methods for the test and control O- and A-MFCs are collected in Figure 4.5; the results from the test and control S-MFCs are displayed in Figure 4.8. Further imaging was performed using scanning electron microscopy (SEM) to confirm trends in electrode colonization and are shown in Figure 4.6. Additionally, optical densities were measured at 600 nm of the anode solutions to monitor planktonic cell growth, OD_{600nm} measurements are listed in Table 4.1.

Comparison of electrode cell coverage in Figures 4.5A and 4.5C shows no

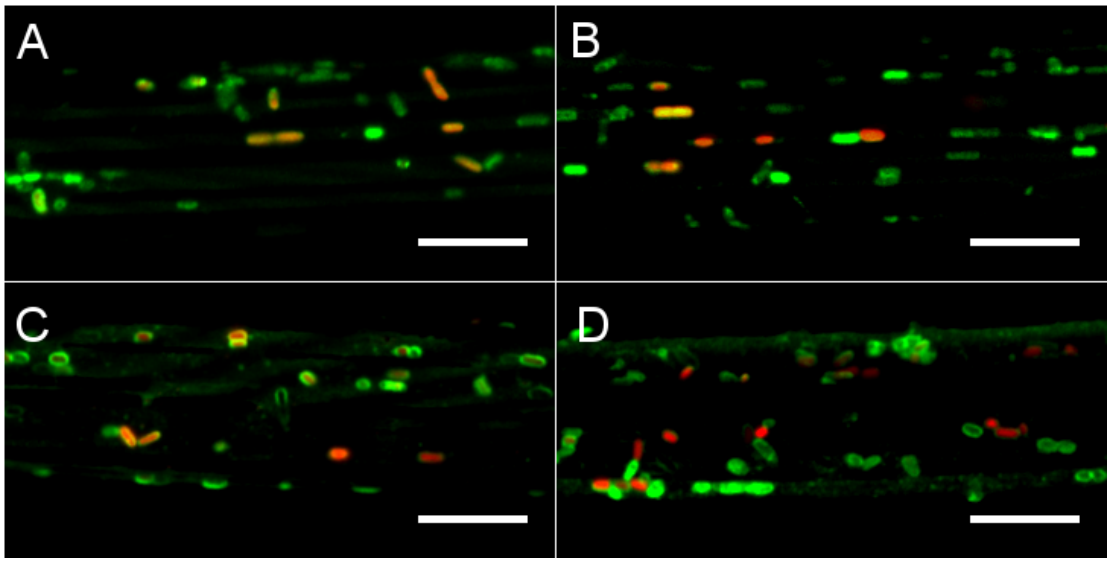

Figure 4.5: Representative confocal micrographs of graphite felt fibers from anodes after operation. O-MFC (A) and A-MFC (B) anode fibers from control groups are compared with O-MFC (C) and A-MFC (D) fibers from DSSN+ modified devices. No emission was detected without COE modification, therefore unmodified cells (A,B) were stained with 5 μM DAPI (green). All fibers were also stained with 5 μM propidium iodide (PI) to observe necrotic cells (red). Laser excitation was 405 nm with emission collected from 420–520 nm for DSSN+ and DAPI. Laser excitation was 559 nm with emission collected from 600–700 nm for PI. Scale bars are 10 μm.

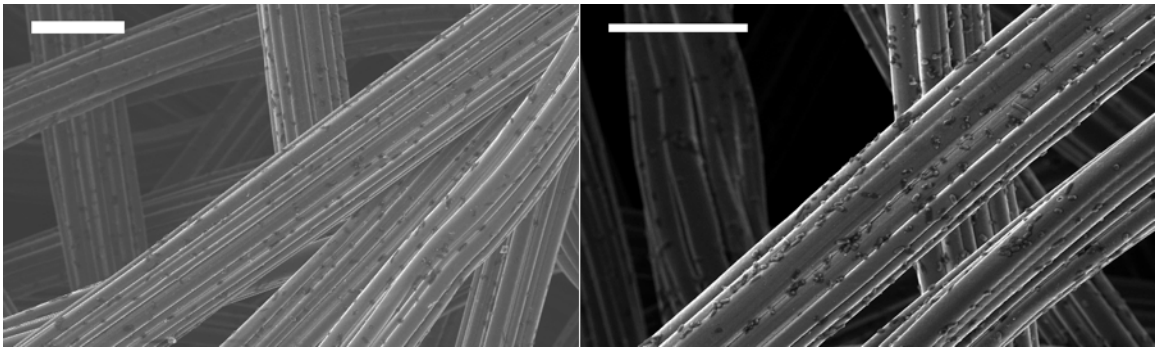

Figure 4.6: Representative SEM of anodes from O-MFCs at the end of operation: without (left) and with DSSN+ modification (right). Scale bars are 20 μm.

discernible difference between the control and DSSN+ modified O-MFCs. The same trend was observed in SEM imagine (Figure 4.6). The average OD_{600nm} of the control and test anode solutions from O-MFCs on day 3 showed no significant difference in planktonic cell growth at this time (Table 4.1). On day 10, the OD_{600nm} between control O-MFC and DSSN+ O-MFCs were still not significantly different. The similarity of cell densities in solution and on the electrode between control and DSSN+ devices suggest that the performance increase observed in Fig 4.2 and Fig. 4.4 is not due to an increase in cell growth in solution nor due to increased colonization on the electrode.

Similarly, in the control A-MFCs and DSSN+ modified A-MFCs, no discernible difference in colonization was observed under confocal microscopy, displayed in Figure 4.5. SEM imaging confirmed this observation (Figure 4.7). The

Table 4.1: OD_{600nm} measurements at day 3 from O-MFCs transferred with and without DSSN+ and day 10 from U-tube O-, A- and S-MFCs with and without DSSN+

	t = 3	t = 10		
Sample	O-MFC	O-MFC	A-MFC	S-MFC
Control	0.68 ± 0.04	0.60 ± 0.12	0.89 ± 0.08	0.58 ± 0.06
With DSSN+	0.65 ± 0.05	0.68 ± 0.01	0.79 ± 0.04	0.58 ± 0.06

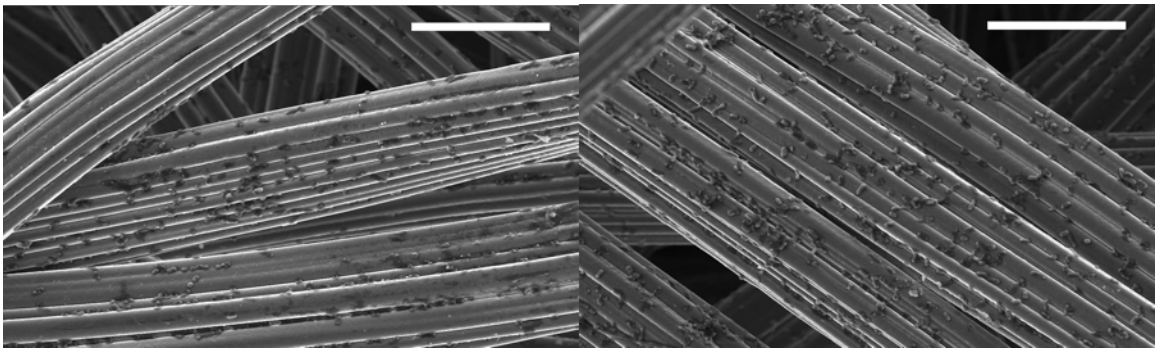

Figure 4.7: Representative SEM of anodes from A-MFCs at the end of operation: without (left) and with DSSN+ modification (right). Scale bars are 20 μm.

OD_{600nm} of the anode solution in control A-MFCs was significantly higher than in DSSN+ A-MFCs (Table 4.1). Although there was a clear difference in cell densities, this was not a positive effect on cell growth in the test group. Therefore, the hypothesis that DSSN+ improves current by increasing cell population in solution in A-MFCs is not supported.

Differences in cell colonization of the anodes were observed between the control and DSSN+ modified S-MFCs in both confocal microscopy and SEM (Figure 4.8 and 4.9, respectively); more cells were present at the electrodes with DSSN+. Although differences were observed, the improvement in performance was negligible compared to the O- and A-MFCs. Cell density in solution was consistent between control and test devices. OD_{600nm} of both control and DSSN+ anode solutions decreased from the OD_{600nm} measured on day 3 to 0.58 ± 0.06 on day 10, indicating some cell death has occurred.

In all cases, no significant difference was observed in PI fluorescence between the anodes with and without DSSN+ (Fig. 4.5 and 4.8), indicating cell death occurs at the same rate in DSSN+ modified cells as in untreated cells. Additionally, this observation signifies DSSN+ insertion does not permeabilize the inner membrane to allow for PI transport into the cytosol. In Chapter 3, we discussed the possibility that small macromolecule transport across the inner membrane may be effected by DSSN+. However, results of PI staining suggest

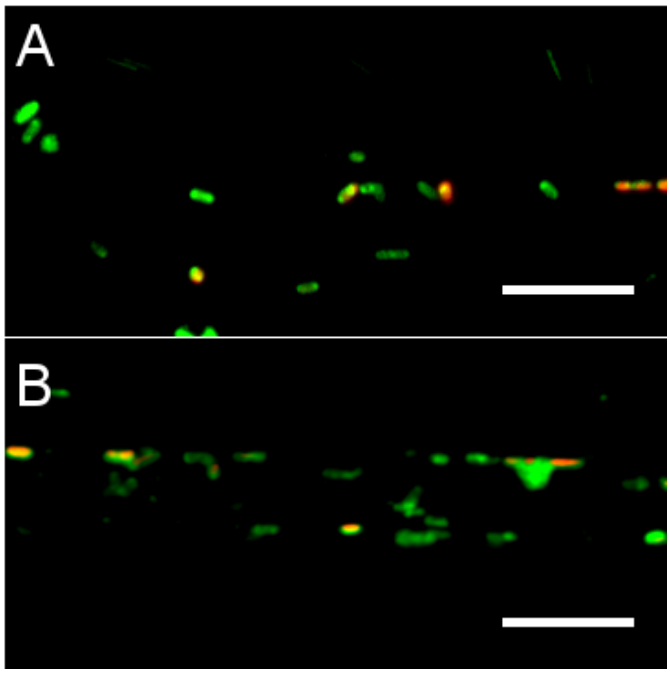

Figure 4.8: Representative confocal micrographs of graphite felt fibers from anodes of S-MFCs after operation. Anode fibers without DSSN+ modification were stained with 5 μM DAPI and 5 μM PI (A), DSSN+ modified fibers were stained with 5 μM PI (B). Scale bars are 10 μm.

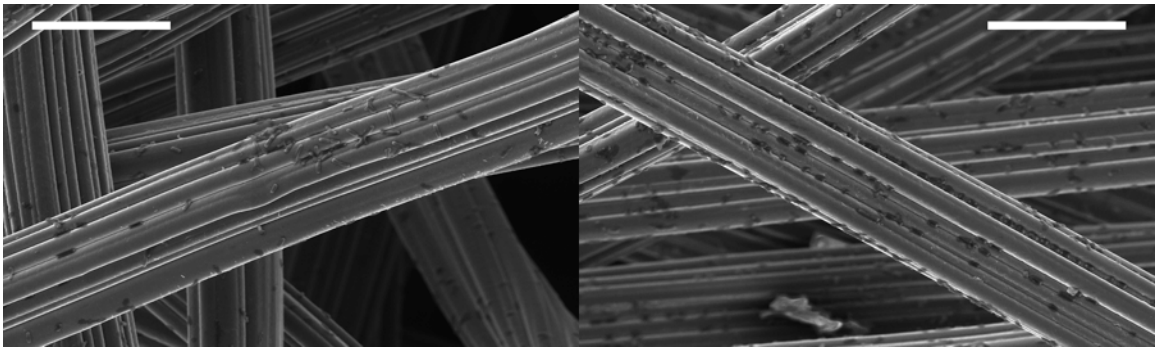

Figure 4.9: Representative SEM of anodes from S-MFCs at the end of operation: without (left) and with DSSN+ modification (right). Scale bars are 20 μm.

that DSSN+ has little effect on improving the transport of this molecule, which has a molecular weight of $\sim$ 668 Da.

It is important to note that for all imaging techniques, anodes were first rinsed with PBS. This process is necessary to fix cells for imaging, however it results in dislodging loosely attached cells from the electrode. Imaging of the electrodes by confocal and SEM did not show differences in cell populations on the electrode, but it is possible that differences may lie in loosely bound cells to the electrode. In order to probe the differences in viable, loosely bound cells, colony forming units (CFUs) were quantified from the cells dislodged from electrodes from O-MFCs after 3 days of operation. CFUs recovered from the anodes of control and DSSN+ modified devices were measured at $6.1\,(\pm 3.6) \times 10^8$ and $1.8\,(\pm 0.5) \times 10^9$ CFU/mL, respectively. This confirms the hypothesis that

DSSN+ affects the population of loosely bound cells to the electrode, however the ∼3-fold increase in CFUs does not correlate with the 10-fold increase in current observed in O-MFCs. This difference could potentially be resolved by the permeability effects DSSN+ has on the outer membrane of *E. coli*, as discussed in Chapter 3, considering LB is known to contain mediators. [95, 208] This hypothesis is further examined in the following section.

4.3.2 Performance in defined media bioreactors

In the previous section, we utilized a U-tube device configuration to determine the origin of performance improvement within cell populations separated into (i) cells on the electrode and (ii) cells and soluble components in solution. These experiments identified performance improvements from DSSN+ to rely on cells on the electrode. However, total cell population on the electrode may have not been accurately accounted for due to device constraints and cell preparation for imaging. It is possible that DSSN+ increases the cell population of loosely adhered to the electrode. Although the increase in CFUs from the DSSN+ modified electrodes did not correlate directly with the increase in current in DSSN+ MFCs.

Here, we utilize a two chamber bioreactor containing a reference electrode

in the anode chamber, sampling ports and use defined media as the electrolyte. By this modification of device configuration, we are able to examine the ability of DSSN+ to improve current production in the absence of exogenous mediators and more accurately assess cell populations in solution verses on the electrode. Additionally, we are able to investigate any changes in redox activity or the release of redox active molecules upon DSSN+ modification in situ.

Electrochemical characterization of DSSN+ modified *E. coli*

To understand how DSSN+ improves the current production of *E. coli* in the absence of exogenous mediators, we first compared the electrochemical behavior of *E. coli* with and without DSSN+ modification in defined media bioelectrochemical reactors. Triplicate bioelectrochemical reactors containing M9 media with 40 mM lactate and a graphite felt electrode poised at $+0.2\,V_{Ag/AgCl}$ were inoculated to an initial OD_{600nm} of 0.5 – 0.6 with *E. coli*. After inoculation, bioreactors produced a current that was $\sim 0.2\,\mu A$ higher than background levels. A concentrated solution of DSSN+ was added to a group of bioreactors at t = 3.6 h to reach final concentration of $10\,\mu M$, resulting in an immediate increase of $\sim 0.6\,\mu A$, a 2.3-fold improvement from untreated *E. coli* bioreactors (Figure 4.10). This immediate current response is consistent with the response of DSSN+ treated *S. oneidensis* observed in previous studies. [53] In both *E.*

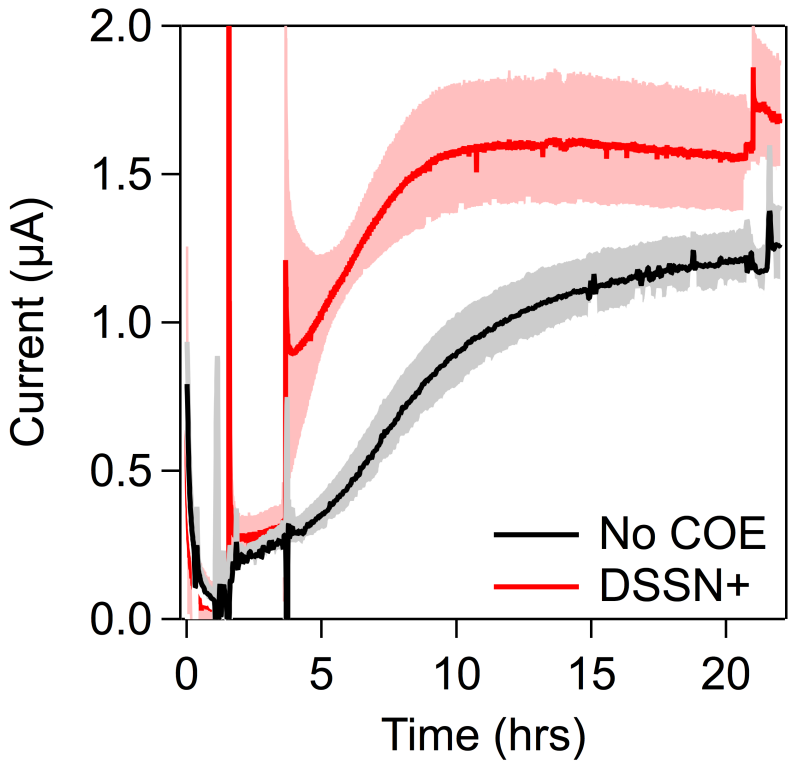

Figure 4.10: Increased current production of DSSN+ treated *E. coli* occurs instantaneously. Current production of untreated (black) *E. coli* and *E. coli* stained with 10 μM DSSN+ is displayed over time. Bioreactors were inoculated at t = 1.5 h and DSSN+ was added at t = 3.6 h. The most significant improvement to current production with DSSN+ is observed during first 24 h of operation, current differences between untreated and DSSN+ modified bioreactors are negligible afterwards. All values are means of triplicate bioreactors, shading shows area between highest and lowest traces.

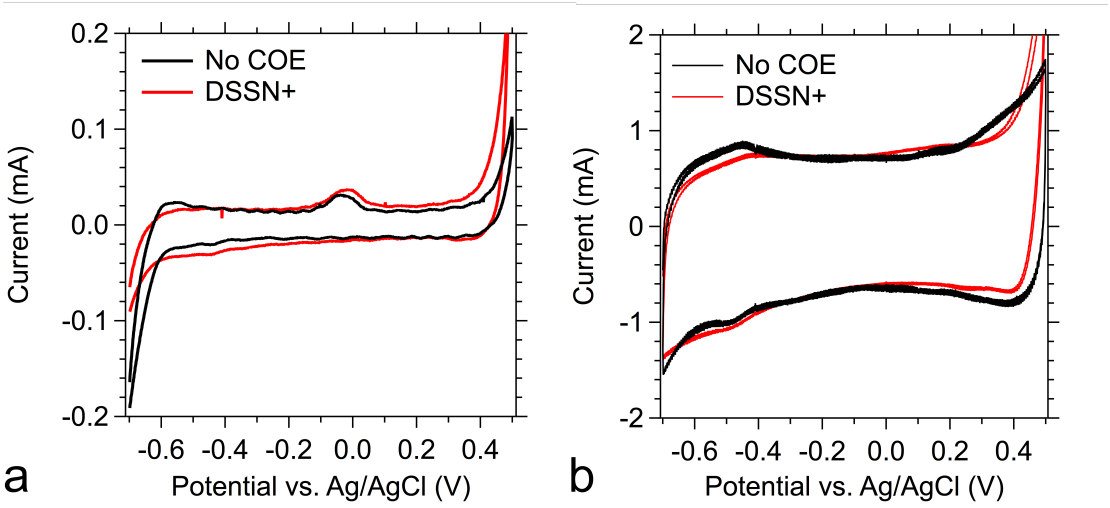

Figure 4.11: Representative cyclic voltammograms of *E. coli* defined media bioreactors without (black) and with 10 μM DSSN+ (red) scanned at (a) 2 mV/s and (b) 100 mV/s.

coli and *S. oneidensis* bioreactors, the current difference between reactors with and without DSSN+ decreased at the end of 24 h, however *S. oneidensis* was not monitored past that time. After t = 72 h, the current of DSSN+ modified *E. coli* bioreactors is within standard deviation of the current produced by untreated *E. coli* bioreactors (data not shown). These results indicate that the main enhancement to current production occurs immediately after DSSN+ addition and this improved performance may not be sustainable in these device configurations.

In order to determine whether or not the increase in current generated by DSSN+ addition is due to an alternative redox mechanism or released redox

active components extracellularly, cyclic voltammetry was performed. Representative cyclic voltammograms of bioreactors with and without DSSN+ are displayed in Figure 4.11. A slow scan rate of 2 mV/s, we expect to examine the catalytic activity of the cells. However, *E. coli* is not naturally electrogenic and has a limited ability to respire on lactate, thus the resulting cyclic voltammogram of unmodified *E. coli* shows negligible catalytic activity. DSSN+ does not appear to effect the catalytic ability of *E. coli* in Figure 4.11a. At a higher scan rate of 100 mV/s, mass-transfer limited reactions are probed, where oxidation at the electrode would be faster than the biological reduction reaction. In this regime, if redox active intracellular species were released from the cells, we would expect to see resulting peaks. However, as in the slower scan rate CV, little difference is observed between reactors with and without DSSN+ (Figure 4.11b). From these CVs, we can conclude that DSSN+ has little to no effect on redox activity and redox species in *E. coli*. Though, it should be noted that CV is not the most accurate method for mediator identification. [209] To accurately identify release of mediators, future spectroscopic analysis should be performed.

Assessing the effect of DSSN+ on cell populations in bioreactors

From Figure 4.12(a) and (b), one notes that the solution in the bioreactors at the time of DSSN+ addition (t = 3.6 h) is visibly turbid due to the high optical density of cells. Along with the immediate increase in current due to DSSN+ addition, it is apparent that DSSN+ affects cell aggregation on the electrode after overnight operation. At t = 12 h, comparison between Figure 4.12 (c) and (d), one notes a decrease in turbidity in DSSN+ modified reactors, with visible cell mass aggregating on the carbon felt electrode. Optical density measurements throughout the course of operation confirm that DSSN+ removes cells from solution at a considerably faster rate than cells inherently fall out of solution, as shown in Figure 4.13. Similar to the difference seen in current generated, the difference in OD_{600nm} between untreated and DSSN+ modified bioreactors is most notable on day 1.

Since we did not see any changes in redox activity with DSSN+ addition, we hypothesize that increased current is likely due to increased cell density on the electrode. To determine whether the increased current produced by DSSN+ modified *E. coli* was due to a greater amount of cells at the electrode, we compared the current recorded as a function of the percent of cells on the electrode from the original inocula from bioreactors with and without DSSN+, calculated

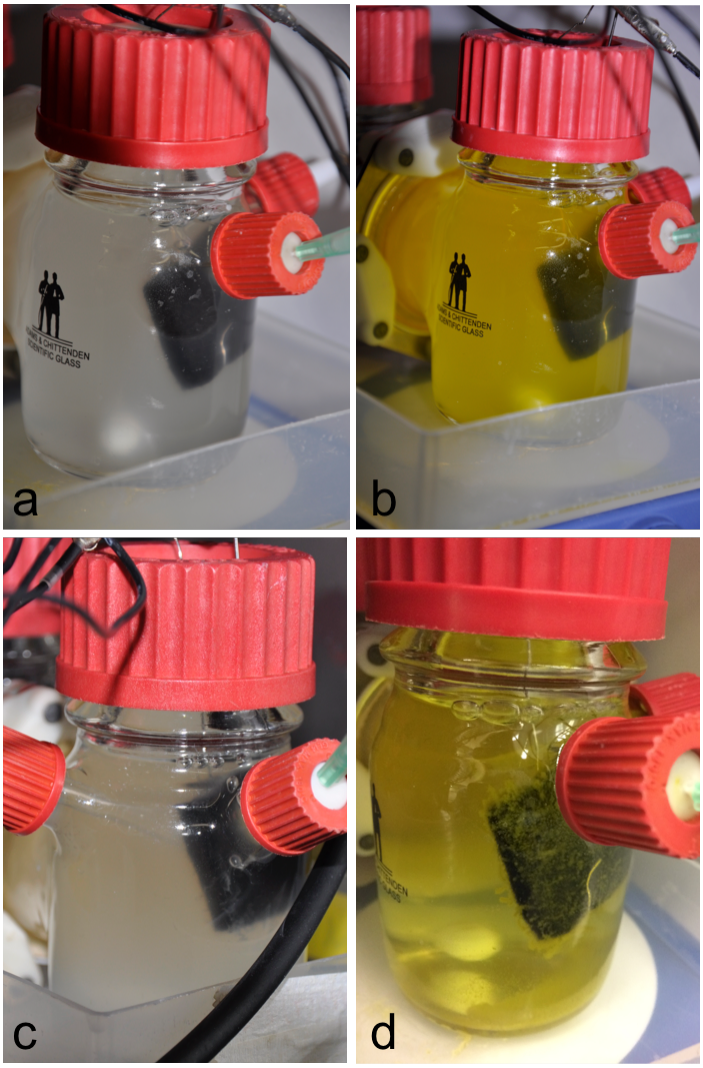

Figure 4.12: Photographs of bioreactors at time of DSSN+ addition (t = 3.6 h) and at t = 12 h. At t = 3.6 h, bioreactor solutions were visibly turbid at $OD_{600nm} = 0.55 \pm 0.04$ for all (a) untreated and (b) DSSN+ treated bioreactors. After overnight operation (t = 12 h) solutions from (c) untreated bioreactors were still visibly turbid, while solutions from (d) DSSN+ modified bioreactors were visibly less turbid with cell mass adhered to electrodes.

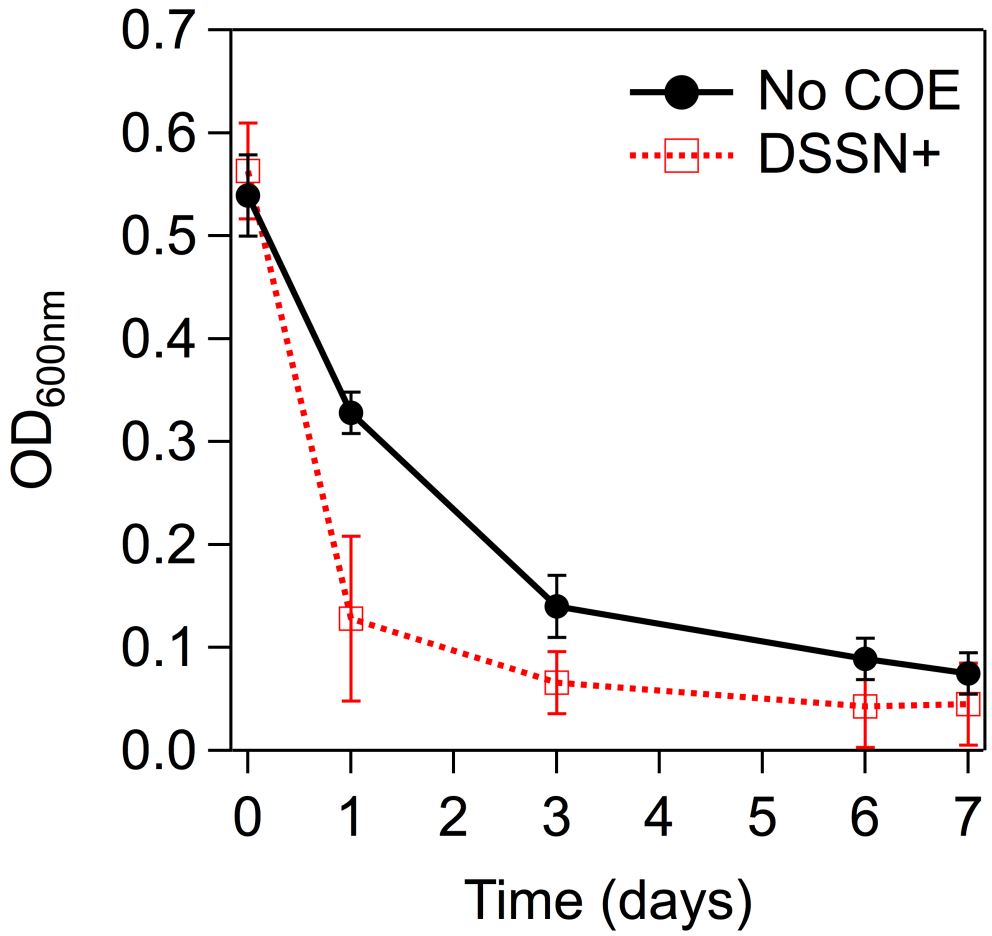

Figure 4.13: Optical density of bioreactor solutions measured at 600 nm over time, representing the rate of cells being removed from solution and adhering to the electrode with (red) and without (black) DSSN+. Measurements are an average of triplicates, error bars display standard deviation.

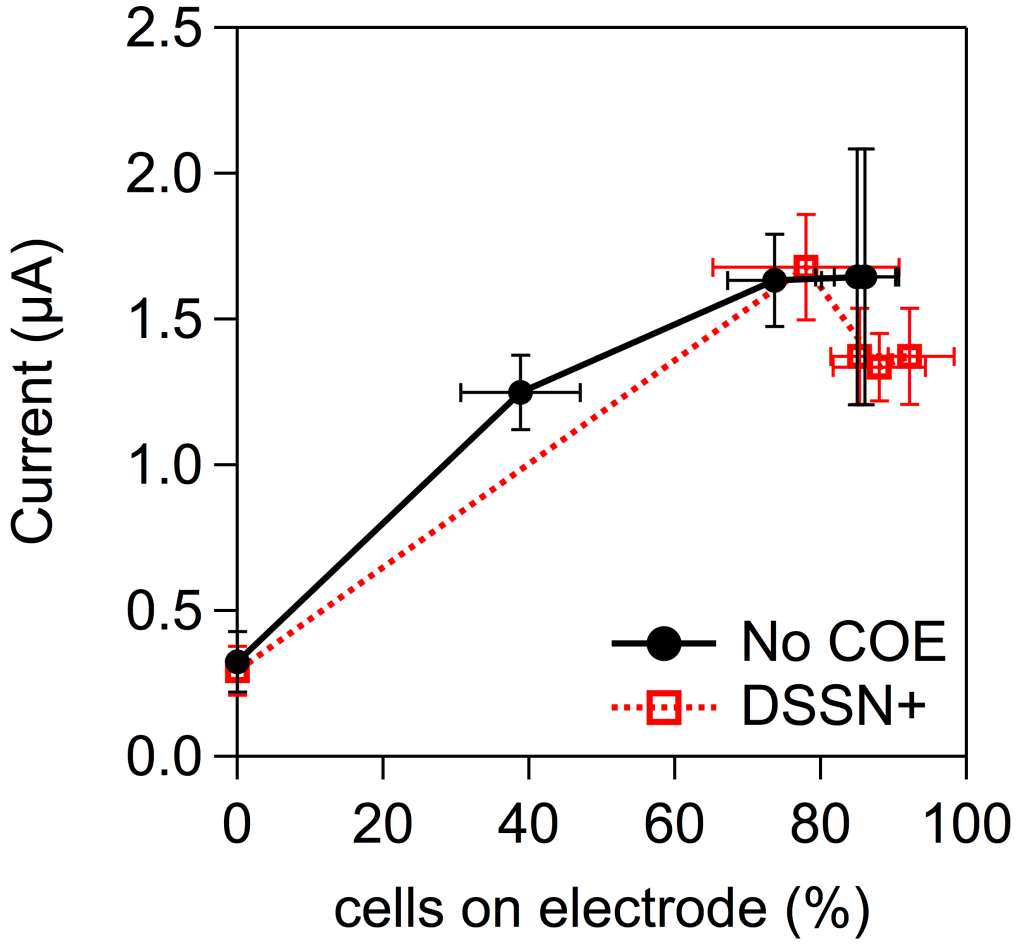

Figure 4.14: Current generated of bioreactors with (red) and without (black) DSSN+ displayed as a function of the percent of cells estimated on the electrode. All measurements are in triplicate, with error bars displaying standard deviation.

as:

$$cells\,on\,electrode(\%) = \frac{OD_0 - OD_t}{OD_0} \times 100$$

where OD_0 and OD_t are the measured OD_{600nm} of the inoculum and of the bioreactor solution at time t of the current measurement, respectively. This calculated current per cells on electrode is displayed in Figure 4.14. One notes that the overall trend of current per cell percent follows the same overall trend with and without DSSN+. These observations indicate that DSSN+ contributes significantly to graphite binding and therefore enhanced adhesion is the direct cause of increased current production by the DSSN+ modified *E. coli* under these conditions.

At the end of device operation, we aimed to directly quantify cell mass on electrodes using total protein content to better characterize the increase in cell adhesion with DSSN+. However, during device operation, we observed that the DSSN+-modified cell mass on the electrode was easily disturbed, indicating that cell adhesion to the electrode was weak. As mentioned previously, we hypothesize that DSSN+ affects cell populations loosely adsorbed onto the electrode. To characterize the cell populations (i) adhered to the electrode, (ii) loosely adsorbed to the electrode, and (iii) in solution, we performed the bicinchoninic acid (BCA) total protein assay at the end of device operation. Before devices were removed from operation, samples were carefully taken and total

Table 4.2: Bicinchoninic acid (BCA) assay of DSSN+ treated and untreated *E. coli* bioreactors measuring total protein content from cells adhered on electrodes, cells loosely bound to the electrode and cells in solution. Values are averages of triplicate measurements with standard deviations.

Total protein content (g)		
Sampling location	**Untreated**	**DSSN+**
Electrodes	5.6 ± 0.5	2.1 ± 0.2
Loosely bound to electrodes	0.5 ± 2.8	8.5 ± 1.6
Solution	5.1 ± 1.1	4.0 ± 1.3
Sum of total protein	11.2 ± 4.4	14.6 ± 3.1

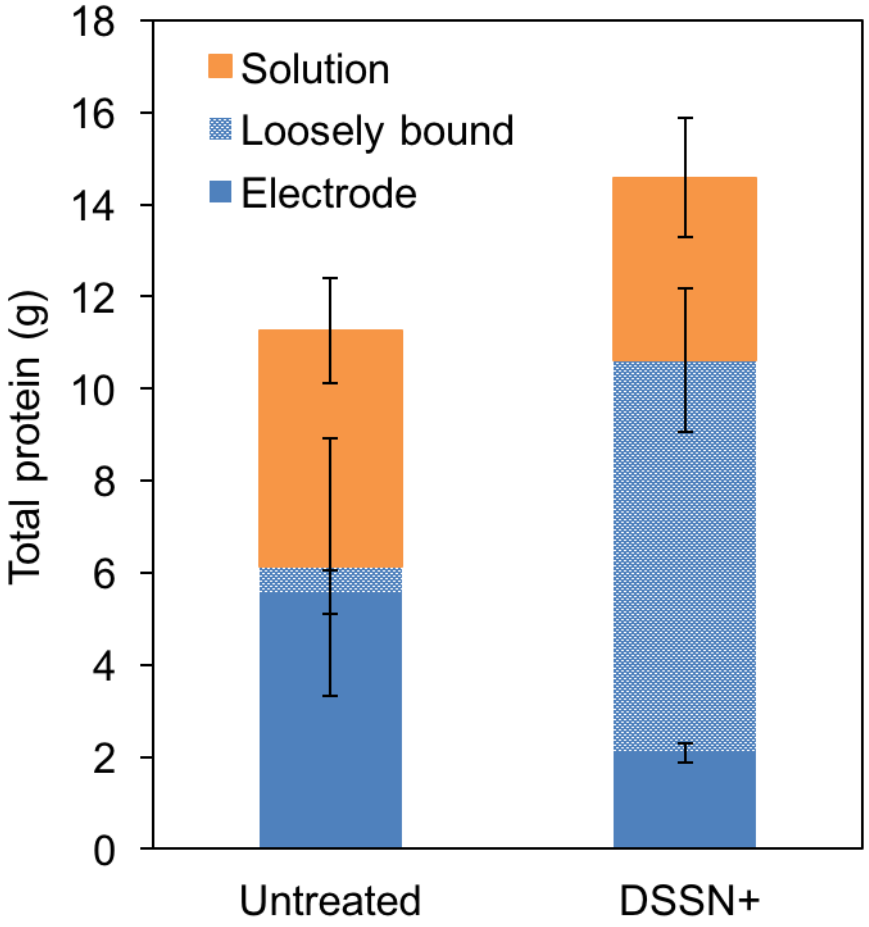

Figure 4.15: Bar graph displaying total protein content in bioreactors from cells adhered on electrodes (dark blue), cells loosely bound to electrodes (patterned blue) and cells in solution (orange). All measurements are averages of triplicates, error bars are standard deviations.

protein content was measured as a representation of the planktonic cell population. Once devices were removed from operation, they were were disturbed by shaking in order to remove loosely adsorbed cell mass from the electrode. Total protein of loosely adsorbed bacteria was quantified as the difference between the total protein of samples after shaking and the total protein in solution. Lastly, total protein content of the electrodes were quantified. Results from this assay are displayed in Figure 4.15 and Table 4.2.

The sum of the total protein content from all cell populations between bioreactors with and without DSSN+ were within error of one another, indicating that cell growth was not significantly influenced by the presence of DSSN+. Protein content measured of the solutions in DSSN+ treated and untreated reactors were within standard deviation, which is consistent with the OD_{600nm} measurement in Figure 4.13, indicating little difference in the planktonic cell count. Protein measured from untreated electrodes was $>$2-fold greater than DSSN+ treated electrodes. Meanwhile, there was a 16-fold increase in the protein content of cells loosely bound to electrodes with DSSN+ compared to the protein content of loosely bound, untreated cells on the electrode. From these results, it is apparent that DSSN+ affects cell-cell and cell-electrode interactions. These interactions have little influence over the current generation at the end of device operation.

The observation that DSSN+ altered cell-cell and cell-electrode interactions is consistent with our previous observations of COEs effects on cell surface properties, discussed in Chapter surfaceprop. It is important to note that in this case, electrostatic attraction of cells to the positively poised electrode does not favor DSSN+ modified cells over untreated cells, due to DSSN+'s ability to neutralize surface charge. [60] The relationship between surface charge and cell adhesion has been utilized to explain increased cell adhesion in net negative charged cells on surfaces. [91, 156] It is therefore possible to attribute this preference of cell-cell interactions in DSSN+ modified cells to the increase in cell hydrophobicity, which was also shown to influence autoaggregation. Thus, it is plausible to attribute the instantaneous increase in current observed to the spontaneous intercalation of COEs into cells and modification of cell surface properties, which would have the most significant effect on current generation at the beginning of device operation. Towards the end of operation, we expect cell adhesion past the total surface coverage of the electrode would no longer influence current generation. This is a plausible hypothesis for the current response with see in DSSN+ treated *E. coli*.

4.4 Conclusions

This work embodies an improvement in elucidating how DSSN+ impacts the increased current and power generation in *E. coli* MFCs. In U-tube MFCs, DSSN+ modification resulted in a 6-fold increase in current and a 10-fold increase in power. This increase in performance originates from the cells on the electrode, which was probed by transferring the anodes from operational MFCs into a new A-MFCs. This resulted in a 4.2-fold increase in current and 3.3-fold increase in power in DSSN+ modified anodes. Enhancements were observed in the S-MFCs, but to a much lesser extent, indicating that the primary improvement to current was not due to released redox active species from the cells with DSSN+ intercalation. This result is not surprising because it is well known that *E. coli* does not produce shuttles. It is inconclusive whether or not the permeabilization of cells by DSSN+ results in the increased current, as this device configuration is limited in its ability to probe electrochemical mechanisms.

In an attempt to separate direct and indirect electron transfer processes into biofilm (A-) versus planktonic (S-) cell MFCs, it was found that A-MFCs containing cells on the electrode had the highest performance improvement comparatively. Unfortunately, this result does not confirm that this improvement is due to increased direct electron transfer, as other mechanisms are still possible, i.e.

increase cell adhesion. In U-tube MFCs, increased cell adhesion on the electrode was not observed via microscopy techniques, however CFU assays indicate that DSSN+ may potentially be increasing loose cell adhesion to the electrode. It should also be noted that an attached biofilm can more effectively utilize intracellular components as an electron shuttle than planktonic cells. Therefore, the biofilm versus planktonic cell study is not evidence for direct electron transfer.

Electrochemical analyses can readily discriminate between direct electron transfer to an electrode and electron transfer with a shuttle. A similar experiment was performed in three-electrode, two chamber bioreactors using a defined media. Increased current was observed in DSSN+ modified *E. coli* instantaneously upon addition. This improvement was not sustainable over time. Using cyclic voltammetry, electrochemical mechanisms were probed. Alternative redox pathways, released intracellular redox species and an improved catalytic current investigated was not observed in DSSN+ treated cells. It was obvious that DSSN+ effects cell adhesion to the electrode, as an aggregated cell mass was visible on the carbon felt electrode. Quantification of cells in solution compared to on the electrode indicated that current production was directly correlated to the amount of cells on the electrode, and that DSSN+ increased cell adhesion. Last, adhesion of DSSN+ treated cells to the electrode was weak, indicating a preference of cell-cell interactions over cell-electrode interactions.

Chapter 5

Summary and future outlook

5.1 Current understanding of conjugated oligoelectrolytes

We have explored in depth and presented an understanding of the effects of COEs on both the membrane properties of *E. coli* and performance of *E. coli* MFCs. COEs were originally designed for molecular wire functionality across lipid bilayers, thus motivating application in MFCs for increasing current and power generation. In this thesis, other hypotheses for the origin of improved MFC performance were investigated. In Chapter 2, we found that COEs modulate cell surface charge and hydrophobicity. Whereby COEs with longer molec-

ular dimensions effect surface properties to a greater degree than shorter COEs. COE association with *E. coli* was quantified and challenged our original assumptions of COE situation within the cell. It is morphologically impossible for the number of COEs associated with cells to be fully intercalated in the cell membrane while maintaining viability. The ability of COEs to modify surface properties suggests that cell-cell and cell-electrode interactions may play a role in increasing MFC performance.

In Chapter 3, we investigated membrane permeabilization by DSSN+ as a possible mode of action COEs may have on *E. coli* that would influence bioelectrochemical performance. We found that DSSN+ is acting as an outer membrane permeabilizer, however specific effects on the inner membrane are still unclear. DSSN+ did not significantly permeabilize the inner membrane for the release of the cytoplasmic enzyme β-galactosidase. The release of smaller molecules from the cytoplasm has yet to be investigated.

In Chapter 4, we examined the mechanism for improved electrochemical performance of DSSN+ modified *E. coli* in a variety of device configurations. Improved performance by DSSN+ was shown to arise from cells adhered to the electrode, while little to no effect was observed on redox activity. It is likely that COEs affect bioelectrochemical performance by multiple modes of action. By modification of surface properties, we observe increased cell adherence to

electrodes resulting in an increase in current production. Increasing membrane permeability allows for improved mediator transport in systems containing redox mediators, such as found in LB media used in U-tube MFCs, which could also improve performance.

These improvements in understanding the modifications of bacterial membranes by COEs pivot future applications towards those where increasing membrane permeability would be most beneficial. For the overall goal of understanding the functionality of these molecules in microbial systems for the rational design of novel membrane-intercalating molecules based on COEs, further understanding of molecular interactions with the cell and on cell behaviors are needed. Future applications and areas of investigation are briefly discussed below.

5.2 Future outlook and applications

5.2.1 Characterization of membrane permeability effects

Conjugated oligoelectrolytes (COEs) have been demonstrated to have a significant effect on the permeability of the outer membrane in gram-negative bacteria, however elucidation of effects on the inner membrane is not well estab-

lished. Further characterization of the influence of COE structure on membrane permeabilities as well as the transport of molecules across the inner and outer membrane is needed for the determination of specific applications of COEs for the improvement of biocatalysis reactions.

We have thus determined that DSSN+ is acting as an outer membrane permeabilizer. For inner membrane permeability effects, we observed less than a 2% release of the total cytoplasmic enzyme target in *E. coli*. When considering the difference between the outer membrane and inner membrane permeability, its important to consider that they were probed by the examination of differently sized proteins. With a molecular weight of 465 kDa, β-galactosidase is $\sim$5 times larger than alkaline phosphatase (M.W. = 89 kDa). [182–184, 190, 191] It is possible that these differences in permeability may be size dependent. and do not reflect intrinsic changes in membrane structure. At this point, we do not have definitive proof that DSSN+ is permeabilizing or, to what extent, even reaching the inner membrane.

That DSSN+ has a significant impact on outer membrane permeability suggests that COEs may be suited for a wide range of whole-cell application. Characterization of the extent of this permeability effects is needed in order to best determine the possible applications of these molecules; for example, the range of macromolecular sizes that can be transported, what extent the inner mem-

brane is affected and the effect of COE structure on membrane permeability.

Investigation of COE molecular structure on outer and inner membrane permeability

Section 3.5 began investigating this subject looking at the overall ONPG turnover in *E. coli* modified with COE1 and COE2 series molecules. Other structural variables can be studied, such as the composition of the backbone and the functionality and number of pendant linkage groups. Characterization of the inner and outer membrane permeability of *E. coli* modified with COE1 and COE2 series is still needed. This can be performed by monitoring extracellular activity of alkaline phosphatase for the determination of outer membrane permeability, and extracellular activity of β-galactosidase for inner membrane permeability, as previously described in Chapter 3.

Examination of permeabilization of *E. coli* is needed in greater detail. The overall level of release protein should be characterized more globally and with the size-dependence of release. To quantify the overall amount of protein released by COE exposure, one can use the bicinchoninic acid assay as well as SDS-Page. The relative abundance of different sized proteins in the media from fully lysed cells, COE treated cells, osmotically shocked or freeze/thaw treated

cells and intact cells can thus be characterized to give a better idea of the extent of COE-induced permeabilization.

Investigation of the size-dependence of released cytoplasmic proteins can be performed utilizing colorimetric and fluorescent assays. Lactate dehydrogenase is a cytoplasmic enzyme with a molecular weight of 114 kDa and the extracellular activity of this enzyme can be monitored using the Pierce LDH Cytotoxicity Assay Kit. Similarly, β-glucuronidase is a cytoplasmic enzyme (MW = 290 kDa) that catalyzes hydrolysis of β-D-glucuronic acid. Quantifying the amount of this enzyme released can be measured by fluorescence spectroscopy, which would monitor the hydrolysis of 4-methylumbelliferyl β-D-glucuronidase into a fluorogenic product. Additionally, engineered strains of *E. coli* expressing green or red fluorescent protein ($\sim$28 kDa) in the periplasm and/or the cytoplasm can be utilized to characterize permeability by the release of GFP/RFP into the media. Confocal microscopy may also be used to examine the dynamics of COE insertion and GRP/RFP release simultaneously. With these assays, one could probe the release of intracellular molecules ranging from 28 kDa to 465 kDa, which would provide a measure of enzymes that can be transported out of the cell by COE modification for specific biocatalysis applications.

5.2.2 How do COEs influence cell physiology?

Little is known about COEs influence on the physiology of microorganisms, apart from viability, which differs in effect between gram-negative and gram-positive microorganisms. [57, 210] It is known that the bacterial cell surface is particularly important in regard to maintaining optimal cell function. [133] The bacterial cell surface is involved in disparate physiological functions such as envelope diffusion, shape maintenance, growth and division, turgor support, chemical sensing and protection from both chemical and physical damage to the cell. Bacteria invest a major part of their metabolic energy for the maintenance of the cell surface. [211] Chemical and physical modification of the cell surface can thus have profound effects on their physiology. A better understanding of COE action may allow control over a wide range of biological processes pertinent to biotechnology as well as the rational design of molecular structures for specific applications.

Do COEs induce a stress response?

It is possible that COE intercalation may induce a stress response specific to the cell envelope, which may have profound influence over energy metabolism and membrane integrity. *E. coli* has been intensively investigated in relation

to stress responses and provides an ideal model to observe the response to COE modification. Five major envelope stress responses have been identified in this organism: the σ^E, Cpx, Rcs, phage-shock protein (Psp) and Bae responses. [212] In studies examining the stress response induced by carbon nanotubes, an up-regulation of σ^s and σ^E were observed, as well as up-regulation in genes relating to glycolysis, fatty acid beta-oxidation, fatty acid biosynthesis, the Tol/Pal system and the PhoPQ two-component system. [213] Another study examining the response of *E. coli* to cationic nanomaterials discerned gene clusters in the lipopolysaccharide biosynthetic pathway, outer membrane transport channels, ubiquinone biosynthetic pathways, flagellar movement, and DNA repair systems as significant to the bacterial response. [214] Both of these previous studies indicate the breadth of cellular processes that can be affected by nanomaterial interactions. To understand the response of *E. coli* to COE exposure, transcriptomic analysis could be performed by either microarray analysis or next generation sequencing.

Is increased current related to metabolic changes?

While COEs have been attributed the ability to link cellular metabolism to electrodes, this effect has yet to be demonstrated in *E. coli* MFCs. Although unlikely considering our presented results, to determine whether COEs are en-

abling a metabolic connection between the intracellular state and extracellular electron transfer, the metabolic activities of *E. coli* should be examined during device operation to test this alternative hypothesis. The alternate hypothesis is that COEs increase current production due to either by a differential oxidation of substrate or a more rapid catabolism of a substrate. It is most likely that rapid catabolism is the case, considering the improved rate of biocatalysis presented in Chapter 3, however changes in cell metabolism are still possible.

Under anaerobic conditions with lactate as the sole carbon source, *E. coli* is limited in its ability for anaerobic respiration and cannot ferment. In these conditions, it is likely that *E. coli* generates ATP and maintains redox balance using an alternative metabolism, such as overflow metabolism. Overflow metabolism allows for the production and reduction of reduced metabolic products, such as ethanol, to mitigate redox balance in the cell. [215, 216]

Previous work has demonstrated that a synthetic conduit for electron transfer can be engineered into *E. coli* through the expression of the Mtr pathway proteins found in *Shewanella oneidensis*, which is shown to couple lactate oxidation to current production. [91] The ability of this strain, referred to as *cymA-mtr E. coli*, to utilize lactate under these conditions is likely due to their ability to access the electrode as an electron acceptor via the Mtr pathway. Under the hypothesis that COE modification increases electron transfer to the electrode, a similar ef-

fect shift in metabolic products would be observed. Investigations of the *E. coli* metabolism has shown that the production of formate and ethanol under anaerobic conditions are caused by a high NADH:NAD+ ratio. [216] Alternatively, increased acetate production and decreased formate and ethanol production are evidence to enhanced oxidation of NADH. [217] The same shift is observed in *cymA-mtr E. coli*, suggestive of increased NADH oxidation and improved redox balance. Similarly, if COEs are enabling *E. coli* to utilize the electrode, we expect to see a similar shift in metabolite production. Currently, no significant evidence of shifts in metabolite production has been observed (data not shown). An area of study left unexamined is the bioenergy utilization/production by COE modified bacteria in order to determine the electron balance in the system. Consideration should be taken when choosing the appropriate carbon source in such experiments.

5.2.3 COE interactions with membrane components

The quantification of COE association with *E. coli* in Chapter 2 suggests that COEs are associating with cells in additional situations other than membrane intercalation. Other situations of COE association with the cell could include, but are not limited to, aggregation on the cell surface or interactions with the

LPS layer. COE disruption of the LPS layer, or removal of LPS from the outer leaflet, are effects that need to be considered. The effects of removing LPS from the outer membrane are inline with the surface property effects of COEs. LPS removal by cationic peptides and surfactants have also shown to render cells more hydrophobic and facilitate uptake of lipophilic carbon substrates. [159, 218, 219]

5.2.4 Future applications

The ability of COEs to increase membrane permeability while maintaining cell viability has promising applications in a wide range of biotechnologies, such as improving the rate of microbial catalysis, recombinant protein recovery, and increasing antibiotic susceptibility. Use of whole cells as biocatalysts is advantageous in processes requiring cofactors and/or multiple enzymatic steps, but the cell envelope is limiting as it provides a permeability barrier for the substrate and product, resulting in low productivities in whole-cell catalytic reactions. *E. coli* is a poor secretor of proteins, but is widely used for recombinant protein production and metabolic engineering. [220] Release of periplasmic proteins by COEs suggests possible application towards extracellular recombinant protein production, with the possibility of mitigating issues in protein purification

and cell toxicity seen in solvent of detergent treatments. [185] Gram-negative bacteria are resistant to a large number of antibiotics due to the effective permeability barrier function of their outer membrane. [159, 160] Application of COEs in combination with antibiotics typically unable to penetrate the outer membrane is a possible method to improve antibiotic susceptibility.

Bibliography

[1] Hengjing Yan, Chelsea Catania, and Guillermo C Bazan. Membrane-Intercalating Conjugated Oligoelectrolytes: Impact on Bioelectrochemical Systems. *Advanced Materials*, 27(19):2958–2973, April 2015.

[2] James T Fleming. Electronic Interfacing with Living Cells. In *Whole Cell Sensing Systems I*, pages 155–178. Springer Berlin Heidelberg, Berlin, Heidelberg, May 2009.

[3] Caroline M Ajo-Franklin and Aleksandr Noy. Crossing Over: Nanostructures that Move Electrons and Ions across Cellular Membranes. *Advanced Materials*, 27(38):5797–5804, April 2015.

[4] Bruce E Logan. Exoelectrogenic bacteria that power microbial fuel cells. *Nature Reviews Microbiology*, 7(5):375–381, May 2009.

[5] Feng Zhao, Robert C T Slade, and John R Varcoe. Techniques for the study and development of microbial fuel cells: an electrochemical perspective. *Chemical Society Reviews*, 38(7):1926, April 2009.

[6] Luo Peng, Shi-Jie You, and Jing-Yuan Wang. Carbon nanotubes as electrode modifier promoting direct electron transfer from Shewanella oneidensis. *Biosensors and Bioelectronics*, 25(5):1248–1251, January 2010.

[7] Yang-Chun Yong, Xiao-Chen Dong, Mary B Chan-Park, Hao Song, and Peng Chen. Macroporous and Monolithic Anode Based on Polyaniline Hybridized Three-Dimensional Graphene for High-Performance Microbial Fuel Cells. *ACS Nano*, 6(3):2394–2400, March 2012.

[8] Korneel Rabaey and Willy Verstraete. Microbial fuel cells: novel biotechnology for energy generation. *Trends in Biotechnology*, 23(6):291–298, June 2005.

[9] Korneel Rabaey and René A Rozendal. Microbial electrosynthesis — revisiting the electrical route for microbial production. *Nature Reviews Microbiology*, 8(10):706–716, October 2010.

[10] Korneel Rabaey, Peter Girguis, and Lars K Nielsen. Metabolic and practical considerations on microbial electrosynthesis. *Current Opinion in Biotechnology*, 22(3):371–377, June 2011.

[11] Fernando Patolsky, Brian P Timko, Gengfeng Zheng, and Charles M Lieber. Nanowire-based nanoelectronic devices in the life sciences. *MRS Bulletin*, 32(2):142–149, February 2007.

[12] Nicholas A Kotov, Jessica O Winter, Isaac P Clements, Edward Jan, Brian P Timko, Stéphane Campidelli, Smita Pathak, Andrea Mazzatenta, Charles M Lieber, Maurizio Prato, Ravi V Bellamkonda, Gabriel A Silva, Nadine Wong Shi Kam, Fernando Patolsky, and Laura Ballerini. Nanomaterials for Neural Interfaces. *Advanced Materials*, 21(40):3970–4004, October 2009.

[13] Diego Ghezzi, Maria Rosa Antognazza, Marco Dal Maschio, Erica Lanzarini, Fabio Benfenati, and Guglielmo Lanzani. A hybrid bioorganic interface for neuronal photoactivation. *Nature Communications*, 2(1):164–7, January 2011.

[14] Byung Hong Kim, In Seop Chang, Geun Cheol Gil, Hyung Soo Park, and Hyung Joo Kim. Novel BOD (biological oxygen demand) sensor using mediator-less microbial fuel cell. *Biotechnology letters*, 25(7):541–545, April 2003.

[15] Avinash Shantaram, Haluk Beyenal, Raaja Raajan Angathevar Veluchamy, and Zbigniew Lewandowski. Wireless Sensors Powered by Microbial Fuel Cells. *Environmental Science & Technology*, 39(13):5037–5042, July 2005.

[16] Leonard M Tender, Sam A Gray, Ethan Groveman, Daniel A Lowy, Peter Kauffman, Julio Melhado, Robert C Tyce, Darren Flynn, Rose Petrecca, and Joe Dobarro. The first demonstration of a microbial fuel cell as a viable power supply: Powering a meteorological buoy. *Journal of Power Sources*, 179(2):571–575, May 2008.

[17] Korneel Rabaey, Kirsten Van de Sompel, Lois Maignien, Nico Boon, Peter Aelterman, Peter Clauwaert, Liesje De Schamphelaire, Hai The Pham, Jan Vermeulen, Marc Verhaege, Piet Lens, and Willy Verstraete. Microbial Fuel Cells for Sulfide Removal †. *Environmental Science & Technology*, 40(17):5218–5224, September 2006.

[18] Derek R Lovley and Kelly P Nevin. A shift in the current: New applications and concepts for microbe-electrode electron exchange. *Current Opinion in Biotechnology*, 22(3):441–448, February 2011.

[19] O Bretschger, A Obraztsova, C A Sturm, I S Chang, Y A Gorby, S B Reed, D E Culley, C L Reardon, S Barua, M F Romine, J Zhou, A.S. Beliaev, R Bouhenni, D Saffarini, F Mansfeld, B H Kim, J K Fredrickson, and K H Nealson. Current Production and Metal Oxide Reduction by Shewanella oneidensis MR-1 Wild Type and Mutants. *Applied and Environmental Microbiology*, 73(21):7003–7012, October 2007.

[20] Susan E Childers, Stacy Ciufo, and Derek R Lovley. Geobacter metallireducens accesses insoluble Fe(III) oxide by chemotaxis. *Nature*, 416(6882):767–769, April 2002.

[21] Dan Coursolle and Jeffrey A Gralnick. Reconstruction of extracellular respiratory pathways for iron(III) reduction in Shewanella oneidensis strain MR-1. *Frontiers in Microbiology*, 3(56):1–11, February 2012.

[22] Leonard M Tender, Clare E Reimers, Hilmar A Stecher, Dawn E Holmes, Daniel R. Bond, Daniel A Lowy, Kanoelani Pilobello, Stephanie J Fertig, and Derek R Lovley. Harnessing microbially generated power on the seafloor. *Nature biotechnology*, 20:821–825, August 2002.

[23] Derek R Lovley. Bug juice: harvesting electricity with microorganisms. *Nature Reviews Microbiology*, 4(7):497–508, July 2006.

[24] Daniel A Lowy and Leonard M Tender. Harvesting energy from the marine sediment–water interface. *Journal of Power Sources*, 185(1):70–75, October 2008.

[25] Nikhil S Malvankar and Derek R Lovley. Microbial Nanowires: A New Paradigm for Biological Electron Transfer and Bioelectronics. *ChemSusChem*, 5(6):1039–1046, May 2012.

[26] Gemma Reguera, Kevin D McCarthy, Teena Mehta, Julie S Nicoll, Mark T Tuominen, and Derek R Lovley. Extracellular electron transfer via microbial nanowires. *Nature*, 435(7045):1098–1101, June 2005.

[27] Yuri A Gorby, Svetlana Yanina, Jeffrey S McLean, Kevin M Rosso, Dianne Moyles, Alice Dohnalkova, Terry J Beveridge, In Seop Chang, Byung Hong Kim, Kyung Shik Kim, David E Culley, Samantha B Reed, Margaret F Romine, Daad A Saffarini, Eric A Hill, Liang Shi, Dwayne A Elias, David W Kennedy, Grigoriy Pinchuk, Kazuya Watanabe, Shun'ichi Ishii, Bruce Logan, Kenneth H Nealson, and Jim K Fredrickson. Electrically conductive bacterial nanowires produced by Shewanella oneidensis strain MR-1 and other microorganisms. *Proceedings of the National Academy of Sciences*, 103(30):11358–11363, July 2006.

[28] Mohamed Y El-Naggar, Greg Wanger, Kar Man Leung, Thomas D Yuzvinsky, Gordon Southam, Jun Yang, Woon Ming Lau, Kenneth H Nealson, and Yuri A Gorby. Electrical transport along bacterial nanowires from Shewanella oneidensis MR-1. *Proceedings of the National Academy of Sciences*, 107(42):18127–18131, 2010.

[29] Korneel Rabaey, Nico Boon, Steven D. Siciliano, and Marc Verhaege. Biofuel Cells Select for Microbial Consortia That Self-Mediate Electron Transfer. *Applied and Environmental Microbiology*, 70(9):5373–5382, September 2004.

[30] Yung-Fu Wang, Seiya Tsujimura, Sheng-Shung Cheng, and Kenji Kano. Self-excreted mediator from Escherichia coli K-12 for electron transfer to carbon electrodes. *Applied Microbiology and Biotechnology*, 76(6):1439–1446, July 2007.

[31] The Hai Pham, Nico Boon, Peter Aelterman, Peter Clauwaert, Liesje De Schamphelaire, Lynn Vanhaecke, Katrien De Maeyer, Monica Höfte, Willy Verstraete, and Korneel Rabaey. Metabolites produced by Pseudomonas sp. enable a Gram-positive bacterium to achieve extracellular electron transfer. *Applied Microbiology and Biotechnology*, 77(5):1119–1129, October 2007.

[32] Enrico Marsili, Daniel B Baron, Indraneel D Shikhare, Dan Coursolle, Jeffrey A Gralnick, and Daniel R. Bond. Shewanella Secretes flavins that mediate extracellular electron transfer. *Proceedings of the National Academy of Sciences*, 105(10):3968–3973, March 2008.

[33] D H Park and J G Zeikus. Utilization of electrically reduced neutral red by Actinobacillus succinogenes: physiological function of neutral red in membrane-driven fumarate reduction and energy conservation. *Journal of bacteriology*, 181(8):2403–2410, March 1999.

[34] D H Park and J G Zeikus. Electricity Generation in Microbial Fuel Cells Using Neutral Red as an Electronophore. *Applied and Environmental Microbiology*, 66(4):1292–1297, April 2000.

[35] Kazuya Watanabe, Mike Manefield, Matthew Lee, and Atsushi Kouzuma. Electron shuttles in biotechnology. *Current Opinion in Biotechnology*, 20(6):633–641, December 2009.

[36] Anuradh Gunawardena, Sandun Fernando, and Filip To. Performance of a Yeast-mediated Biological Fuel Cell. *International Journal of Molecular Sciences*, 9(10):1893–1907, October 2008.

[37] Stuart Wilkinson, Jason Klar, and Shawn Applegarth. Optimizing Biofuel Cell Performance Using a Targeted Mixed Mediator Combination. *Electroanalysis*, 18(19-20):2001–2007, October 2006.

[38] H. M Jensen, A.E. Albers, K.R. Malley, Y.Y. Londer, B.E. Cohen, B.A. Helms, P. Weigele, J.T. Groves, and C.M. Ajo-Franklin. Engineering of a synthetic electron conduit in living cells. *Proceedings of the National Academy of Sciences*, 107(45):19213–19218, October 2010.

[39] Cheryl P Goldbeck, Heather M Jensen, Michaela A TerAvest, Nicole Beedle, Yancey Appling, Matt Hepler, Guillaume Cambray, Vivek Mutalik, Largus T Angenent, and Caroline M Ajo-Franklin. Tuning Promoter Strengths for Improved Synthesis and Function of Electron Conduits in Escherichia coli. *ACS Synthetic Biology*, 2(3):150–159, March 2013.

[40] Shaoan Cheng and Bruce E Logan. Ammonia treatment of carbon cloth anodes to enhance power generation of microbial fuel cells. *Electrochemistry Communications*, 9(3):492–496, March 2007.

[41] Yanzhen Fan, Shoutao Xu, Rebecca Schaller, Jun Jiao, Frank Chaplen, and Hong Liu. Nanoparticle decorated anodes for enhanced current generation in microbial electrochemical cells. *Biosensors and Bioelectronic*, 26(5):1908–1912, January 2011.

[42] Cui-e Zhao, Jiansheng Wu, Yuanzhao Ding, Victor Bochuan Wang, Yingdan Zhang, Staffan Kjelleberg, Joachim Say Chye Loo, Bin Cao, and Qichun Zhang. Hybrid Conducting Biofilm with Built-in Bacteria for High-Performance Microbial Fuel Cells. *ChemElectroChem*, 2(5):654–658, February 2015.

[43] Jenny Du, Chelsea Catania, and Guillermo C Bazan. Modification of Abiotic–Biotic Interfaces with Small Molecules and Nanomaterials for Improved Bioelectronics. *Chemistry of Materials*, 26(1):686–697, January 2014.

[44] Igor Vostiar, E E Ferapontova, and Lo Gorton. Electrical "wiring" of viable Gluconobacter oxydans cells with a flexible osmium-redox polyelectrolyte. *Electrochemistry Communications*, 6(7):621–626, July 2004.

[45] Suna Timur, Behzad Haghighi, Jan Tkac, Nurdan Pazarlıoğlu, Azmi Telefoncu, and Lo Gorton. Electrical wiring of Pseudomonas putida and Pseudomonas fluorescens with osmium redox polymers. *Bioelectrochemistry*, 71(1):38–45, September 2007.

[46] Xuee Wu, Feng Zhao, Nelli Rahunen, John R Varcoe, Claudio Avignone-Rossa, Alfred E Thumser, and Robert C T Slade. A Role for Microbial

Palladium Nanoparticles in Extracellular Electron Transfer. *Angewandte Chemie International Edition*, 50(2):427–430, December 2010.

[47] Jia Geng, Kyunghoon Kim, Jianfei Zhang, Artur Escalada, Ramya Tunuguntla, Luis R Comolli, Frances I Allen, Anna V Shnyrova, Kang Rae Cho, Dayannara Munoz, Y Morris Wang, Costas P Grigoropoulos, Caroline M Ajo-Franklin, Vadim A Frolov, and Aleksandr Noy. Stochastic transport through carbon nanotubes in lipid bilayers and live cell membranes. *Nature*, 514(7524):612–615, April 2015.

[48] Renqiang Yang, Yunhua Xu, Xuan-Dung Dang, Thuc-Quyen Nguyen, Yong Cao, and Guillermo C Bazan. Conjugated Oligoelectrolyte Electron Transport/Injection Layers for Organic Optoelectronic Devices. *Journal of the American Chemical Society*, 130(11):3282–3283, March 2008.

[49] Logan E Garner, Juhyun Park, Scott M Dyar, Arkadiusz Chworos, James J Sumner, and Guillermo C Bazan. Modification of the Optoelectronic Properties of Membranes via Insertion of Amphiphilic Phenylenevinylene Oligoelectrolytes. *Journal of the American Chemical Society*, 132(29):10042–10052, July 2010.

[50] Victor Bochuan Wang, Jenny Du, Xiaofen Chen, Alexander W Thomas, Nathan D Kirchhofer, Logan E Garner, Myat Thiri Maw, Wee Han Poh, Jamie Hinks, Stefan Wuertz, Staffan Kjelleberg, Qichun Zhang, Joachim Say Chye Loo, and Guillermo C Bazan. Improving charge collection in Escherichia coli–carbon electrode devices with conjugated oligoelectrolytes. *Physical Chemistry Chemical Physics*, 15(16):5867–5872, February 2013.

[51] Huijie Hou, Xiaofen Chen, Alexander W Thomas, Chelsea Catania, Nathan D Kirchhofer, Logan E Garner, Arum Han, and Guillermo C Bazan. Conjugated Oligoelectrolytes Increase Power Generation in E. coli Microbial Fuel Cells. *Advanced Materials*, 25(11):1593–1597, January 2013.

[52] Alexander W Thomas, Logan E Garner, Kelly P Nevin, Trevor L Woodard, Ashley E Franks, Derek R Lovley, James J Sumner, Christian J Sund, and

Guillermo C Bazan. A lipid membrane intercalating conjugated oligoelectrolyte enables electrode driven succinate production in Shewanella. *Energy & Environmental Science*, 6(6):1761, April 2013.

[53] Nathan D Kirchhofer, Xiaofen Chen, Enrico Marsili, James J Sumner, Frederick W Dahlquist, and Guillermo C Bazan. The conjugated oligoelectrolyte DSSN+ enables exceptional coulombic efficiency via direct electron transfer for anode-respiring Shewanella oneidensis MR-1–a mechanistic study. *Physical Chemistry Chemical Physics*, 16:20436–20443, September 2014.

[54] Logan E Garner, Alexander W Thomas, James J Sumner, Steven P Harvey, and Guillermo C Bazan. Conjugated oligoelectrolytes increase current response and organic contaminant removal in wastewater microbial fuel cells. *Energy & Environmental Science*, 5(11):9449–9452, September 2012.

[55] Jamie Hinks, Wee Han Poh, Justin Jang Hann Chu, Joachim Say Chye Loo, Guillermo C Bazan, Lynn E Hancock, and Stefan Wuertz. Oligopolyphenylenevinylene-Conjugated Oligoelectrolyte Membrane Insertion Molecules Selectively Disrupt Cell Envelopes of Gram-Positive Bacteria. *Applied and Environmental Microbiology*, 81(6):1949–1958, February 2015.

[56] Jamie Hinks, Yaofeng Wang, Wee Han Poh, Bogdan C Donose, Alexander W Thomas, Stefan Wuertz, Say Chye Joachim Loo, Guillermo C Bazan, Staffan Kjelleberg, Yuguang Mu, and Thomas Seviour. Modeling Cell Membrane Perturbation by Molecules Designed for Transmembrane Electron Transfer. *Langmuir*, 30(9):2429–2440, March 2014.

[57] Hengjing Yan, Zachary D Rengert, Alexander W Thomas, Carolin Rehermann, Jamie Hinks, and Guillermo C Bazan. Influence of molecular structure on the antimicrobial function of phenylenevinylene conjugated oligoelectrolytes. *Chemical Science*, 7:5714–5722, June 2016.

[58] Jenny Du, Alexander W Thomas, Xiaofen Chen, Logan E Garner, Carol A Vandenberg, and Guillermo C Bazan. Increased ion conduc-

tance across mammalian membranes modified with conjugated oligoelectrolytes. *Chemical Communications*, 49(83):9624, 2013.

[59] Justin P Jahnke, Guillermo C Bazan, and James J Sumner. Effect of Modified Phospholipid Bilayers on the Electrochemical Activity of a Membrane-Spanning Conjugated Oligoelectrolyte. *Langmuir*, 31(42):11613–11620, October 2015.

[60] Chelsea Catania, Alexander W Thomas, and Guillermo C Bazan. Tuning cell surface charge in E. coli with conjugated oligoelectrolytes. *Chemical Science*, 7:2023–2029, February 2016.

[61] Alexander W Thomas, Chelsea Catania, Logan E Garner, and Guillermo C Bazan. Pendant ionic groups of conjugated oligoelectrolytes govern their ability to intercalate into microbial membranes. *Chemical Communications*, 51:9294–9297, May 2015.

[62] H D Sikes. Rapid Electron Tunneling Through Oligophenylenevinylene Bridges. *Science*, 291(5508):1519–1523, February 2001.

[63] C R Myers and J M Myers. Localization of Cytochromes to the Outer-Membrane of Anaerobically Grown Shewanella-Putrefaciens Mr-1. *Journal of bacteriology*, 174(11):3429–3438, June 1992.

[64] C R Myers and J M Myers. Outer membrane cytochromes of Shewanella putrefaciens MR-1: spectral analysis, and purification of the 83-kDa c-type cytochrome. *Biochimica et Biophysica Acta*, 1326(2):307–318, June 1997.

[65] Robert S Hartshorne, Catherine L Reardon, Daniel Ross, Jochen Nuester, Thomas A Clarke, Andrew J Gates, Paul C Mills, Jim K Fredrickson, John M Zachara, Liang Shi, Alex S Beliaev, Matthew J Marshall, Ming Tien, Susan Brantley, Julea N Butt, and David J Richardson. Characterization of an electron conduit between bacteria and the extracellular environment. *PNAS*, 106(52):22169–22174, December 2009.

[66] M Fonseca Bruno, M Paquete Catarina, E Neto Sonia, Pacheco Isabel, M Soares Claudio, and O Louro Ricardo. Mind the gap: cytochrome

interactions reveal electron pathways across the periplasm of Shewanella oneidensis MR-1. *Biochemical Journal*, 449(1):101–108, 2013.

[67] D Baron, E LaBelle, D Coursolle, J A Gralnick, and D.R. Bond. Electrochemical Measurement of Electron Transfer Kinetics by Shewanella oneidensis MR-1. *Journal of Biological Chemistry*, 284(42):28865–28873, October 2009.

[68] David J Richardson, Julea N Butt, Jim K Fredrickson, John M Zachara, Liang Shi, Marcus J Edwards, Gaye White, Nanakow Baiden, Andrew J Gates, Sophie J Marritt, and Thomas A Clarke. The 'porin-cytochrome' model for microbe-to-mineral electron transfer. *Molecular Microbiology*, 85(2):201–212, May 2012.

[69] Dan Coursolle and Jeffrey A Gralnick. Modularity of the Mtr respiratory pathway of Shewanella oneidensis strain MR-1. *Molecular Microbiology*, pages no–no, July 2010.

[70] Lisa A Fitzgerald, Emily R Petersen, Richard I Ray, Brenda J Little, Candace J Cooper, Erinn C Howard, Bradley R Ringeisen, and Justin C Biffinger. Shewanella oneidensis MR-1 Msh pilin proteins are involved in extracellular electron transfer in microbial fuel cells. *Process Biochemistry*, 47(1):170–174, January 2012.

[71] Kar Man Leung, Greg Wanger, Mohamed Y El-Naggar, Yuri Gorby, Gordon Southam, Woon Ming Lau, and Jun Yang. Shewanella oneidensisMR-1 Bacterial Nanowires Exhibit p-Type, Tunable Electronic Behavior. *Nano Letters*, 13(6):2407–2411, June 2013.

[72] S Pirbadian, S E Barchinger, K M Leung, H S Byun, Y Jangir, R A Bouhenni, S B Reed, M F Romine, D A Saffarini, L Shi, Y A Gorby, J H Golbeck, and M Y El-Naggar. Shewanella oneidensis MR-1 nanowires are outer membrane and periplasmic extensions of the extracellular electron transport components. *PNAS*, 111(35):12883–12888, September 2014.

[73] Sarah M Strycharz-Glaven, Rachel M Snider, Anthony Guiseppi-Elie, and Leonard M Tender. On the electrical conductivity of microbial nanowires and biofilms. *Energy & Environmental Science*, 4(11):4366, July 2011.

[74] Sahand Pirbadian and Mohamed Y El-Naggar. Multistep hopping and extracellular charge transfer in microbial redox chains. *Physical Chemistry Chemical Physics*, 14(40):13802, June 2012.

[75] Shuai Xu, Yamini Jangir, and Mohamed Y El-Naggar. Electrochimica Acta. *Electrochimica Acta*, 198:49–55, April 2016.

[76] H von Canstein, J Ogawa, S Shimizu, and J R Lloyd. Secretion of Flavins by Shewanella Species and Their Role in Extracellular Electron Transfer. *Applied and Environmental Microbiology*, 74(3):615–623, February 2008.

[77] Sharon B Velasquez-Orta, Ian M Head, Thomas P Curtis, Keith Scott, Jonathan R Lloyd, and Harald Canstein. The effect of flavin electron shuttles in microbial fuel cells current production. *Applied Microbiology and Biotechnology*, 85(5):1373–1381, August 2009.

[78] Uwe Schröder. Anodic electron transfer mechanisms in microbial fuel cells and their energy efficiency. *Physical Chemistry Chemical Physics*, 9(21):2619, April 2007.

[79] Victor Bochuan Wang, Nathan D Kirchhofer, Xiaofen Chen, Melissa Yuan Li Tan, Krishnakumar Sivakumar, Bin Cao, Qichun Zhang, Staffan Kjelleberg, Guillermo C Bazan, Say Chye Joachim Loo, and Enrico Marsili. Electrochemistry Communications. *Electrochemistry Communications*, 41(C):55–58, April 2014.

[80] Robert B Gennis. The cytochromes of Escherichia coli. *FEMS Microbiology Letters*, 46(4):387–399, May 1987.

[81] Erin Ching, Robert B Gennis, and Randy W Larsen. Kinetics of Intramolecular Electron Transfer in Cytochrome bo3 from Escherichia coli. *Biophysical Journal*, 84(4):2728–2733, April 2003.

[82] Natividad Ruiz, Daniel Kahne, and Thomas J Silhavy. Advances in understanding bacterial outer-membrane biogenesis. *Nature Reviews Microbiology*, 4(1):57–66, January 2006.

[83] C Iobbi-Nivol, H Crooke, L Griffiths, J Grove, H Hussain, J Pommier, V Mejean, and J A Cole. A reassessment of the range of c-type cytochromes synthesized by Escherichia coli K-12. *FEMS Microbiology Letters*, 119(1-2):89–94, June 1994.

[84] Krishnakumar Sivakumar, Victor Bochuan Wang, Xiaofen Chen, Guillermo C Bazan, Staffan Kjelleberg, Say Chye Joachim Loo, and Bin Cao. Membrane permeabilization underlies the enhancement of extracellular bioactivity in Shewanella oneidensis by a membrane-spanning conjugated oligoelectrolyte. *Applied Microbiology and Biotechnology*, 98(21):9021–9031, August 2014.

[85] Victor Bochuan Wang, Natalia Yantara, Teck Ming Koh, Staffan Kjelleberg, Qichun Zhang, Guillermo C Bazan, Say Chye Joachim Loo, and Nripan Mathews. Uncovering alternate charge transfer mechanisms in Escherichia coli chemically functionalized with conjugated oligoelectrolytes. *Chemical Communications*, 50(60):8223–8226, June 2014.

[86] G Unden and J Bongaerts. Alternative respiratory pathways of Escherichia coli: energetics and transcriptional regulation in response to electron acceptors. *Biochimica et biophysica acta*, 1320(3):217–234, July 1997.

[87] Poonam Sharma, Maarten J Teixeira de Mattos, Klaas J Hellingwerf, and Martijn Bekker. On the function of the various quinone species in Escherichiacoli. *FEBS Journal*, 279(18):3364–3373, May 2012.

[88] B Soballe and R K Poole. Microbial ubiquinones: multiple roles in respiration, gene regulation and oxidative stress management. *Microbiology-Sgm*, 145:1817–1830, August 1999.

[89] Huijie Hou, Xiaofen Chen, Jia Liu, Xiuping Zhu, Guillermo C Bazan, and Bruce E Logan. ScienceDirect. *International Journal of Hydrogen Energy*, 39(34):19407–19415, November 2014.

[90] Jia Liu, Huijie Hou, Xiaofen Chen, Guillermo C Bazan, Hiroyuki Kashima, and Bruce E Logan. Bioelectrochemistry. *Bioelectrochemistry*, 106(PB):379–382, December 2015.

[91] Michaela A TerAvest, Tom J Zajdel, and Caroline M Ajo-Franklin. The Mtr Pathway of Shewanella oneidensis MR-1 Couples Substrate Utilization to Current Production in Escherichia coli. *ChemElectroChem*, 1(11):1874–1879, November 2014.

[92] Michaela A TerAvest and Caroline M Ajo-Franklin. Transforming exoelectrogens for biotechnology using synthetic biology. *Biotechnology and Bioengineering*, 113(4):687–697, April 2016.

[93] Bruce E Logan. Essential Data and Techniques for Conducting Microbial Fuel Cell and other Types of Bioelectrochemical System Experiments. *ChemSusChem*, 5(6):988–994, April 2012.

[94] Xiaoxin Cao, Xia Huang, Xiaoyuan Zhang, Peng Liang, and Mingzhi Fan. A mini-microbial fuel cell for voltage testing of exoelectrogenic bacteria. *Frontiers of Environmental Science & Engineering in China*, 3(3):307–312, July 2009.

[95] Marc Sugnaux, Sophie Mermoud, Ana Ferreira da Costa, Manuel Happe, and Fabian Fischer. Probing electron transfer with Escherichia coli: A method to examine exoelectronics in microbial fuel cell type systems. *Bioresource Technology*, 148(C):567–573, November 2013.

[96] I M Keseler, C Bonavides-Martinez, J Collado-Vides, S Gama-Castro, R P Gunsalus, D A Johnson, M Krummenacker, L M Nolan, S Paley, I T Paulsen, M Peralta-Gil, A Santos-Zavaleta, A G Shearer, and P D Karp. EcoCyc: A comprehensive view of Escherichia coli biology. *Nucleic Acids Research*, 37(Database):D464–D470, January 2009.

[97] F C Neidhardt. *Escherichia coli and Salmonella typhimurium: Cellular and Molecular Biology*. Escherichia Coli and Salmonella Typhimurium: Cellular and Molecular Biology. American Society for Microbiology, Washington DC, 1 edition, 1987.

[98] Rawil F Fakhrullin and Yuri M Lvov. "Face-Lifting" and "Make-Up" for Microorganisms: Layer-by-Layer Polyelectrolyte Nanocoating. *ACS Nano*, 6(6):4557–4564, June 2012.

[99] B Liu and G C Bazan. *Conjugated Polyelectrolytes; Fundamentals and Applications*. Wiley-VCH, 2013.

[100] Aidee Duarte, Kan-Yi Pu, Bin Liu, and Guillermo C Bazan. Recent Advances in Conjugated Polyelectrolytes for Emerging Optoelectronic Applications †. *Chemistry of Materials*, 23(3):501–515, February 2011.

[101] Hui Jiang, Prasad Taranekar, John R Reynolds, and Kirk S Schanze. Conjugated Polyelectrolytes: Synthesis, Photophysics, and Applications. *Angewandte Chemie International Edition*, 48(24):4300–4316, June 2009.

[102] Wonho Lee, Jung Hwa Seo, and Han Young Woo. Conjugated polyelectrolytes: A new class of semiconducting material for organic electronic devices. *Polymer*, 54(19):5104–5121, August 2013.

[103] Fude Feng, Fang He, Lingling An, Shu Wang, Yuliang Li, and Daoben Zhu. Fluorescent Conjugated Polyelectrolytes for Biomacromolecule Detection. *Advanced Materials*, 20(15):2959–2964, August 2008.

[104] Ruoyu Zhan and Bin Liu. Benzothiadiazole-Containing Conjugated Polyelectrolytes for Biological Sensing and Imaging. *Macromolecular Chemistry and Physics*, 216(2):131–144, November 2014.

[105] K Peter R Nilsson and Per Hammarström. Luminescent Conjugated Polymers: Illuminating the Dark Matters of Biology and Pathology. *Advanced Materials*, 20(13):2639–2645, July 2008.

[106] Guangxue Feng, Dan Ding, and Bin Liu. Fluorescence bioimaging with conjugated polyelectrolytes. *Nanoscale*, 4(20):6150–16, August 2012.

[107] Therése Klingstedt and K Peter R Nilsson. Conjugated polymers for enhanced bioimaging. *BBA - General Subjects*, 1810(3):286–296, March 2011.

[108] A Herland, P Björk, K P R Nilsson, J D M Olsson, P Åsberg, P Konradsson, P Hammarström, and O Inganäs. Electroactive Luminescent Self-Assembled Bio-organic Nanowires: Integration of Semiconducting Oligoelectrolytes within Amyloidogenic Proteins. *Advanced Materials*, 17(12):1466–1471, June 2005.

[109] Therése Klingstedt, Andreas Åslund, Rozalyn A Simon, Leif B G Johansson, Jeffrey J Mason, Sofie Nyström, Per Hammarström, and K Peter R Nilsson. Synthesis of a library of oligothiophenes and their utilization as fluorescent ligands for spectral assignment of protein aggregates. *Organic & Biomolecular Chemistry*, 9(24):8356–15, 2011.

[110] N Sakai, D Gerard, and S Matile. Electrostatics of Cell Membrane Recognition: Structure and Activity of Neutral and Cationic Rigid Push-Pull Rods in Isoelectric, Anionic, and Polarized Lipid Bilayer Membranes. *Journal of the American Chemical Societry*, 123:2517–2524, February 2001.

[111] Ying Wang, Emmalee M Jones, Yanli Tang, Eunkyung Ji, Gabriel P Lopez, Eva Y Chi, Kirk S Schanze, and David G Whitten. Effect of Polymer Chain Length on Membrane Perturbation Activity of Cationic Phenylene Ethynylene Oligomers and Polymers. *Langmuir*, 27(17):10770–10775, September 2011.

[112] Eric H Hill, Kelly Stratton, David G Whitten, and Deborah G Evans. Molecular Dynamics Simulation Study of the Interaction of Cationic Biocides with Lipid Bilayers: Aggregation Effects and Bilayer Damage. *Langmuir*, 28(42):14849–14854, October 2012.

[113] Ping Yan, Aifang Xie, Meide Wei, and Leslie M Loew. Amino(oligo)thiophene-Based Environmentally Sensitive Biomembrane Chromophores. *The Journal of Organic Chemistry*, 73(17):6587–6594, September 2008.

[114] Alexander W Thomas, Zachary B Henson, Jenny Du, Carol A Vandenberg, and Guillermo C Bazan. Synthesis, Characterization, and Biological Affinity of a Near-Infrared-Emitting Conjugated Oligoelectrolyte. *Journal of the American Chemical Society*, 136(10):3736–3739, March 2014.

[115] Paulina Gwozdzinska, Roza Pawlowska, Justyna Milczarek, Logan E Garner, Alexander W Thomas, Guillermo C Bazan, and Arkadiusz Chworos. Phenylenevinylene conjugated oligoelectrolytes as fluorescent dyes for

mammalian cell imaging. *Chemical Communications*, 50:14859–14861, October 2014.

[116] Artur Cieślar-Pobuda, Marcus Bäck, Karin Magnusson, Mayur V Jain, Mehrdad Rafat, Saeid Ghavami, K Peter R Nilsson, and Marek J Łos. Cell type related differences in staining with pentameric thiophene derivatives. *Cytometry*, 85(7):628–635, February 2014.

[117] Sylvia Schmid, E Marion Schneider, Eduard Brier, and Peter Bäuerle. Self-organizing carbohydrate-oligothiophene-hybrids for eukaryotic membrane-labelling. *Journal of Materials Chemistry B*, 2:7861–7865, October 2014.

[118] Marta Dal Molin, Quentin Verolet, Adai Colom, Romain Letrun, Emmanuel Derivery, Marcos Gonzalez-Gaitan, Eric Vauthey, Aurélien Roux, Naomi Sakai, and Stefan Matile. Fluorescent Flippers for Mechanosensitive Membrane Probes. *Journal of the American Chemical Society*, 137(2):568–571, January 2015.

[119] Ilaria Palamà, Francesca Di Maria, Ilenia Viola, Eduardo Fabiano, Giuseppe Gigli, Cristian Bettini, and Giovanna Barbarella. Live-Cell-Permeant Thiophene Fluorophores and Cell-Mediated Formation of Fluorescent Fibrils. *Journal of the American Chemical Society*, 133(44):17777–17785, November 2011.

[120] Therése Klingstedt, Hamid Shirani, K O Andreas Åslund, Nigel J Cairns, Christina J Sigurdson, Michel Goedert, and K Peter R Nilsson. The Structural Basis for Optimal Performance of Oligothiophene-Based Fluorescent Amyloid Ligands: Conformational Flexibility is Essential for Spectral Assignment of a Diversity of Protein Aggregates. *Chemistry - A European Journal*, 19(31):10179–10192, June 2013.

[121] Jens Wigenius, Gustav Persson, Jerker Widengren, and Olle Inganäs. Interactions Between a Luminescent Conjugated Oligoelectrolyte and Insulin During Early Phases of Amyloid Formation. *Macromolecular Bioscience*, 11(8):1120–1127, May 2011.

[122] Aidee Duarte, Arkadiusz Chworos, Suvi F Flagan, Grady Hanrahan, and Guillermo C Bazan. Identification of Bacteria by Conjugated Oligoelectrolyte/Single-Stranded DNA Electrostatic Complexes. *Journal of the American Chemical Society*, 132(36):12562–12564, September 2010.

[123] Huaping Li and Guillermo C Bazan. Conjugated Oligoelectrolyte/ssDNA Aggregates: Self-Assembled Multicomponent Chromophores for Protein Discrimination. *Advanced Materials*, 21(9):964–967, March 2009.

[124] Liping Cai, Ruoyu Zhan, Kan-Yi Pu, Xiaoying Qi, Hua Zhang, Wei Huang, and Bin Liu. Butterfly-Shaped Conjugated Oligoelectrolyte/Graphene Oxide Integrated Assay for Light-Up Visual Detection of Heparin. *Analytical Chemistry*, 83(20):7849–7855, October 2011.

[125] Lakshmi P Kotra, Dasantila Golemi, Nabil A Amro, Gang-Yu Liu, and Shahriar Mobashery. Dynamics of the Lipopolysaccharide Assembly on the Surface of Escherichiacoli. *Journal of the American Chemical Society*, 121(38):8707–8711, September 1999.

[126] H Nikaido. Molecular Basis of Bacterial Outer Membrane Permeability Revisited. *Microbiology and Molecular Biology Reviews*, 67(4):593–656, December 2003.

[127] Bettina Franz, Shantanu S Balkundi, Christiane Dahl, Yuri M Lvov, and Alexander Prange. Layer-by-Layer Nano-Encapsulation of Microbes: Controlled Cell Surface Modification and Investigation of Substrate Uptake in Bacteria. *Macromolecular Bioscience*, 10(2):164–172, February 2010.

[128] Shantanu S Balkundi, Nalinkanth G Veerabadran, D Matthew Eby, Glenn R Johnson, and Yuri M Lvov. Encapsulation of Bacterial Spores in Nanoorganized Polyelectrolyte Shells †. *Langmuir*, 25(24):14011–14016, December 2009.

[129] D Matthew Eby, Svetlana Harbaugh, Randi N Tatum, Karen E Farrington, Nancy Kelley-Loughnane, and Glenn R Johnson. Bacterial Sunscreen: Layer-by-Layer Deposition of UV-Absorbing Polymers on Whole-Cell Biosensors. *Langmuir*, 28(28):10521–10527, July 2012.

[130] Han Young Woo, Bin Liu, Bernhard Kohler, Dmitry Korystov, Alexander Mikhailovsky, and Guillermo C Bazan. Solvent Effects on the Two-Photon Absorption of Distyrylbenzene Chromophores. *Journal of the American Chemical Society*, 127(42):14721–14729, October 2005.

[131] Julia H Ortony, Tirtha Chatterjee, Logan E Garner, Arkadiusz Chworos, Alexander Mikhailovsky, Edward J Kramer, and Guillermo C Bazan. Self-Assembly of an Optically Active Conjugated Oligoelectrolyte. *Journal of the American Chemical Society*, 133(21):8380–8387, June 2011.

[132] Ivan Sondi and Branka Salopek-Sondi. Silver nanoparticles as antimicrobial agent: a case study on E. coli as a model for Gram-negative bacteria. *Journal of Colloid and Interface Science*, 275(1):177–182, July 2004.

[133] W William Wilson, Mary Margaret Wade, Steven C Holman, and Franklin R Champlin. Status of methods for assessing bacterial cell surface charge properties based on zeta potential measurements. *Journal of Microbiological Methods*, 43(3):153–164, January 2001.

[134] Anna L Hillberg and Maryam Tabrizian. Biorecognition through Layer-by-Layer Polyelectrolyte Assembly: In-Situ Hybridization on Living Cells. *Biomacromolecules*, 7(10):2742–2750, October 2006.

[135] Mehmet Kahraman, Alsu I Zamaleeva, Rawil F Fakhrullin, and Mustafa Culha. Layer-by-layer coating of bacteria with noble metal nanoparticles for surface-enhanced Raman scattering. *Analytical and Bioanalytical Chemistry*, 395(8):2559–2567, October 2009.

[136] A G Lee. Lipid–protein interactions in biological membranes: a structural perspective. *Biochimica et Biophysica Acta (BBA)-Biomembranes*, 1612(1):1–40, May 2003.

[137] M Kastowsky, T Gutberlet, and H Bradaczek. Molecular modelling of the three-dimensional structure and conformational flexibility of bacterial lipopolysaccharide. *Journal of bacteriology*, 174(14):4798–4806, July 1992.

[138] Justin C Biffinger, Hong Woo Kim, and Stephen G DiMagno. The Polar Hydrophobicity of Fluorinated Compounds. *ChemBioChem*, 5(5):622–627, April 2004.

[139] Kan-Yi Pu, Kai Li, Xinhai Zhang, and Bin Liu. Conjugated Oligoelectrolyte Harnessed Polyhedral Oligomeric Silsesquioxane as Light-Up Hybrid Nanodot for Two-Photon Fluorescence Imaging of Cellular Nucleus. *Advanced Materials*, 22(37):4186–4189, June 2010.

[140] Dan Ding, Kan-Yi Pu, Kai Li, and Bin Liu. Conjugated oligoelectrolyte-polyhedral oligomeric silsesquioxane loaded pH-responsive nanoparticles for targeted fluorescence imaging of cancer cell nucleus. *Chemical Communications*, 47(35):9837–3, August 2011.

[141] Wen Li Song, Rong Cui Jiang, Yan Yuan, Xiao Mei Lu, Wen Bo Hu, Qu Li Fan, and Wei Huang. Star-shaped conjugated oligoelectrolyte for bioimaging in living cells. *Chinese Science Bulletin*, 58(21):2570–2575, May 2013.

[142] Yebin Lee, Ilseung Yang, Jung Eun Lee, Sunjin Hwang, Jong Woo Lee, Seung-Soo Um, Thanh Luan Nguyen, Pil J Yoo, Han Young Woo, Juhyun Park, and Seong Keun Kim. Enhanced Photocurrent Generation by Förster Resonance Energy Transfer between Phospholipid-Assembled Conjugated Oligoelectrolytes and Nile Red. *Journal of Physical Chemistry C*, 117(7):3298–3307, February 2013.

[143] Nathan D Kirchhofer, Michelle A Rasmussen, Frederick W Dahlquist, Shelley D Minteer, and Guillermo C Bazan. The photobioelectrochemical activity of thylakoid bioanodes is increased via photocurrent generation and improved contacts by membrane-intercalating conjugated oligoelectrolytes. *Energy & Environmental Science*, 8:2698–2706, August 2015.

[144] Ryoma Nakao, Madeleine Ramstedt, Sun Nyunt Wai, and Bernt Eric Uhlin. Enhanced Biofilm Formation by Escherichia coli LPS Mutants Defective in Hep Biosynthesis. *PLoS ONE*, 7(12):e51241, December 2012.

[145] A T Poortinga, R Bos, W Norde, and H J BUSSCHER. Electric double layer

interactions in bacterial adhesion to surfaces. *Surface Science Reports*, 47:1–32, January 2002.

[146] Jon Palmer, Steve Flint, and John Brooks. Bacterial cell attachment, the beginning of a biofilm. *Journal of Industrial Microbiology & Biotechnology*, 34(9):577–588, July 2007.

[147] Yu Liu, Shu-Fang Yang, Yong Li, Hui Xu, Lei Qin, and Joo-Hwa Tay. The influence of cell and substratum surface hydrophobicities on microbial attachment. *Journal of Biotechnology*, 110(3):251–256, June 2004.

[148] A Zita and M Hermansson. Effects of bacterial cell surface structures and hydrophobicity on attachment to activated sludge flocs. *Applied and Environmental Microbiology*, 63(3):1168–1170, March 1997.

[149] W M Dunne. Bacterial Adhesion: Seen Any Good Biofilms Lately? *Clinical Microbiology Reviews*, 15(2):155–166, April 2002.

[150] François Ahimou, Frédéric A Denis, Ahmed Touhami, and Yves F Dufrêne. Probing Microbial Cell Surface Charges by Atomic Force Microscopy. *Langmuir*, 18(25):9937–9941, December 2002.

[151] Mark C M van Loosdrecht, W Norde, and A J B Zehnder. Physical Chemical Description of Bacterial Adhesion. *Journal of Biomaterials Applications*, 5(2):91–106, October 1990.

[152] Rob Van Houdt and Chris W Michiels. Role of bacterial cell surface structures in Escherichia coli biofilm formation. *Research in Microbiology*, 156(5-6):626–633, June 2005.

[153] M ROSENBERG. Bacterial Adherence to Hydrocarbons - a Useful Technique for Studying Cell-Surface Hydrophobicity. *FEMS Microbiology Letters*, 22(3):289–295, 1984.

[154] R M Goulter, I R Gentle, and G A Dykes. Issues in determining factors influencing bacterial attachment: a review using the attachment of Escherichia colito abiotic surfaces as an example. *Letters in Applied Microbiology*, 49(1):1–7, July 2009.

[155] Rebecca M Goulter, Ian R Gentle, and Gary A Dykes. Characterisation of Curli Production, Cell Surface Hydrophobicity, Autoaggregation and Attachment Behaviour of Escherichia coli O157. *Current Microbiology*, 61(3):157–162, February 2010.

[156] Baikun Li and Bruce E Logan. Bacterial adhesion to glass and metal-oxide surfaces. *Colloids and Surfaces B: Biointerfaces*, 36(2):81–90, July 2004.

[157] Mel Rosenberg. Microbial adhesion to hydrocarbons: twenty-five years of doing MATH. *FEMS Microbiology Letters*, 262(2):129–134, September 2006.

[158] C Catania, C.M. Ajo-Franklin, and G C Bazan. Membrane permeabilization by conjugated oligoelectrolytes accelerates whole-cell catalysis. *RSC Advances*, 6(102):100300–100306, October 2016.

[159] M Vaara. Agents that increase the permeability of the outer membrane. *Microbiological reviews*, 56(3):395–411, September 1992.

[160] M Vaara. Antibiotic-supersusceptible mutants of Escherichia coli and Salmonella typhimurium. *Antimicrobial Agents and Chemotherapy*, 37(11):2255–2260, November 1993.

[161] H Nikaido and M Vaara. Molecular basis of bacterial outer membrane permeability. *Microbiological reviews*, 49(1):1–32, March 1985.

[162] M Vaara and M Nurminen. Outer membrane permeability barrier in Escherichia coli mutants that are defective in the late acyltransferases of lipid A biosynthesis. *Antimicrobial Agents and Chemotherapy*, 43(6):1459–1462, April 1999.

[163] S P Denyer and J-Y Maillard. Cellular impermeability and uptake of biocides and antibiotics in Gram-negative bacteria. *Journal of Applied Microbiology*, 92 Suppl:35S–45S, 2002.

[164] R Benz and K Bauer. Permeation of hydrophilic molecules through the outer membrane of gram-negative bacteria. *European Journal of Biochemistry*, 176:1–19, May 1988.

[165] Rachel Ruizhen Chen. Permeability issues in whole-cell bioprocesses and cellular membrane engineering. *Applied Microbiology and Biotechnology*, 74(4):730–738, January 2007.

[166] Carla C C R de Carvalho. Enzymatic and whole cell catalysis: Finding new strategies for old processes. *Biotechnology Advances*, 29(1):75–83, January 2011.

[167] M J de Smet, H Wynberg, and B Witholt. Synthesis of 1,2-Epoxyoctane by Pseudomonas oleovorans During Growth in a Two-Phase System Containing High Concentrations of 1-Octene. *Applied and Environmental Microbiology*, 42(5):811–816, November 1981.

[168] A Kondo, Y Liu, M Furuta, Y Fujita, Takeyuki Itabashi, T Matsumoto, and H Fukuda. Preparation of high activity whole cell biocatalyst by permeabilization of recombinant flocculent yeast with alcohol. *Enzyme and Microbial Technology*, 27(10):806–811, December 2000.

[169] M J Van der Werf and S Hartmans. Permeabilization and lysis of Pseudomonas pseudoalcaligenes cells by Triton X-100 for efficient production of d-malate. *Applied Microbiology and Biotechnology*, 43:590–594, November 1995.

[170] R Y K Yang, O Bayraktar, and H T Pu. Plant-cell bioreactors with simultaneous electropermeabilization and electrophoresis. *Journal of Biotechnology*, 100(1):13–22, January 2003.

[171] M W Breedveld, L P Zevenhuizen, and A J Zehnder. Synthesis of cyclic beta-(1,2)-glucans by Rhizobium leguminosarum biovar trifolii TA-1: factors influencing excretion. *Journal of bacteriology*, 174(20):6336–6342, October 1992.

[172] P Fontanille and C Larroche. Optimization of isonovalal production from α-pinene oxide using permeabilized cells of Pseudomonas rhodesiae CIP 107491. *Applied Microbiology and Biotechnology*, 60(5):534–540, January 2003.

[173] C Dupont and A J Clarke. In vitro synthesis and O acetylation of peptidoglycan by permeabilized cells of Proteus mirabilis. *Journal of bacteriology*, 173(15):4618–4624, August 1991.

[174] M Cánovas, T Torroglosa, and J L Iborra. Permeabilization of Escherichia coli cells in the biotransformation of trimethylammonium compounds into l-carnitine. *Enzyme and Microbial Technology*, 37(3):300–308, August 2005.

[175] J H Choi and S Y Lee. Secretory and extracellular production of recombinant proteins using Escherichia coli. *Applied Microbiology and Biotechnology*, 64(5):625–635, June 2004.

[176] M J Weickert, D H Doherty, E A Best, and P O Olins. Optimization of heterologous protein production in Escherichia coli. *Current Opinion in Biotechnology*, 7(5):494–499, October 1996.

[177] Ye Ni and Rachel R Chen. Accelerating whole-cell biocatalysis by reducing outer membrane permeability barrier. *Biotechnology and Bioengineering*, 87(6):804–811, August 2004.

[178] Ye Ni, Zichao Mao, and Rachel R Chen. Outer membrane mutation effects on UDP-glucose permeability and whole-cell catalysis rate. *Applied Microbiology and Biotechnology*, 73(2):384–393, September 2006.

[179] Ye Ni, John Reye, and Rachel R Chen. lpp deletion as a permeabilization method. *Biotechnology and Bioengineering*, 97(6):1347–1356, January 2007.

[180] T Tsuchido, N Katsui, A Takeuchi, M Takano, and I Shibasaki. Destruction of the outer membrane permeability barrier of Escherichia coli by heat treatment. *Applied and Environmental Microbiology*, 50(2):298–303, August 1985.

[181] M B Martinez, M C Flickinger, and G L Nelsestuen. Steady-state enzyme kinetics in the Escherichia coli periplasm: a model of a whole cell biocatalyst. *Journal of Biotechnology*, 71(1-3):59–66, May 1999.

[182] M L Applebury and J E Coleman. Escherichia coli alkaline phosphatase. Metal binding, protein conformation, and quaternary structure. *The Journal of biological chemistry*, 244(2):308–318, January 1969.

[183] R A Anderson and B L Vallee. Cobalt(III), a probe of metal binding sites of Escherichia coli alkaline phosphatase. *Proceedings of the National Academy of Sciences*, 72(1):394–397, January 1975.

[184] H Inouye and J Beckwith. Synthesis and processing of an Escherichia coli alkaline phosphatase precursor in vitro. *Proceedings of the National Academy of Sciences*, 74:1440–1444, April 1977.

[185] Brian H Johnson and Michael H Hecht. Recombinant Proteins Can Be Isolated from E. coli Cells by Repeated Cycles of Freezing and Thawing. *Nature biotechnology*, 12(12):1357–1360, December 1994.

[186] H R Ibrahim, Y Sugimoto, and T Aoki. Ovotransferrin antimicrobial peptide (OTAP-92) kills bacteria through a membrane damage mechanism. *Biochimica et biophysica acta*, 1523(2-3):196–205, October 2000.

[187] Kevin L Griffith and Richard E Wolf, Jr. Measuring β-Galactosidase Activity in Bacteria: Cell Growth, Permeabilization, and Enzyme Assays in 96-Well Arrays. *Biochemical and biophysical research communications*, 290(1):397–402, January 2002.

[188] Raquel F Epand, Brendan P Mowery, Sarah E Lee, Shannon S Stahl, Robert I Lehrer, Samuel H Gellman, and Richard M Epand. Dual Mechanism of Bacterial Lethality for a Cationic Sequence-Random Copolymer that Mimics Host-Defense Antimicrobial Peptides. *Journal of Molecular Biology*, 379(1):38–50, May 2008.

[189] M W Slein and G F Logan. Lysis of Escherichia coli by Ethylenediaminetetraacetate and Phospholipases as Measured by β-Galactosidase Activity. *Journal of bacteriology*, 94:934–941, June 1967.

[190] G R Craven, E Steers, and C B Anfinsen. Purification, Composition, and Molecular Weight of the Beta-Galactosidase of Escherichia coli K12. *The Journal of biological chemistry*, 240(240):2468–2477, June 1965.

[191] A V Fowler and I Zabin. The amino acid sequence of beta-galactosidase of Escherichia coli. *Proceedings of the National Academy of Sciences*, 74:1507–1510, January 1977.

[192] A Smita, H Mohammad A, and N Vidyanand. β-Galactosidase leakage from Escherichia coli points to mechanical damageas likely cause of carbon nanotube toxicity. *Soft Nanoscience Letters*, 2:41–45, May 2012.

[193] Faustino Vidal-Aroca, Michele Giannattasio, Elisa Brunelli, Alessandro Vezzoli, Paolo Plevani, Marco Muzi-Falconi, and Giovanni Bertoni. One-step high-throughput assay for quantitative detection of β-galactosidase activity in intact Gram-negative bacteria, yeast, and mammalian cells. *BioTechniques*, 40(4):433–440, April 2006.

[194] W Li, X Zhao, S Zou, Y Ma, K Zhang, and M Zhang. Scanning assay of β-galactosidase activity. *Applied Biochemistry and Microbiology*, 48(6):603–607, October 2012.

[195] Yang-Chun Yong, Yang-Yang Yu, Yun Yang, Jing Liu, Jing-Yuan Wang, and Hao Song. Enhancement of extracellular electron transfer and bioelectricity output by synthetic porin. *Biotechnology and Bioengineering*, 110(2):408–416, February 2013.

[196] Yan Qiao, Chang Ming Li, Shu-Juan Bao, Zhisong Lu, and Yunhan Hong. Direct electrochemistry and electrocatalytic mechanism of evolved Escherichia coli cells in microbial fuel cells. *Chemical Communications*, (11):1290–1292, February 2008.

[197] Yan Qiao, Chang Ming Li, Zhisong Lu, Hua Ling, Aram Kang, and Matthew Wook Chang. A time-course transcriptome analysis of Escherichia coli with direct electrochemistry behavior in microbial fuel cells. *Chemical Communications*, (41):6183–6183, September 2009.

[198] Tian Zhang, Changzheng Cui, Shengli Chen, Xinping Ai, Hanxi Yang, Ping Shen, and Zhenrong Peng. A novel mediatorless microbial fuel cell based on direct biocatalysis of Escherichia coli. *Chemical Communications*, (21):2257–2259, April 2006.

[199] Jing Liu, Yan Qiao, Zhi Song Lu, Hao Song, and Chang Ming Li. Enhance electron transfer and performance of microbial fuel cells by perforating the cell membrane. *Electrochemistry Communications*, 15(1):50–53, February 2012.

[200] Jörg S Deutzmann, Merve Sahin, and Alfred M Spormann. Extracellular Enzymes Facilitate Electron Uptake in Biocorrosion and Bioelectrosynthesis. *mBio*, 6(2):e00496–15, April 2015.

[201] Bangaru Balasundaram, Sue Harrison, and Daniel G Bracewell. Advances in product release strategies and impact on bioprocess design. *Trends in Biotechnology*, 27(8):477–485, August 2009.

[202] Erik Strandberg, Santi Esteban-Martín, Anne S Ulrich, and Jesús Salgado. Hydrophobic mismatch of mobile transmembrane helices: Merging theory and experiments. *BBA - Biomembranes*, 1818(5):1242–1249, May 2012.

[203] Jamie Hinks, Yaofeng Wang, Artur Matysik, Rachel Kraut, Staffan Kjelleberg, Yuguang Mu, Guillermo C Bazan, Stefan Wuertz, and Thomas Seviour. Increased Microbial Butanol Tolerance by Exogenous Membrane Insertion Molecules. *ChemSusChem*, 8(21):3718–3726, September 2015.

[204] Peter Clauwaert, Peter Aelterman, The Hai Pham, Liesje Schamphelaire, Marta Carballa, Korneel Rabaey, and Willy Verstraete. Minimizing losses in bio-electrochemical systems: the road to applications. *Applied Microbiology and Biotechnology*, 79(6):901–913, May 2008.

[205] H C Neu and L A Heppel. *The release of enzymes from Escherichia coli by osmotic shock and during the formation of spheroplasts*, volume 240. Journal of Biological Chemistry, March 1965.

[206] A Shokri A Sand x000E9 n G Larss. Growth rate-dependent changes in Escherichia coli membrane structure and protein leakage. *Applied Microbiology and Biotechnology*, 58(3):386–392, March 2002.

[207] S C Williams, Y Hong, DCA Danavall, M H Howard-Jones, D Gibson, M E Frischer, and P G Verity. Distinguishing between living and nonliving

bacteria: Evaluation of the vital stain propidium iodide and its combined use with molecular probes in aquatic samples. *Journal of Microbiological Methods*, 32(3):225–236, May 1998.

[208] Raphaël Ducommun, Marie-France Favre, Delphine Carrard, and Fabian Fischer. Outward electron transfer by Saccharomyces cerevisiae monitored with a bi-cathodic microbial fuel cell-type activity sensor. *Yeast*, 27(3):139–148, November 2010.

[209] Falk Harnisch and Stefano Freguia. A Basic Tutorial on Cyclic Voltammetry for the Investigation of Electroactive Microbial Biofilms. *Chemistry - An Asian Journal*, 7(3):466–475, January 2012.

[210] Jamie Hinks, Wee Han Poh, Justin Jang Hann Chu, Joachim Say Chye Loo, Guillermo C Bazan, Lynn E Hancock, and Stefan Wuertz. Oligopolyphenylenevinylene-Conjugated Oligoelectrolyte Membrane Insertion Molecules Selectively Disrupt Cell Envelopes of Gram-Positive Bacteria. *Applied and Environmental Microbiology*, 81(6):1949–1958, February 2015.

[211] T.J. Beveridge and L L Graham. Surface-Layers of Bacteria. *Microbiological reviews*, 55(4):684–705, December 1991.

[212] Gisela Storz and Regine Hengge. *Bacterial Stress Responses*. American Society for Microbiology Press, November 2010.

[213] Seoktae Kang, Moshe Herzberg, Debora F Rodrigues, and Menachem Elimelech. Antibacterial Effects of Carbon Nanotubes: Size Does Matter! *Langmuir*, 24(13):6409–6413, July 2008.

[214] Angela Ivask, Elizabeth Suarez, Trina Patel, David Boren, Zhaoxia Ji, Patricia Holden, Donatello Telesca, Robert Damoiseaux, Kenneth A Bradley, and Hilary Godwin. Genome-Wide Bacterial Toxicity Screening Uncovers the Mechanisms of Toxicity of a Cationic Polystyrene Nanomaterial. *Environmental Science & Technology*, 46(4):2398–2405, February 2012.

[215] G N Vemuri, M A Eiteman, J E McEwen, L Olsson, and J Nielsen. Increasing NADH oxidation reduces overflow metabolism in Saccharomyces

cerevisiae. *Proceedings of the National Academy of Sciences*, 104(7):2402–2407, February 2007.

[216] M R Leonardo, Y Dailly, and D P Clark. Role of NAD in regulating the adhE gene of Escherichia coli. *Journal of bacteriology*, 178(20):6013–6018, October 1996.

[217] Q Wang, M S Ou, Y Kim, L O Ingram, and K T Shanmugam. Metabolic Flux Control at the Pyruvate Node in an Anaerobic Escherichia coli Strain with an Active Pyruvate Dehydrogenase. *Applied and Environmental Microbiology*, 76(7):2107–2114, March 2010.

[218] R A Al-Tahhan, T R Sandrin, A A Bodour, and R M Maier. Rhamnolipid-induced removal of lipopolysaccharide from Pseudomonas aeruginosa: Effect on cell surface properties and interaction with hydrophobic substrates. *Applied and Environmental Microbiology*, 66(8):3262–3268, August 2000.

[219] A Bhattacharjee and T D Nusca. Rhamnolipids Mediate an Interspecies Biofilm Dispersal Signaling Pathway. *ACS Chemical Biology*, 11(11):3068–3076, September 2016.

[220] Ye Ni and Rachel Chen. Extracellular recombinant protein production from Escherichia coli. *Biotechnology letters*, 31(11):1661–1670, July 2009.

Appendix A

Additional electrochemical characterization experiments

A.1 Cyclic voltammetry of U-tube MFC components

U-tube MFC devices were utilized in Chapter 4 to determine the origin of DSSN+ performance improvements by physical separation of components to discern between cells adhered on the electrode vs. planktonic cells. In these devices, it is difficult to ascertain the mechanism of improved charge transfer due to the lack of in situ electrochemical characterization. In an attempt to elucidate charge transfer mechanism using cyclic voltammetry (CV), anode components from U-tube MFCs are once again transferred into 3-electrode electrochemical cells.

A.1.1 Experimental Methods

3-electrode electrochemical cell construction and cyclic voltammetry (CV)

3-electrode electrochemical cells were constructed following previous experiments. [53] Glass reactor vials with a 20 mL working volume were sealed with rubber septa. Ag/AgCl reference electrodes were constructed out of silver wire,

treated with bleach, in 3.5 M KCl and a 3.2 mm Vycor frit. The counter electrode was a coiled 0.25 mm Ti wire. The working electrode was either a new piece of graphite felt (1 cm $\times$ 1 cm) woven with Ti or the anodes (2 cm $\times$ 5 cm) removed from the U-tube devices. Anaerobic conditions were maintained through constant purging of the headspace with humidified N_2:CO_2 (80:20), however anodes were still briefly exposed to aerobic conditions.

Devices were connected to a Gamry potentiostat (Reference 600) and multiplexer (model ECM8) for cyclic voltammetry (CV) analyses. CVs were measured of the anodes removed from U-tubes in the anode solution, of anodes in 50 mM PBS and of new working electrodes in the anode solution. After CV of anodes in the anode solution, anodes were then rinsed in 50 mM PBS prior to CV analysis in PBS to remove any residual LB media. Control CVs were measured of abiotic LB and PBS with and without 10 μM DSSN+. Potentials were scanned from -0.7 V to 0.2 V vs Ag/AgCl at a scan rate of 5 mV/s for 3 or 4 cycles. The last scan of representative devices was used for comparison.

A.1.2 Results and Discussion

Cyclic voltammetry (CV) was utilized to determine whether DSSN+ improves current by increasing catalytic activity, inducing redox processes, or releasing redox mediators from the cell. In order to perform CV analyses, components from U-tube devices needed to be transferred to a 3-electrode electrochemical cell, since the U-tube configuration lacks a references electrode. Anodes and anode solutions from O-, A- and S-MFCs were carefully transferred from U-tube devices to electrochemical cells. Voltammograms of anodes in anode solutions are displayed in Figure A.1. In both the O- and A-MFCs, DSSN+ increased both the anodic and cathodic currents. Less of an effect was observed in the S-MFC CVs (Figure A.1c).

The use of LB as the electrolyte solution in this study, as well as in previous studies [50, 51], convolutes the mechanism of electron transfer with DSSN+ in MFCs. LB is known to contain mediators, such as flavins, present in yeast extract [93, 95, 208]. The presence of redox mediators makes it difficult to observe any potential signals from redox active components that were potentially

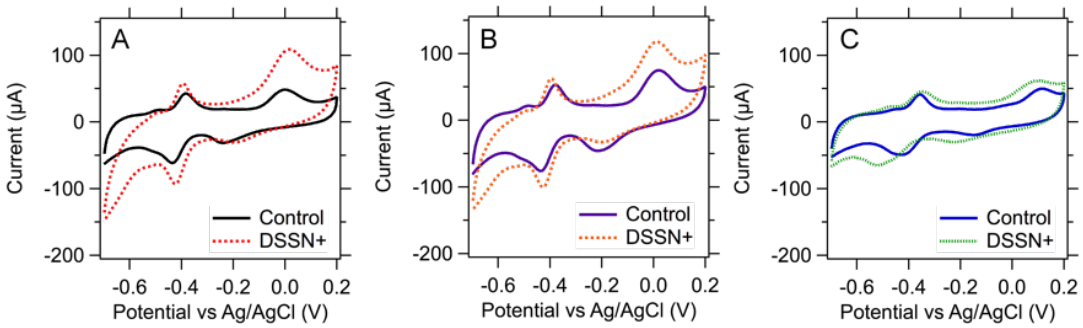

Figure A.1: Representative cyclic voltammograms of anodes in media from the anode chambers removed from (A) O-MFCs, (B) A-MFCs and (C) S-MFCs with and without DSSN+ modification. The anode from the U-tubes were used as the working electrode and have a geometric area of 10 cm^2 Scan rate: 5 mV/s

released from the cells. Redox activity of abiotic LB shows two reversible reactions in Figure A.2a, representing the background redox activity. It is possible that membrane disruption by DSSN+ would produce an increased current when in the presence of a sufficient concentration of mediators, therefore it is hard to ascertain this effect of DSSN+ to be from mediators in the media or a release of intracellular components upon DSSN+ intercalation.

To address this concern, anodes from all devices were rinsed in 50 mM PBS solution in order to remove any soluble mediators then transferred to a 3-electrode electrochemical cell for cyclic voltammetry (CV) analyses in a buffer solution devoid of potential mediators. Thus, CV was performed on cells remaining on electrodes under non-turnover conditions and scans are displayed in Figure A.3. Similar increases in anodic and cathodic currents are observed from the O- and A-MFC electrodes under non-turnover conditions and the characteristic peaks from LB media are no longer present (Figure A.3a-b). This could suggest enhanced electroactivity in the DSSN+ modified biofilms, however it is unclear as to what reactions are taking place under these conditions.

CV was also performed on the anode solutions from the U-tube MFCs using a new carbon felt working electrode with an area of 1 cm^2. Negligible differences in currents are observed between DSSN+ and control CVs in all O-, A-, and S-MFCs, displayed in Figure A.4. Under these conditions, release of redox mediators from *E. coli* upon DSSN+ intercalation is not apparent.

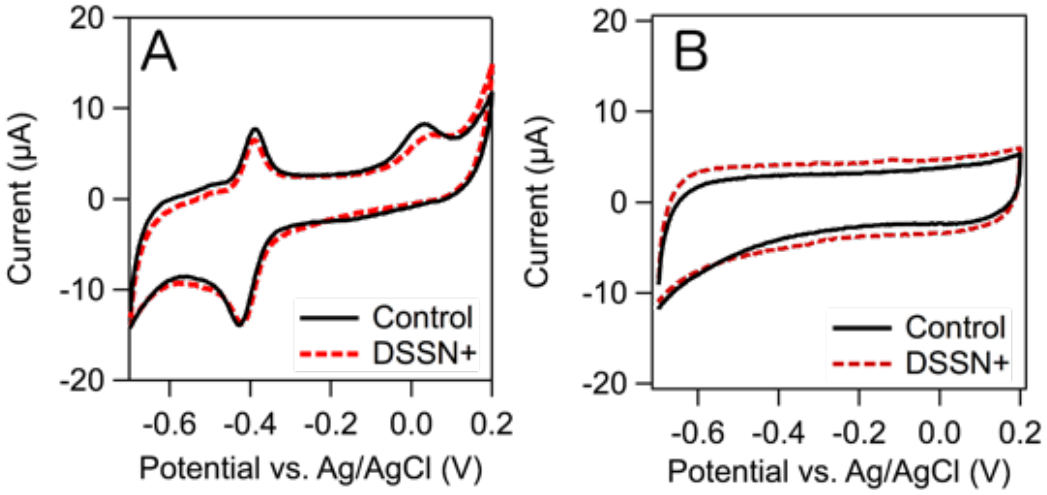

Figure A.2: Cyclic voltammograms of sterile abiotic solutions of (a) LB and (b) PBS, with and without 10 μM DSSN+. The carbon felt working electrode used has a geometric surface area of 1 cm^2. Scan rate: 5 mV/s

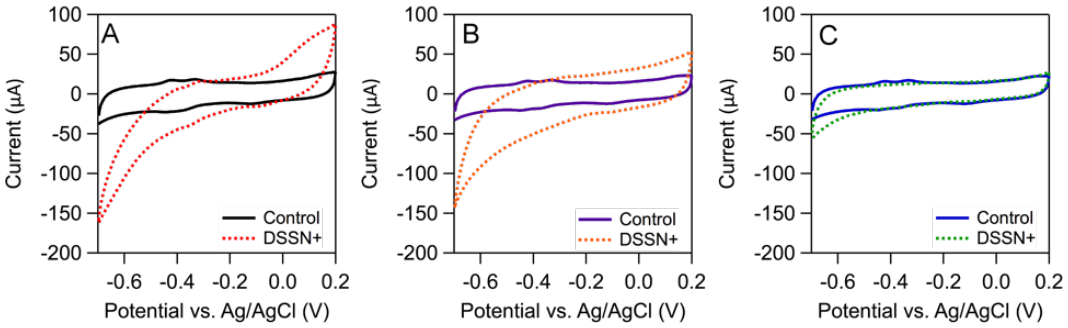

Figure A.3: Representative non-turnover cyclic voltammograms of anodes removed from the (a) O-MFCs, (b) A-MFCs, and (c) S-MFCs with and without DSSN+ modification in PBS. Scan rate: 5 mV/s

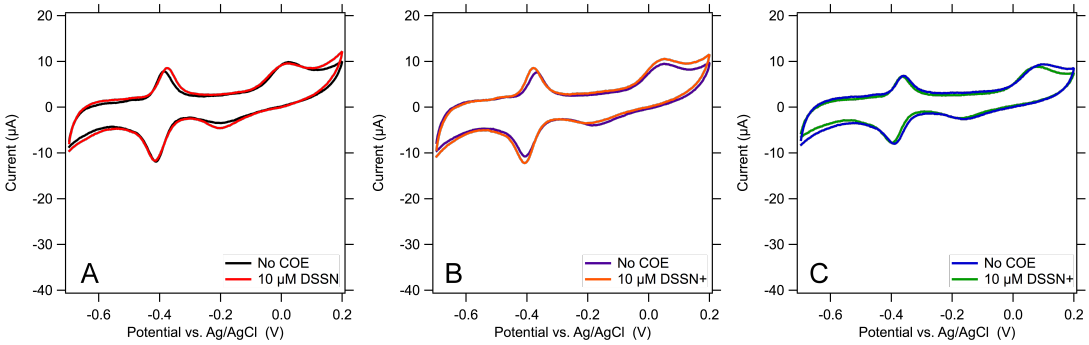

Figure A.4: Representative cyclic voltammograms of planktonic cell solutions from anode chambers of devices after operation from (a) O-MFCs, (b) A-MFCs and (c) S-MFCs with and without DSSN+ modification. The working electrode used was new carbon felt ($1\,cm^2$). Scan rate: $5\,mV/s$

A.2 3-electrode electrochemical cell experiments

In order to beat a dead horse, similar experiments were performed in 3-electrode electrochemical cells. In these experiments, as well at the previous bioreactor experiments from Chapter 4, lactate was chosen as the carbon source. Under anaerobic conditions with lactate as the sole carbon source, *E. coli* is limited in its ability for anaerobic respiration and cannot ferment. However, if *E. coli* is able to utilize an external electron acceptor, such as the electrode, lactate can be metabolized. Current production is evaluated via chronoamperometry under a poised potential of 0.2 V. Additionally, cyclic voltammetry is performed to probe any changes in redox or catalytic behavior with the addition of DSSN+. Four devices were used for each test group; control, $10\,\mu$M DSSN+ present initially (t=0 hr), and $10\,\mu$M DSSN+ added after 23 hours. Two devices in each group were running chronoamperometry uninterrupted, while the other two in the group were used for cyclic voltammetry.

Figure A.5 shows the current data from chronoamperometry. As demonstrated previously, DSSN+ is shown to improve current production compared to untreated *E. coli* up to 200%. Adding DSSN+ to devices at t=23 hr results in an instantaneous increase in current. CV was taken immediately before and after DSSN+ addition in devices not continuously poised for chronoamperometry,

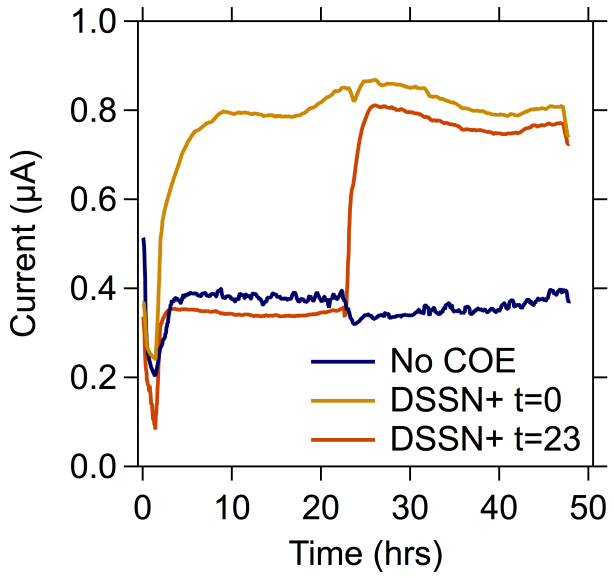

Figure A.5: Chronoamerometry of *E. coli* in 3-electrode electrochemical cells. Current generation is plotted over time from *E. coli* with no COEs (blue), initial DSSN+ modified *E. coli* (gold), and DSSN+ added at t=23 hr (orange).

shown in Figure A.6. No significant redox activity appears after DSSN+ modification. Figure A.7 shows CV data at the end of device operation of the two devices that were consistently under chronoamperometric conditions. Similar to results shown in Chapter 4, OD measurements were taken over time, indicating a significant decrease in planktonic cells after DSSN+ addition (Figure A.8).

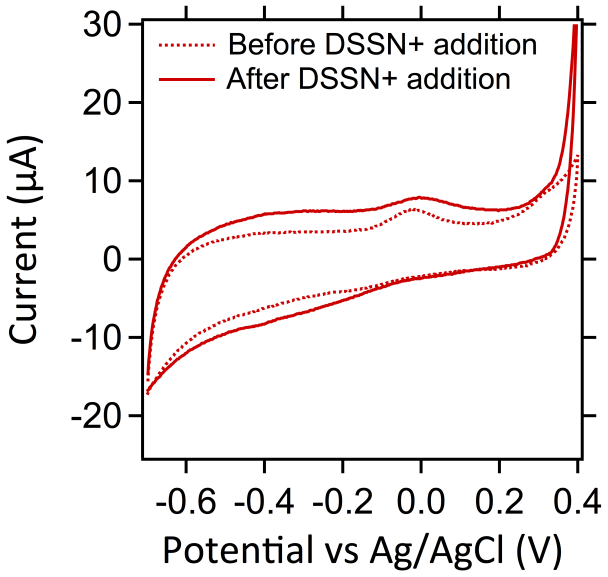

Figure A.6: Cyclic voltammetry before (dotted) and after (solid) DSSN+ addition.

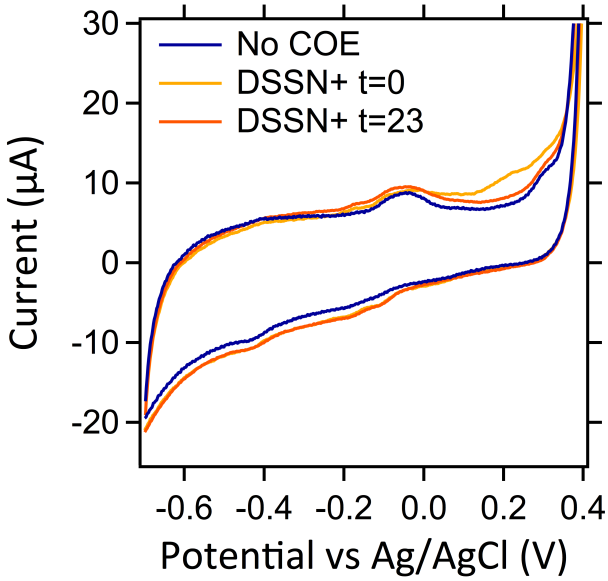

Figure A.7: Cyclic voltammetry of DSSN+ modified electrochemical cells at the end of operation.

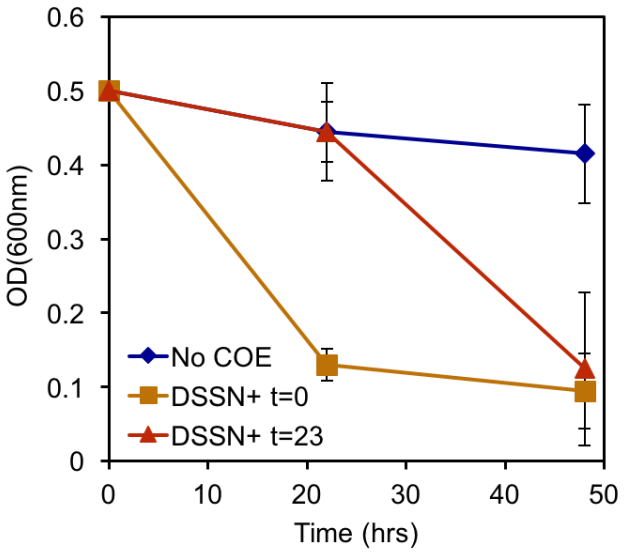

Figure A.8: Optical density measurements in electrochemical cells over time from untreated (blue), initially treated (gold), and DSSN+ added at t=23 h treated *E. coli*. Error bars show standard deviation of quadruplicates.